UNIVERSITY OF OKLAHOMA

GRADUATE COLLEGE

BRINE DRIVEN ALTERATION OF PHYLLOSILICATES

A DISSERTATION

SUBMITTED TO THE GRADUATE FACULTY

in partial fulfillment of the requirements for the

Degree of

DOCTOR OF PHILOSPOHY

By

CHRISTOPHER JOHN GEYER

Norman, Oklahoma

2024

BRINE DRIVEN ALTERATION OF PHYLLOSILICATES

A DISSERTATION APPROVED FOR THE

SCHOOL OF GEOSCIENCES

BY THE COMMITTEE CONSISTING OF

Dr. Megan E. Elwood Madden, Chair

Dr. Andrew S. Elwood Madden

Dr. Caitlin Hodges

Dr. Gordon Macleod

Dr. Mashhad Fahes

Acknowledgements

There are many people who help us throughout our journeys, I am grateful to so many. I'd like to thank my advisor, Dr. Megan Elwood Madden, for her guidance and patience. Thanks to Dr. Andy Elwood Madden for the thought-provoking conversations and inspirations. Thanks also to Dr. Gordon Macleod, for his sage counsel and guidance. I'd like to thank the other members of my committee, Dr. Caitlin Hodges and Dr. Mashhad Fahes for their support and critical feedback.

I would like to thank Steve Chipera for inspiring me and sharing his incredible command of mineralogy and XRD methodology. Also, I have never been so well trained on instrumentation than by Dr. Preston Larson, and so I am incredibly grateful. A special thank you is owed to the OU support staff, particularly Rebecca Fay and Ginger Leivas; OU culture has created an environment so supportive of the students that I continue to be overwhelmed.

And most importantly, I would like to thank my wife Natalie, for her patience, encouragement, and support, for suffering through moments when I was absent minded and especially for engaging with me as I thought through some complicated rationale.

Financial support statement: This project was funded by NASA grants 80NSSC18K0512 and 80NSSC23K0037. Additional funding was provided by the University of Oklahoma and the Mewbourne College of Earth and Energy School of Geosciences.

Dissertation Summary

The sedimentary structures and mineralogy of the Martian surface record a complex and inconsistently active hydrosphere throughout the planet's history (Bibring et al., 2006; Elwood Madden et al., 2009). Phyllosilicates in particular are useful for interpreting the influence water has had on the planet, and have been detected using remote sensing, as well as ground-based lander and rover analyses (Bishop, 2018; Bishop et al., 2008). On Earth, phyllosilicates have been studied extensively, not only because of their economic value, but also because they are a product of the fluids they formed in as well as the fluids they have been subsequently exposed to (Ayari et al., 2007; Kerr, 1952; McKinley et al., 1999).

The fluid chemistry of the Martian hydrosphere likely differed from Earth's significantly, thus, interpretations of aqueous alteration derived from common terrestrial analogues may not fully reflect aqueous alteration on Mars. In the geologic past, Mars likely had a wetter (and possibly warmer) climate which transitioned into a present-day cold and dry climate (Carter et al., 2015). As water became increasingly restricted, fluids would have become increasingly briny. This desiccation would have led to temporally and spatially variable fluid chemistries, multiple aqueous alteration mechanisms, and therefore multiple pathways for alteration of phyllosilicates (Bristow et al., 2021).

This dissertation examines aqueous processes which may have influenced and/or continues to influence phyllosilicates on Mars. Through a series of investigations, techniques including X-ray diffraction (XRD), Environmental Scanning Electron Microscopy (ESEM), Raman spectroscopy and elemental fluid composition via Inductively Coupled Plasma – Optical Emission Spectrometry (ICP-OES) are used to determine the effects of brine exposure to kaolinite

($Al_2Si_2O_5(OH)_4$), nontronite ($Na_{0.4}Fe^{III}_2(Si_{3.6}Al_{0.4})O_{10}(OH)_2$), and montmorillonite ($Na_{0.4}(Al_{1.6}Mg_{0.4})Si_4O_{10}(OH)_2$) (Essington, 2015).

Chapter 1 details two sets of experiments which were conducted to investigate how rock-fluid interactions on Mars could have facilitated precipitation of Ca-sulfate phases such as gypsum. It was found that brine concentration as well as the specific cation/anion pairing influenced cation exchange by montmorillonite. Chapter 1 has been published in The Planetary Science Journal (Geyer et al., 2023). In **Chapter 2**, ESEM was used to observe cation exchange facilitated by the deliquescence of a salt. A sample of montmorillonite mixed with a Na_2SO_4 or $MgSO_4$ salt underwent a cycle where relative humidity was increased from 3% to 100% and back to 3%. During this relative humidity cycle, in the absence of liquid water, the salt deliquesced and exchanged Na^+ or Mg^{2+} with the montmorillonite. As cation exchange occurred, the Ca^{2+} originally in the montmorillonite grain migrated out of the grain and formed new gypsum crystals. Chapter 2 has been submitted for publication in Clays and Clay Minerals and is currently under review. **Chapter 3** investigated potential aqueous alteration of kaolinite by twelve brines at 25°C and 100°. It was found that an interdependent relationship exists between temperature and brine concentration which significantly influenced kaolinite alteration, specifically, the preferential Al release from the kaolinite. Finally, **Chapter 4** details a similar set of experiments to those in Chapter 3, except the clays reacted were montmorillonite and nontronite. Here it was found that both illite formation during dissolution as well as preferential release of different elements by montmorillonite and nontronite was significantly influenced by temperature-brine dependent smectite alteration pathways.

References

Ayari, F., Srasra, E., & Trabelsi-Ayadi, M. (2007). Effect of exchangeable cations on the physicochemical properties of smectite. Surface Engineering and Applied Electrochemistry, 43, 369-378.

Bibring, J.-P., Langevin, Y., Mustard, J. F., Poulet, F., Arvidson, R., Gendrin, A., . . . Forget, F. (2006). Global mineralogical and aqueous Mars history derived from OMEGA/Mars Express data. Science, 312(5772), 400-404.

Bishop, J. L. (2018). Remote detection of phyllosilicates on Mars and implications for climate and habitability. In From habitability to life on Mars (pp. 37-75): Elsevier.

Bishop, J. L., Dobrea, E. Z. N., McKeown, N. K., Parente, M., Ehlmann, B. L., Michalski, J. R., . . . Mustard, J. F. (2008). Phyllosilicate diversity and past aqueous activity revealed at Mawrth Vallis, Mars. Science, 321(5890), 830-833.

Bristow, T., Grotzinger, J. P., Rampe, E., Cuadros, J., Chipera, S., Downs, G., . . . Morris, R. (2021). Brine-driven destruction of clay minerals in Gale crater, Mars. Science, 373(6551), 198-204.

Carter, J., Loizeau, D., Mangold, N., Poulet, F., & Bibring, J.-P. (2015). Widespread surface weathering on early Mars: A case for a warmer and wetter climate. Icarus, 248, 373-382.

Elwood Madden, M. E., Madden, A. S., & Rimstidt, J. D. (2009). How long was Meridiani Planum wet? Applying a jarosite stopwatch to determine the duration of aqueous diagenesis. Geology, 37(7), 635-638.

Essington, M. E. (2015). Soil and water chemistry: an integrative approach: CRC press.

Geyer, C., Madden, A. S. E., Rodriguez, A., Bishop, J. L., Mason, D., & Madden, M. E. (2023). The Role of Sulfate in Cation Exchange Reactions: Applications to Clay–Brine Interactions on Mars. The planetary science journal, 4(3), 48.

Kerr, P. F. (1952). Formation and occurrence of clay minerals. Clays and clay minerals, 1, 19-32.

McKinley, J., Worden, R., & Ruffell, A. (1999). Smectite in sandstones: a review of the controls on occurrence and behaviour during diagenesis. Clay mineral cements in sandstones, 109-128.

Chapter 1. The role of sulfate in cation exchange reactions: applications to clay-brine interactions on Mars

Christopher Geyer[1], Andrew S. Elwood Madden[1,2], Andrew Rodriguez, Janice L. Bishop[3], Daniel Mason[4], Megan Elwood Madden[1]

[1] School of Geosciences, University of Oklahoma, Norman, OK, USA

[2] Samuel Roberts Noble Microscopy Laboratory, University of Oklahoma, Norman, OK, USA

[3] NASA Ames and SETI Institute, Mountain View, CA, USA

[4] Department of Earth and Planetary Science, University of New Mexico, Albuquerque, NM, USA

Key Words: cation exchange; clay alteration; mars

Citation:

Geyer, C., Madden, A. S. E., Rodriguez, A., Bishop, J. L., Mason, D., & Madden, M. E. (2023). The Role of Sulfate in Cation Exchange Reactions: Applications to Clay–Brine Interactions on Mars. The planetary science journal, 4(3), 48.

Abstract

Phyllosilicates on Mars record a complex history of aqueous activity, including at Gale crater and Meridiani Planum, where stratigraphic differences in clay mineralogy have been recorded in outcrops that also contain calcium sulfate minerals. Thus, characterizing associations between phyllosilicates and calcium sulfates may provide constraints useful for constraining the geochemical environments that formed these outcrops. Previous studies have documented calcium sulfate precipitation as a result of clay-salt-atmospheric H_2O interactions, but the composition of brines throughout Mars' history would have depended on the volume of water available on the Martian surface. Variations in brine composition likely influence the type and extent of reactions between the brines and minerals they come in contact with. To better understand how clay–brine interactions affected near-surface mineral assemblages on Mars, we performed two sets of experiments. The first set of experiments examines the effect of differing total brine concentration and the second set explores variations in Na^+ and SO_4^{2-} concentrations independently. The results of this study show that gypsum readily forms due to cation exchange between montmorillonite and Na_2SO_4 brines of any concentration, but only near saturated $MgSO_4$ brines produced gypsum, and these also produced higher quantities of epsomite. Additionally, we found that the amount of gypsum produced from clay–Na_2SO_4 brine reactions was more strongly influenced by SO_4^{2-} than Na^+ or Cl^- concentrations. Understanding how rapidly gypsum forms as a product of clay-brine interactions, as well as the influence of SO_4^{2-} on cation exchange, will aid interpretations of sediments and environments observed on Mars.

1. Introduction

The spatial and stratigraphic heterogeneity of phyllosilicates and sulfate minerals on Mars is illustrative of a complex relationship between Mars' rock units and its hydrosphere. Several phyllosilicates have been identified, including different varieties of smectites, namely montmorillonite, saponite, and nontronite (Bibring et al., 2006; Janice L. Bishop et al., 2008; John Carter, Loizeau, Mangold, Poulet, & Bibring, 2015). A variety of sulfate minerals have been observed on Mars including kieserite, szomolnokite, polyhydrated sulfates consistent with starkeyite, hexahydrite, or rozenite (Janice L Bishop et al., 2009; Murchie et al., 2019), gypsum, bassanite (J. Carter, Poulet, Bibring, Mangold, & Murchie, 2013; S. W. Squyres et al., 2004; James J Wray et al., 2010) and anhydrite (Rampe et al., 2020). Gypsum has been identified at the Olympia Undae North Polar Dunes (Langevin, Poulet, Bibring, & Gondet, 2005), Noctis Labyrinthus west of Valles Marineris (Weitz, Bishop, & Grant, 2013), Gale Crater (D. T. Vaniman et al., 2018), and Meridiani Planum (S. W. Squyres et al., 2004). Terrestrial clay minerals are commonly interpreted as products of aqueous chemical weathering and it is likely similar processes influenced clay mineral formation on Mars (Cornelius, Hurlbyt, & Klein, 1977; Grim, 1968). Noachian age clay-bearing units in Gale Crater and Mawrth Vallis are commonly interpreted as products of authigenic lacustrine diagenesis. Alternative formation mechanisms such as hydrothermal alteration, burial diagenesis, pedogenesis, or detrital (eolian or alluvial) transport have been proposed for the wide variety of phyllosilicates observed across Mars (Murchie et al., 2019) and no single process likely describes the origin of all clay mineral assemblages on Mars (Thomas F Bristow et al., 2015; Thomas F. Bristow & Milliken, 2011; Ehlmann et al., 2011; Grotzinger et al., 2014). Several outcrops on Mars exhibit phyllosilicates

associated with sulfates, including Gale Crater (Rampe et al., 2020), Mawrth Vallis (James J Wray et al., 2010), and Noctis Labyrinthus (Weitz, Bishop, Thollot, Mangold, & Roach, 2011).

Spatial and temporal variations in fluid chemistry may also have influenced clay mineralogy on Mars. There is evidence that aqueous chemistry evolved over time to form high salinity fluids (brines) due to evapo-concentration, mineral hydration reactions, and freezing, decreasing the availability of liquid water in near-surface environments. As the total volume of liquid water decreased, salt concentrations in the remaining water would have increased, progressing towards hypersaline conditions, and ending with precipitation of the salts (Ehlmann et al., 2011; Hurowitz et al., 2017; Michalski & Noe Dobrea, 2007).

Reactions between brines and primary rocks, clays, and other secondary minerals have likely left a detailed, though complicated, record of water on Mars. Part of that record can be interpreted through investigation of clay-brine reaction products. The close relationship between clay minerals and hydrated sulfates has been observed across the Martian surface and studied in detail at locations such as Gale crater and Meridiani Planum (Andrews-Hanna, Phillips, & Zuber, 2007; S. Squyres et al., 2004; D. T. Vaniman et al., 2018; J. J. Wray et al., 2009). It is thought that brines have also influenced smectite mineralogy after their initial deposition, affecting smectite stratigraphic distribution (Thomas F Bristow et al., 2015; V. M. Tu et al., 2021) as well as producing Mg/Ca-sulfate concretions within the rock units (Nachon et al., 2014; S. P. Schwenzer et al., 2016). For example, Al-rich smectites are commonly observed overlaying Fe/Mg-rich smectites on Mars; this progression could be the result of alteration by transitory brines (Janice L. Bishop et al., 2008; T. Bristow et al., 2021; John Carter et al., 2015; V. M. Tu et al., 2021). While gypsum is considered an evaporite mineral that commonly forms from brines on Earth, the mechanism(s) and fluids which provided Ca^{2+} to SO_4^{2-} laden fluids is not uniform

171 across Mars (Fishbaugh, Poulet, Chevrier, Langevin, & Bibring, 2007; Gendrin, Mangold,
172 Bibring, Langevin, & et al., 2005; D. T. Vaniman & Chipera, 2006). For instance, sediments at
173 Gale Crater are thought to have been deposited in a lacustrine environment, but the presence of
174 Ca-sulfate minerals occurring in the rock matrix, as nodules or as fracture fill, indicates several
175 different diagenetic environments pre– and post–lithification (T. Bristow et al., 2021; Thomas F
176 Bristow et al., 2015; S. P. Schwenzer et al., 2016; D. T. Vaniman et al., 2018). Compared to Gale
177 crater, an even more complex record of water has been interpreted at Meridiani Planum where up
178 to four short-lived episodes of groundwater fluctuations may have been needed to create the
179 observed chemically distinct stratigraphic sections (Andrews-Hanna et al., 2007; M. Elwood
180 Madden, Bodnar, & Rimstidt, 2004; M. E. Elwood Madden, Madden, & Rimstidt, 2009;
181 Grotzinger et al., 2005; McLennan et al., 2005; Squyres & Knoll, 2005). The effects of different
182 diagenetic processes may be distinguished by determining the gypsum formation mechanism at
183 play, including gypsum precipitation as a product of clay-brine reactions (Deocampo, 2015).

184 Previous studies have shown that clay-brine interactions can readily form calcium sulfate
185 minerals through cation exchange, even in the absence of liquid water (Chipera et al., 1997,
186 Wilson and Bish, 2012). In Wilson and Bish (2011) smectite was mixed with a Mg-sulfate salt
187 prior to XRD analysis as relative humidity was cycled; gypsum was observed to form in these
188 experiments even in the absence of liquid water (Wilson & Bish, 2011). A later study by Wilson
189 and Bish (2012), found that besides forming hydrated $CaSO_4$ minerals, H_2O exchange between
190 Mg-sulfate minerals and a Ca-smectite might also buffer relative humidity on Mars. Cation
191 exchange driven alteration of clays caused by evolving brine chemistry as the prevalence of free
192 water changed throughout Mars' history may also explain the heterogeneous nature of Martian
193 smectites. During Noachian wet periods, acidic weathering of basalt likely liberated Na^+, Mg^{2+},

194 Ca^{2+}, SO_4^{2-} and Cl^- ions into solution (Thomas F Bristow et al., 2015; Zolotov & Mironenko,
195 2016). Later, a drier climate beginning in the Hesperian, reduced the volume of lakes and
196 lowered the water table through evaporation/sublimation; the resulting brine compositions would
197 have evolved as the remaining free water volume decreased as well as interactions between pore
198 waters and sediments. Chemical stratification of the water column, caused by intermittent wet
199 periods, may also have resulted in stratigraphically different clay-brine interactions.

200 The temporally and chemically transient nature of brines and their reactions with clays could
201 explain the provenance of gypsum coincident with clay deposits on Mars. Cation exchange has
202 been previously found to dominate reactions between nontronite (an Fe-smectite) and $MgSO_4$
203 brine (D. Vaniman, Bish, Chipera, & Rearick, 2011); similarly, exchange of Na^+ for smectite
204 bound Ca^{2+} is believed to enrich Ca^{2+} concentrations in hypersaline lake waters in Antarctica's
205 McMurdo Dry Values, a terrestrial Mars analogue site (Tu, Ming, & Sletten, 2021). Gypsum
206 formation has also been observed as a result of cation exchange between montmorillonite and
207 hydrated Mg-sulfate salts in the absence of liquid H_2O (Wilson & Bish, 2011). As brines formed
208 and became enriched in Mg^{2+} and Na^+ through evaporation and diagenesis and interacted with
209 clays, Mg^{2+} would have readily exchanged with clay bound Ca^{2+}. Similarly, as brines became yet
210 more concentrated, Na^+ would have also exchanged for Ca^+. Thus SO_4^{2-} laden pore waters may
211 have become enriched with Ca^{2+} eventually leading to $CaSO_4$ mineral precipitation.

212 To further test this hypothesis, we investigated the effects of varying cation and anion
213 concentrations within brines on cation exchange mechanisms and controls on gypsum
214 precipitation resulting from clay-brine interactions. We focused on smectites because they often
215 contain exchangeable Ca^{2+} and their specific composition provides detailed information that can

aid interpretations of both formation fluid chemistry and subsequent diagenetic fluid composition.

2. Materials & Methods

2.1 Brines

Most aqueous fluids active near the surface of Mars, both in the geologic past and the present, were/are likely salty (Schwenzer et al., 2016, Wang et al., 2006, Schwenzer et al., 2012). It is improbable that one singular brine composition is responsible for the spatial and stratigraphic variability of the mineralogy seen on Mars (Schwenzer et al., 2016, Schwenzer et al., 2012, Squyres et al., 2004b). Therefore, this study employed $MgSO_4$, NaCl, and Na_2SO_4 brines in different concentrations and ratios to study the effects of clay reaction with brines, representing different diagenetic conditions on Mars. $MgSO_4$ and Na_2SO_4 brines were chosen due to their potential presence on Mars and abundant sulfate, as well as the cations involved. Cation exchange and selectivity in clays is complex and highly variable even within a specific clay group the cations and concentrations used in this study were chosen based on the conceptual model: $Na^+ > Ca^{2+} > Mg^{2+}$ (Appelo & Postma, 2004; Singh & Turner, 1965; Sposito, Holtzclaw, Charlet, Jouany, & Page, 1983; Suarez & Zahow, 1989; Tang & Sparks, 1993). Where Na^+ is the most likely to exchange into the interlayer from solution, followed by Ca^{2+}, and then Mg^{2+}, which is the least likely ion to move from solution into the interlayer due to a combination of size, charge, and hydration sphere effects.

To better constrain the factors that influence clay-brine interactions on Mars, two sets of experiments were conducted. The first investigated $MgSO_4$ and Na_2SO_4 brine-smectite reactions at varying total salt concentrations (0.1 *M*, 0.2 *M*, and 2.0 *M* Na_2SO_4, as well as 0.1 *M*, 0.3 *M*,

and 3.0 *M* $MgSO_4$, see Table 1). These reactions are referred to as "variable brine concentration" experiments. The second set of experiments, referred to as "variable cation/anion concentration" experiments, investigated the influence of individual cation/anion concentrations on gypsum precipitation. We analyzed the resulting solids with Raman and XRD, both of which are currently available for in-situ analyses on Mars (Marshall & Olcott Marshall, 2015).

Table 1. Molar concentrations for the six brines used in the brine concentration experiments. Water activities calculated based on Guendouzi et al. (Guendouzi, Mounir, & Dinane, 2003)

Brine	$MgSO_4$ (*M*)	Na_2SO_4 (*M*)	*a* H_2O
a	0.1	0	1.00
b	0.3	0	0.99
c	3.0	0	0.91
d	0	0.1	1.00
e	0	0.2	0.99
f	0	2.0	0.91

To investigate the effects of varied individual cation and anion concentrations we also prepared brines with independently varying Na^+ and SO_4^{2-} concentrations by adding chloride salts (Table 2). Substitution of Na_2SO_4 with NaCl was used to manipulate Na^+ concentrations independently of SO_4^{2-} concentrations. NaCl was used because, for the purposes of this study, Cl^- can be considered conservative. Of the ten separate brines prepared, Brines 1-5 had constant SO_4^{2-} concentrations and linearly increasing Na^+ concentrations, while Brines 6-10 had constant Na^+ concentrations and linearly increasing SO_4^{2-} concentrations; all had similar water activities (Table 2).

All brines used in this study were prepared by adding high–purity salts to 18.2 MΩ-H_2O in appropriate quantities to yield the desired concentrations. Brines were allowed to equilibrate for

>24 hours to ensure complete dissolution before filtering with a 0.45 μm filter and subsequent reactions with smectite.

Table 2. Molar ion concentrations for variable cation-anion concentration experiments. Water activities calculated based on Guendouzi et al. (Guendouzi et al., 2003)

		Brine Solution	Na^+ (*M*)	SO_4^{2-} (*M*)	*Cl*$^-$	*a* H_2O
Increasing	Na^+	1	0.6	0.3	0.0	0.99
		2	0.8	0.3	0.2	0.98
		3	1.0	0.3	0.4	0.98
		4	1.2	0.3	0.6	0.97
		5	1.4	0.3	0.8	0.96
Increasing	SO_4^{2-}	6	1.0	0.1	0.8	0.97
		7	1.0	0.2	0.6	0.97
		8	1.0	0.3	0.4	0.98
		9	1.0	0.4	0.2	0.98
		10	1.0	0.5	0.0	0.98

2.2 Smectite

We used Ca-montmorillonite "SAz-1" (Apache County, Arizona USA) $[(Ca_{0.39}Na_{0.36}K_{0.02})(Al_{2.71}Mg_{1.11}Fe_{0.12}Mn_{0.01}Ti_{0.03})(Si_8)O_{20}(OH)_4]$ obtained from the Clay Minerals Society (Mermut, 2001a, Mermut, 2001b, Chipera and Bish, 2001) as our model smectite phase. While other smectites such as nontronite and saponite are observed in greater abundances than montmorillonite on Mars (Bibring et al., 2005), SAz-1 was chosen for several reasons. First, SAz-1 is relatively pure compared to other widely available smectite clay standards and second, it will allow direct comparisons to previous studies of cation-exchange induced gypsum formation (Wilson and Bish, 2012, Wilson and Bish, 2011, Garrels and Christ, 1965, Lafuente et al., 2015). Lastly, SAz-1 is similar in structure and layer-charge to nontronite and saponite (Grim, 1968, Essington, 2015). While both nontronite and montmorillonite are dioctahedral smectites, saponite is trioctahedral; however, cation exchange behavior should be similar across

all three mineral species since it is primarily controlled by the magnitude of the layer-charge and the ion concentration of the fluid involved, not the source of the layer charge. In addition, SAz-1 exhibits some of the highest cation exchange capacity (CEC) observed in clays- 110-123 cmol•kg^{-1} (Essington, 2015; Mermut, 2001), whereas other smectites such as nontronite have slightly lower CEC values between 75-96 cmol•kg^{-1} (Bischoff, 1972).

We saturated the SAz-1 with Ca^{2+} by allowing the clay to react with ~3.5 M $CaCl_2$ for 24 hours followed by four cycles of washing with 18.2 MΩ H_2O, then centrifugation at 10,000 RPM for 20 minutes and decanting the supernatant. After washing, the Ca-exchanged SAz-1 was freeze-dried using a Labconco freeze dryer.

2.3 Analyses

Clay-brine pastes were created by mixing 0.5 g of clay with 0.5 mL brine and mixing thoroughly using a vortex mixer for 30 seconds. We analyzed the samples immediately using powder XRD and Raman spectroscopy to characterize the reaction products.

We used a Rigaku Ultima IV X-Ray diffractometer (Cu tube, 40 kV and 44 mA, curved graphite monochromator) to analyze the mineralogy of the samples via powder XRD. XRD slides were prepared following the smear technique (Moore and Reynolds, 1997) and analyzed immediately. XRD patterns were interpreted using MDI Jade Pro with the ICDD PDF4+ database; mineral phase weight percent were calculated using FULLPAT (Chipera and Bish, 2002). It is worth noting that one of the key diagnostic XRD peaks for smectites, the 001 basal reflection, is sensitive to both cation saturation and relative humidity; however, Chipera, Carey & Bish (1997) demonstrated Ca-exchanged SAz-1 001 spacing to be stable in laboratory conditions (Chipera et al., 1997, Moore and Reynolds, 1997). Thus, for the time scales involved

in these analyses (<4 hours), any shift detected in the 001 reflection can be ascribed to a change in the intercalating cation (Moore and Reynolds, 1997).

We used a Renishaw InVia Raman microscope equipped with a 500 mW 785 nm red laser and 1200 l/cm grating centered at 900 cm^{-1} to acquire Raman spectra from 300 to 1500 wavenumbers. The laser was set at 1% power to minimize sample heating and possible mineral degradation. Immediately before Raman analysis SAz-1 and the individual brines were mixed to a paint like consistency on a glass slide. Spectra were collected for 300 seconds, with repeat sampling to determine if laser-induced alteration occurred.

3. Results

3.1 Variable Brine Concentration Experiments

Gypsum was observed in all of the variable brine concentration $NaSO_4$ experiments (0.1 *M*, 0.2 *M*, and 2.0 *M* Na_2SO_4). However, of the $MgSO_4$ clay-brine mixtures, only 3.0 *M* $MgSO_4$ produced detectable gypsum (~2 wt%) along with 58 wt% epsomite ($MgSO_4 \cdot 7H_2O$) (Table 3; Figure 1).

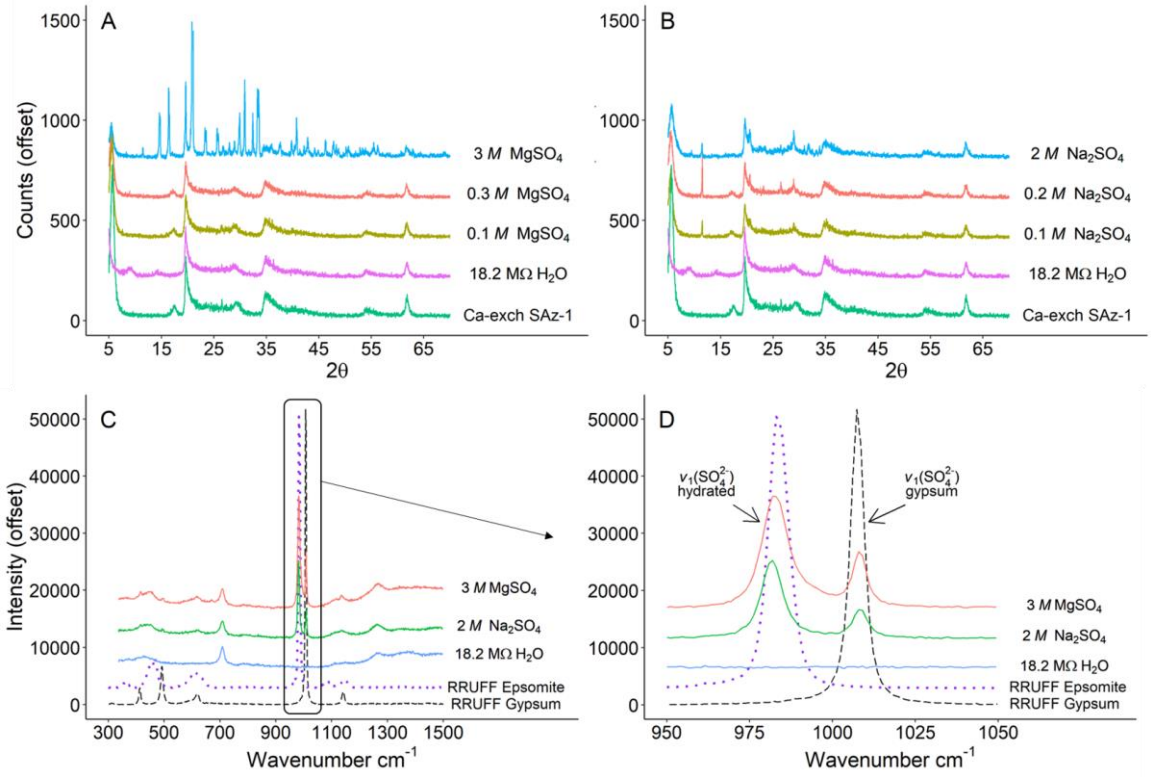

308

309 **Figure 1.** XRD patterns (A&B) and Raman spectra (C&D) collected from the clay-brine pastes.
310 A) variable $MgSO_4$ brine concentration experiments and B) variable Na_2SO_4 brine concentration
311 experiments; dashed black box in A & B highlighting characteristic gypsum 7.6 Å peak observed
312 at ~11.7 2θ. C) Full Raman spectra collected for the 18.2 MΩ H_2O, 3.0 M $MgSO_4$ and 2.0 M
313 Na_2SO_4 brines mixed with Ca-exchanged SAz-1. RRUFF gypsum (dashed line) and epsomite
314 (dotted line) included for reference (Lafuente et al., 2015). Note the broad peak at ~415-450 cm^{-1}
315 and intense peaks observed at ~980 and ~1008 cm^{-1}, black box highlighting area shown in D. D)
316 Close up of characteristic v_1 (SO_4^{2-}) symmetric stretching peak for gypsum and hydrated SO_4^{2-}.
317 The peak at ~980 cm^{-1} is commonly considered the indicative peak for epsomite, however, a
318 peak at 980 cm^{-1} is common for many SO_4^{2-} compounds as discussed in Section 3.1.

Table 3. Mineral phases observed in variable brine concentration experiments (wt %).

Brine with SAz-1	Montmorillonite	Quartz	Gypsum	Epsomite
Ca-exch SAz-1 (starting)	98%	2%	0%	0%
18.2 MΩ H_2O	98%	2%	0%	0%
0.1 *M* $MgSO_4$	98%	2%	0%	0%
0.3 *M* $MgSO_4$	98%	2%	0%	0%
3.0 *M* MgSO4	38%	2%	2%	58%
0.1 *M* Na_2SO_4	90%	2%	8%	0%
0.2 *M* Na_2SO_4	89%	2%	9%	0%
2.0 *M* Na_2SO_4	90%	2%	8%	0%

Raman spectra of Ca-exchanged SAz-1 reacted with 18.2 MΩ H_2O exhibited peaks typical of SAz-1, such as the SiO_4 and Al_2O_3 structural lattice modes at 435 cm^{-1} and 700 cm^{-1}, while lacking any vibrational modes associated with SO_4^{2-} (Janice L Bishop & Murad, 2004) (Figure 1c,d). Raman spectra of the 3.0 *M* $MgSO_4$ and 2.0 *M* Na_2SO_4 clay-brine mixtures clearly exhibit a $v_1(SO_4^{2-})$ peak at 981 cm^{-1} as well as a characteristic gypsum peak at 1007 cm^{-1} (Ben Mabrouk, Kauffmann, Aroui, & Fontana, 2013; Lafuente, Downs, Yang, & Stone, 2015; Wang, Freeman, Jolliff, & Chou, 2006)(Figure 1d).

Epsomite formation was only observed in the 3.0 *M* $MgSO_4$ XRD analysis (Figure 1a). However, in the Raman spectra, the vibrational modes commonly associated with hydrated SO_4^{2-} in epsomite ($v_2(SO_4^{2-})$ at 450 cm^{-1} and $v_3(SO_4^{2-})$ at 1100 cm^{-1} (Wang et al., 2006)) were not observed (Figure 1c,d). Although a peak at ~983 cm^{-1} (Figure 1d) is commonly assigned as $v_1(SO_4^{2-})$ for epsomite, the same frequency has been observed in sulfate brines regardless of the cation (Ben Mabrouk et al., 2013; Mason & Madden, 2022). Therefore, we interpret the ~980 cm^{-1} Raman peak as residual aqueous sulfate remaining in the sample since the secondary peaks, v_2(450 cm^{-1}) and v_3(1100 cm^{-1}), indicative of epsomite, are missing. The absence of epsomite in

the Raman analysis of the 3.0 *M* $MgSO_4$ clay-brine mixture is confirmed by examining the relative intensity ratio of the 980 cm^{-1} to 450 cm^{-1} peaks as the experimental sample has a lower relative intensity ratio (60%) as compared to the RRUFF epsomite reference spectrum.

3.2 Variable Cation-Anion Concentration Experiments

Gypsum formation was observed in all experiments where a brine containing Na^+ and SO_4^{2-} was reacted with Ca-exchanged SAz-1. In the experiments investigating variable Na^+ concentrations (SO_4^{2-} concentrations held constant), the volume of gypsum produced was relatively constant ~7 wt% (Figure 1c). However, in the experiments investigating varying SO_4^{2-} concentrations (Na^+ concentrations held constant), gypsum increased non-linearly with increasing sulfate concentration (Figure 1d). Closer inspection of the 10-25 Å d-spacings reveals that varying the Na^+ and SO_4^{2-} brine concentrations also influenced the 001 basal reflection (Figure 3). The swelling observed in SAz-1 reacted with 0.6 *M* Na^+ brine to ~19.5 Å can be explained by the presence of an added water layer. Slade et al. (1991) found that in lower concentration ionic solutions a transition from two to three water layers between the silicate layers will occur when the hydration enthalpy of the interlayer cations substantially overwhelms the layer charge deficit (Slade, Quirk, & Norrish, 1991).

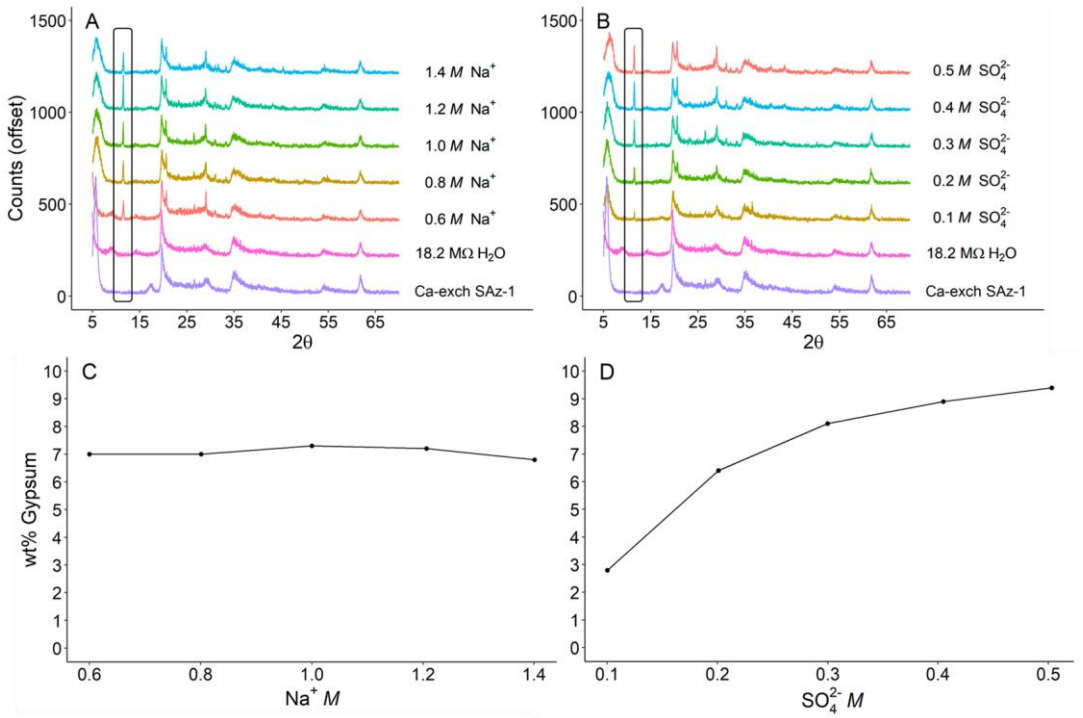

352

353 **Figure 2.** XRD patterns (A&B) and weight percent gypsum (C&D) formed from reacting Ca-
354 exchanged SAz-1 with Na_2SO_4 brines containing different concentrations of cations and anions.
355 A & C: The volume of gypsum produced was relatively constant despite increasing Na^+
356 concentrations (SO_4^{2-} concentrations held constant). B & D: Gypsum volumes increase with
357 increasing SO_4^{2-} concentrations (Na^+ concentrations held constant). Black box in A & B
358 highlighting characteristic gypsum 7.6 Å peak observed at ~11.7 2θ.

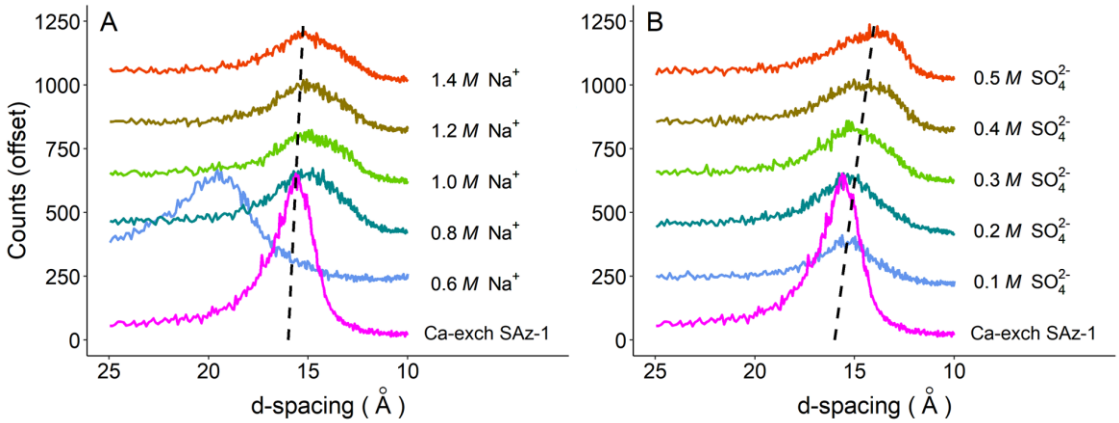

359

360 **Figure 3.** View of the 001 basal reflection of Ca-exchanged SAz-1 reacted with Na_2SO_4 brines
361 containing different concentrations of cations and anions. A) Increasing Na^+ concentration with

362 constant SO_4^{2-} concentration; note, with the exception of swelling observed at 0.6 M Na^+, a
363 minor but largely uniform shift toward smaller d-spacing is observed. B) Unlike the experiment
364 where SO_4^{2-} was held constant, the 001 reflection consistently progresses towards smaller d-
365 spacings with increasing SO_4^{2-} concentration (constant Na^+).

366 # 4. Discussion

367 ## 4.1 Effects from brine concentration

368 Results from these experiments demonstrate that gypsum formation is a function of both the
369 concentration and composition of the aqueous solution. Gypsum formed in less than one minute,
370 as observed in our Raman analyses, corroborating rapid gypsum formation rates observed by
371 Wilson and Bish (2011 & 2012). The amount of gypsum formed in montmorillonite reactions
372 with all three Na_2SO_4 brines was uniform at 7-9 wt%; however, gypsum formation was not
373 observed in reactions involving the lower concentrations of $MgSO_4$ brines.

374 Considering the rapid nature of the reactions, as well as the preponderance of gypsum
375 formation from Na_2SO_4 clay-brine reactions, cation exchange is likely the dominant mechanism
376 leading to gypsum formation in our experiments. Montmorillonite ion selectivity (retention in the
377 interlayer) generally follows $Mg^{2+} > Ca^{2+} > Na^+$, but replacement is also dependent on ion
378 activities, both in solution and at the exchanging sites (Essington, 2015; Garrels & Christ, 1965;
379 Grim, 1968; Sumner & Miller, 1996).

380 To complicate matters, it is not only the cation activity that must be considered but also the
381 anion(s); as shown in Figures 2C and 2D, gypsum precipitation increased with increasing SO_4^{2-}
382 concentrations but was mostly unaffected by variations in Na^+ concentrations.

4.2 Impacts of evolving brine chemistry

While cation exchange adequately explains reactions between clays, brines, and the resulting gypsum precipitation, it is unlikely clays on Mars experienced a sudden shift in concentration of a singular brine. Rather, evapo-concentration, fluid mixing, and an evolving climate likely altered the chemistry of brines in contact with clays (T. Bristow et al., 2021; V. M. Tu et al., 2021).

The experiments in this study which include varied concentrations of Na^+ and SO_4^{2-} shed some light on how cation exchange reactions may have progressed as brines on Mars evolved. The correlation between gypsum precipitation and SO_4^{2-} concentration seen in Figure 1 is not unexpected, as SO_4^{2-} is a primary constituent of gypsum. And yet, the apparent irrelevance of Na^+ concentrations requires some consideration. The constant amount of gypsum precipitated from the variable Na^+ brines, in juxtaposition with the variable SO_4^{2-} brines, demonstrates that although cation exchange may be the driving mechanism, the anions present in solution also influence cation exchange beyond just contributing to the ionic strength of a brine. As SO_4^{2-} concentrations are increased, a progressive reduction in the 001 reflection d-spacings by 11.9% is observed (Figure 2). However, as Na^+ concentrations increase, the shift to smaller d-spacings is less pronounced (4.0%). We interpret this reduction in d-spacings as evidence that interlayer-bound Ca^{2+} has been exchanged for Na^+ originating from the brine, causing collapse of the basal spacings. Progressive shifts to smaller d-spacings as a function of ion concentration are observed in both the variable SO_4^{2-} and Na^+ brines, however the shift was almost three times greater for increasing concentrations of SO_4^{2-} than for the Na^+. The substantially larger shift due to cation exchange in the variable SO_4^{2-} brines demonstrates that SO_4^{2-} concentration influences cation

405 exchange considerably more than Na^+ or Cl^-, at least in the concentrations that were investigated
406 in this study.

407 While it is unsurprising that an overwhelming concentration of Na^+ will displace interlayer
408 bonded Ca^{2+} in smectites, the increased cation exchange as a response to SO_4^{2-} and the apparent
409 irrelevance of Cl^- is worth noting. Early studies examining the cation selectivity of smectites
410 record a history of inconsistent interpretations regarding the influence of Cl^-, SO_4^{2-} and ClO_4^- and
411 the mechanisms driving cation exchange; however, previous studies focused on more dilute
412 solutions, where ion concentrations were significantly lower (maximum 0.1 *M* $Na^+/Ca^{2+}/Mg^{2+}$)
413 compared to the present study (Singh, 1982; Singh & Turner, 1965; Sposito, 1991; Sposito et al.,
414 1983; Suarez & Zahow, 1989; Teppen & Miller, 2006). Some of the aforementioned studies did
415 observe increased cation exchange in the presence of SO_4^{2-} as compared to solutions dominated
416 by Cl^-, NO_3^- or ClO_4^-, indicating that cation exchange is more active as SO_4^{2-} concentrations
417 increase, given similar brine chemistry.

418 The variable brine concentration experiments demonstrate that lower concentrations of
419 $MgSO_4$ brines will not induce gypsum formation. As free liquid water availability decreased on
420 Mars, brines would have become increasingly concentrated, eventually reaching saturation. The
421 results shown above suggest that gypsum would not have precipitated from clay-brine reactions
422 until the clays were exposed to brines with significant concentrations of $MgSO_4$ and in this case
423 there would be more epsomite present than gypsum, so the gypsum may not be discernable from
424 orbit at Mars. However, exposure to brines containing both Na^+ and SO_4^{2-} could readily produce
425 gypsum, even at relatively low concentrations of either ion.

426

5. Applications to Mars

Since the discovery of clay minerals on Mars, there has been a focused and concerted effort to better understand the environments in which they may have formed. Particular attention has been paid to smectites, since they are both relatively widespread and their chemical variability strongly correlates to the fluids they were exposed to during and after deposition. The results of this study may be used to refine interpretations of aqueous alteration where both smectites and calcium sulfates are observed, such as Gale crater and Meridiani Planum. For example, estimates for the length of intermittent "wet" periods at Meridiani Planum total less than 1 Ma, possibly fewer than 10,000 years. This study demonstrates clay-brine reactions can result in near-instantaneous gypsum formation, making one or more periods of brine-mediated alteration possible well within that time frame (M. E. Elwood Madden et al., 2009; Squyres & Knoll, 2005). Montmorillonite is not the only smectite observed on Mars; saponite and nontronite are also abundant, though the three clays do not have exactly the same chemistry or CEC and thus, additional research to determine the similarities between the three with respect to gypsum formation via cation exchange is advisable. The influence of SO_4^{2-} on gypsum formation shown in this study also provides insight into how clay-brine reactions may have progressed as brine chemistry changed, such as with the evapo-concentration believed to occur at Gale crater (S. Schwenzer et al., 2012; V. M. Tu et al., 2021).

6. Conclusions

While the CEC of montmorillonite is well-known, and gypsum precipitation as a result of clay-brine/salt reactions has been discussed in previous studies, these experiments provide further context through which we can interpret gypsum formation as brine chemistry evolved on Mars. The results of this study demonstrate that interactions between montmorillonite and brines

with subsequent formation of Ca-sulfates is rapid, and in fact almost instantaneous with respect to the geologic time scale. Although epsomite was seen to form within 2-3 hours using XRD analysis, Raman spectra reveal epsomite precipitation was not immediate and likely required evaporation. Conversely, gypsum formation from clay-brine reactions was nearly instantaneous. An important observation from the variable brine concentration experiments was that $NaSO_4$ brines reacted with SAz-1 would produce gypsum at any concentration; on the other hand, $MgSO_4$ brines only produced gypsum when they were at near saturation.

Acknowledgements

This project was partially funded by NASA PDART grant 80NSSC18K0512 and the University of Oklahoma.

References

Andrews-Hanna, J. C., Phillips, R. J., & Zuber, M. T. (2007). Meridiani Planum and the global hydrology of Mars. *Nature, 446*(7132), 163-166.

Appelo, C. A. J., & Postma, D. (2004). *Geochemistry, groundwater and pollution*: CRC press.

Ben Mabrouk, K., Kauffmann, T. H., Aroui, H., & Fontana, M. D. (2013). Raman study of cation effect on sulfate vibration modes in solid state and in aqueous solutions: Raman study of cation effect on sulfate vibration modes. *Journal of Raman spectroscopy, 44*(11), 1603-1608. doi:10.1002/jrs.4374

Bibring, J.-P., Langevin, Y., Mustard, J. F., Poulet, F., Arvidson, R., Gendrin, A., . . . Forget, F. (2006). Global Mineralogical and Aqueous Mars History Derived from OMEGA/Mars Express Data. *Science (American Association for the Advancement of Science), 312*(5772), 400-404. doi:10.1126/science.1122659

Bischoff, J. L. (1972). A ferroan nontronite from the Red Sea geothermal system. *Clays and clay minerals, 20*(4), 217-223.

Bishop, J. L., & Murad, E. (2004). Characterization of minerals and biogeochemical markers on Mars: A Raman and IR spectroscopic study of montmorillonite. *Journal of Raman spectroscopy, 35*(6), 480-486.

Bishop, J. L., Noe Dobrea, E. Z., McKeown, N. K., Parente, M., Ehlmann, B. L., Michalski, J. R., . . . Bibring, J.-P. (2008). Phyllosilicate diversity and past aqueous activity revealed at

Mawrth Vallis, Mars. *Science (American Association for the Advancement of Science), 321*(5890), 830-833. doi:10.1126/science.1159699

Bishop, J. L., Parente, M., Weitz, C. M., Noe Dobrea, E. Z., Roach, L. H., Murchie, S. L., . . . Brown, A. J. (2009). Mineralogy of Juventae Chasma: Sulfates in the light-toned mounds, mafic minerals in the bedrock, and hydrated silica and hydroxylated ferric sulfate on the plateau. *Journal of Geophysical Research: Planets, 114*(E2).

Bristow, T., Grotzinger, J. P., Rampe, E., Cuadros, J., Chipera, S., Downs, G., . . . Morris, R. (2021). Brine-driven destruction of clay minerals in Gale crater, Mars. *science, 373*(6551), 198-204.

Bristow, T. F., Bish, D. L., Vaniman, D. T., Morris, R. V., Blake, D. F., Grotzinger, J. P., . . . Ming, D. W. (2015). The origin and implications of clay minerals from Yellowknife Bay, Gale crater, Mars. *American Mineralogist, 100*(4), 824-836.

Bristow, T. F., & Milliken, R. E. (2011). Terrestrial perspective on authigenic clay mineral production in ancient Martian lakes. *Clays and clay minerals, 59*(4), 339-358. doi:10.1346/CCMN.2011.0590401

Carter, J., Loizeau, D., Mangold, N., Poulet, F., & Bibring, J.-P. (2015). Widespread surface weathering on early Mars: A case for a warmer and wetter climate. *Icarus (New York, N.Y. 1962), 248*, 373-382. doi:10.1016/j.icarus.2014.11.011

Carter, J., Poulet, F., Bibring, J.-P., Mangold, N., & Murchie, S. (2013). Hydrous minerals on Mars as seen by the CRISM and OMEGA imaging spectrometers: Updated global view. *Journal of Geophysical Research: Planets*, *118*(4), 831-858. doi:https://doi.org/10.1029/2012JE004145

Chipera, S. J., Carey, J. W., & Bish, D. L. (1997). Controlled-humidity XRD analyses: Application to the study of smectite expansion/contraction. *Advances in X-ray Analysis, 39*, 713-722.

Cornelius, S., Hurlbyt, J., & Klein, C. (1977). *Manual of Mineralogy (after James D. Dana)* (19th ed. Vol. 3): John Wiley & Sons, Inc.

Deocampo, D. M. (2015). Authigenic clay minerals in lacustrine mudstones. *Geological Society of America Special Papers, 515*, SPE515-503.

Ehlmann, B. L., Mustard, J. F., Murchie, S. L., Bibring, J.-P., Meunier, A., Fraeman, A. A., & Langevin, Y. (2011). Subsurface water and clay mineral formation during the early history of Mars. *Nature, 479*(7371), 53-60.

Elwood Madden, M., Bodnar, R., & Rimstidt, J. (2004). Jarosite as an indicator of water-limited chemical weathering on Mars. *Nature, 431*(7010), 821-823.

Elwood Madden, M. E., Madden, A. S., & Rimstidt, J. D. (2009). How long was Meridiani Planum wet? Applying a jarosite stopwatch to determine the duration of aqueous diagenesis. *Geology, 37*(7), 635-638.

Essington, M. E. (2015). *Soil and water chemistry: an integrative approach*: CRC press.

Fishbaugh, K. E., Poulet, F., Chevrier, V., Langevin, Y., & Bibring, J. P. (2007). On the origin of gypsum in the Mars north polar region. *Journal of Geophysical Research: Planets, 112*(E7).

Garrels, R. M., & Christ, C. L. (1965). *Solutions, minerals, and equilibria [by] Robert M. Garrels [and] Charles L. Christ*. New York: New York, Harper & Row.

Gendrin, A., Mangold, N., Bibring, J.-P., Langevin, Y., & et al. (2005). Sulfates in Martian Layered Terrains: The OMEGA/Mars Express View. *science, 307*(5715), 1587-1591.

Grim, R. E. (1968). *Clay Mineralogy* (2nd ed.): McGraw-Hill.

Grotzinger, J. P., Arvidson, R., Bell Iii, J., Calvin, W., Clark, B., Fike, D., . . . Herkenhoff, K. E. (2005). Stratigraphy and sedimentology of a dry to wet eolian depositional system, Burns formation, Meridiani Planum, Mars. *Earth and planetary science letters, 240*(1), 11-72.

Grotzinger, J. P., Sumner, D. Y., Kah, L., Stack, K., Gupta, S., Edgar, L., . . . Mangold, N. (2014). A habitable fluvio-lacustrine environment at Yellowknife Bay, Gale Crater, Mars. *science, 343*(6169), 1242777.

Guendouzi, M. E., Mounir, A., & Dinane, A. (2003). Water activity, osmotic and activity coefficients of aqueous solutions of Li2SO4, Na2SO4, K2SO4, (NH4)2SO4, MgSO4, MnSO4, NiSO4, CuSO4, and ZnSO4 at T= 298.15 K. *The Journal of Chemical Thermodynamics, 35*(2), 209-220.

Hurowitz, J. A., Grotzinger, J. P., Fischer, W. W., McLennan, S. M., Milliken, R. E., Stein, N., . . . Eigenbrode, J. L. (2017). Redox stratification of an ancient lake in Gale crater, Mars. *science, 356*(6341), eaah6849.

Lafuente, B., Downs, R. T., Yang, H., & Stone, N. (2015). The power of databases: The RRUFF project. In (pp. 1-30). Berlin, MΓjnchen, Boston: Berlin, MΓjnchen, Boston: DE GRUYTER.

Langevin, Y., Poulet, F., Bibring, J.-P., & Gondet, B. (2005). Sulfates in the north polar region of Mars detected by OMEGA/Mars Express. *science, 307*(5715), 1584-1586.

Marshall, C. P., & Olcott Marshall, A. (2015). Challenges analyzing gypsum on Mars by Raman spectroscopy. *Astrobiology, 15*(9), 761-769.

Mason, D. P., & Madden, M. E. E. (2022). Raman spectroscopy of high salinity brines and ices. *Icarus, 372*, 114759.

McLennan, S. M., Bell, J. F., Calvin, W. M., Christensen, P. R., Clark, B. C., de Souza, P. A., . . . Yen, A. (2005). Provenance and diagenesis of the evaporite-bearing Burns formation, Meridiani Planum, Mars. *Earth and planetary science letters, 240*(1), 95-121. doi:10.1016/j.epsl.2005.09.041

Mermut, A. R., & Cano, A. F. (2001). Baseline Studies of the Clay Minerals Society Source Clays: Chemical Analyses of Major Elements. *Clays and clay minerals, 49*(5), 381-386.

Mermut, A. R., & Lagaly, G. (2001). Baseline Studies of the Clay Minerals Society Source Clays: Layer-Charge Determination and Characteristics of those Minerals Containing 2:1 Layers. *Clays and clay minerals, 49*(5), 393-397. doi:10.1346/CCMN.2001.0490506

Michalski, J. R., & Noe Dobrea, E. Z. (2007). Evidence for a sedimentary origin of clay minerals in the Mawrth Vallis region, Mars. *Geology, 35*(10), 951-954.

Moore, D. M., & Reynolds, R. C., Jr. (1997). *X-Ray Diffraction and the Identification and Analysis of Clay Minerals* (2nd Edition ed.): Oxford University Press.

Murchie, S. L., Bibring, J.-P., Arvidson, R. E., Bishop, J. L., Carter, J., Ehlmann, B. L., . . . Riu, L. (2019). Visible to short-wave Infrared spectral analyses of Mars from orbit using CRISM and OMEGA. *Remote Compositional Analysis: Techniques for understanding spectroscopy, mineralogy, and geochemistry of planetary surfaces*, 453-483.

Nachon, M., Clegg, S., Mangold, N., Schröder, S., Kah, L., Dromart, G., . . . Bridges, J. (2014). Calcium sulfate veins characterized by ChemCam/Curiosity at Gale crater, Mars. *Journal of Geophysical Research: Planets, 119*(9), 1991-2016.

Rampe, E. B., Blake, D. F., Bristow, T., Ming, D. W., Vaniman, D., Morris, R., . . . Tu, V. (2020). Mineralogy and geochemistry of sedimentary rocks and eolian sediments in Gale crater, Mars: A review after six Earth years of exploration with Curiosity. *Geochemistry, 80*(2), 125605.

Schwenzer, S., Abramov, O., Allen, C., Bridges, J., Clifford, S., Filiberto, J., . . . Newsom, H. (2012). Gale Crater: Formation and post-impact hydrous environments. *Planetary and Space Science, 70*(1), 84-95.

Schwenzer, S. P., Bridges, J. C., Wiens, R. C., Conrad, P. G., Kelley, S. P., Leveille, R., . . . Meslin, P. Y. (2016). Fluids during diagenesis and sulfate vein formation in sediments at Gale Crater, Mars. *Meteoritics & planetary science, 51*(11), 2175-2202. doi:10.1111/maps.12668

Singh, S. S. (1982). Effect of chloride and sulfate anions on the chemical characteristics of some acid soils. *Canadian Journal of Soil Science, 62*(4), 549-557.

Singh, S. S., & Turner, R. (1965). Sulphate ions and cation exchange reactions with clays. *Canadian Journal of Soil Science, 45*(3), 271-279.

Slade, P., Quirk, J., & Norrish, K. (1991). Crystalline swelling of smectite samples in concentrated NaCl solutions in relation to layer charge. *Clays and clay minerals, 39*(3), 234-238.

Sposito, G. (1991). Effect of Chloride Ions on Sodium-Calcium and Sodium-Magnesium Exchange on Montmorillonite. *Soil Science Society of America journal, 55*(4), 965-967.

Sposito, G., Holtzclaw, K. M., Charlet, L., Jouany, C., & Page, A. (1983). Sodium-calcium and sodium-magnesium exchange on Wyoming bentonite in perchlorate and chloride background ionic media. *Soil Science Society of America journal, 47*(1), 51-56.

Squyres, S., Arvidson, R., Bell, J. F., Brückner, J., Cabrol, N., Calvin, W., . . . Crumpler, L. (2004). The Opportunity Rover's Athena Science Investigation at Meridiani Planum, Mars. *science, 306*(5702), 1698-1703.

Squyres, S. W., Grotzinger, J. P., Arvidson, R. E., Bell, J. F., Calvin, W. M., Christensen, P. R., . . . Soderblom, L. A. (2004). In situ evidence for an ancient aqueous environment at Meridiani

Planum, Mars. *Science (American Association for the Advancement of Science), 306*(5702), 1709-1714. doi:10.1126/science.1104559

Squyres, S. W., & Knoll, A. H. (2005). Sedimentary rocks at Meridiani Planum: Origin, diagenesis, and implications for life on Mars. *Earth and planetary science letters, 240*(1), 1-10.

Suarez, D., & Zahow, M. (1989). Calcium-Magnesium Exchange Selectivity of Wyoming Montmorillonite in Chloride, Sulfate and Perchlorate Solutions. *Soil Science Society of America journal, 53*(1), 52-57.

Sumner, M. E., & Miller, W. P. (1996). Cation exchange capacity and exchange coefficients. *Methods of soil analysis: Part 3 Chemical methods, 5*, 1201-1229.

Tang, L., & Sparks, D. L. (1993). Cation-exchange kinetics on montmorillonite using pressure-jump relaxation. *Soil Science Society of America journal, 57*(1), 42-46.

Teppen, B. J., & Miller, D. M. (2006). Hydration Energy Determines Isovalent Cation Exchange Selectivity by Clay Minerals. *Soil Science Society of America journal, 70*(1), 31-40. doi:10.2136/sssaj2004.0212

Tu, V., Ming, D., & Sletten, R. (2021). The Mineralogy and Cation Exchange of Sediments in Don Juan Pond, Antarctica Dry Valley: Implications for Mars. *LPI Contributions, 2614*, 6021.

Tu, V. M., Rampe, E. B., Bristow, T. F., Thorpe, M. T., Clark, J. V., Castle, N., . . . Bedford, C. (2021). A Review of the Phyllosilicates in Gale Crater as Detected by the CheMin Instrument on the Mars Science Laboratory, Curiosity Rover. *Minerals, 11*(8), 847.

Vaniman, D., Bish, D., Chipera, S., & Rearick, M. (2011). *Relevance to Mars of cation exchange between nontronite and Mg-sulfate brine.* Paper presented at the Lunar and Planetary Science Conference.

Vaniman, D. T., & Chipera, S. J. (2006). Transformations of Mg- and Ca-sulfate hydrates in Mars regolith. *American Mineralogist, 91*(10), 1628-1642.

Vaniman, D. T., Martínez, G. M., Rampe, E. B., Bristow, T. F., Blake, D. F., Yen, A. S., . . . Morookian, J. M. (2018). Gypsum, bassanite, and anhydrite at Gale crater, Mars. *American Mineralogist: Journal of Earth and Planetary Materials, 103*(7), 1011-1020.

Wang, A., Freeman, J. J., Jolliff, B. L., & Chou, I. M. (2006). Sulfates on Mars: a systematic Raman spectroscopic study of hydration states of magnesium sulfates. *Geochimica et cosmochimica acta, 70*(24), 6118-6135. doi:10.1016/j.gca.2006.05.022

Weitz, C. M., Bishop, J. L., & Grant, J. A. (2013). Gypsum, opal, and fluvial channels within a trough of Noctis Labyrinthus, Mars: Implications for aqueous activity during the Late Hesperian to Amazonian. *Planetary and Space Science, 87*, 130-145.

Weitz, C. M., Bishop, J. L., Thollot, P., Mangold, N., & Roach, L. H. (2011). Diverse mineralogies in two troughs of Noctis Labyrinthus, Mars. *Geology, 39*(10), 899-902.

630 Wilson, S. A., & Bish, D. L. (2011). Formation of gypsum and bassanite by cation exchange
631 reactions in the absence of free-liquid H2O: Implications for Mars. *Journal of Geophysical*
632 *Research: Planets, 116*(E9).

633 Wilson, S. A., & Bish, D. L. (2012). Stability of Mg-sulfate minerals in the presence of
634 smectites: Possible mineralogical controls on H2O cycling and biomarker preservation on
635 Mars. *Geochimica et cosmochimica acta, 96*, 120-133.

636 Wray, J. J., Noe Dobrea, E. Z., Arvidson, R. E., Wiseman, S. M., Squyres, S. W., McEwen, A.
637 S., . . . Murchie, S. L. (2009). Phyllosilicates and sulfates at Endeavour Crater, Meridiani
638 Planum, Mars. *Geophysical research letters, 36*(21), n/a. doi:10.1029/2009GL040734

639 Wray, J. J., Squyres, S. W., Roach, L. H., Bishop, J. L., Mustard, J. F., & Dobrea, E. Z. N.
640 (2010). Identification of the Ca-sulfate bassanite in Mawrth Vallis, Mars. *Icarus, 209*(2),
641 416-421.

642 Zolotov, M. Y., & Mironenko, M. V. (2016). Chemical models for martian weathering profiles:
643 Insights into formation of layered phyllosilicate and sulfate deposits. *Icarus (New York, N.Y.*
644 *1962), 275*, 203-220. doi:10.1016/j.icarus.2016.04.011

Chapter 2. Microscopic Observations of Smectite Cation Exchange in the Absence of Free Water: Implications for the Evolution of Mars Sediments

Christopher Geyer[1], Andrew S. Elwood Madden[1,2], Preston R. Larson[2], Megan Elwood Madden[1]

[1] School of Geosciences, University of Oklahoma, Norman, OK, USA

[2] Samuel Roberts Noble Microscopy Laboratory, University of Oklahoma, Norman, OK, USA

Key Words: cation exchange; clay alteration; mars; scanning electron microscopy

Abstract

Models of cation exchange mechanisms and driving forces have proven effective predictors of clay behavior and chemistry, but are largely theoretical, particularly in complex systems involving high ionic strength brines or systems where hydration is controlled by relative humidity. This study examines the effects of relative humidity on clay-salt mixtures using Environmental Scanning Electron Microscopy to observe the physiochemical effects of salt deliquescence and desiccation on clay textures and elemental distributions. Our results demonstrate that even reaction periods as short as a few minutes allow ample time for relative humidity to affect the clay-salt mixtures. In addition to clay swelling and salt deliquescence, we also observed changes in element distributions within the clay and new crystal growth in the presence of high relative humidity. Even in the absence of bulk liquid water, exchangeable cations migrated out of the clay and formed new crystals at the clay-salt interface. The observed microscopic changes in elemental distributions indicate that the migration of cations and resulting secondary mineral precipitation were likely the result of cation exchange within a sub-micrometer thick layer of water on the clay grains.

1. Introduction

Clays are ubiquitous across Earth and have also been detected on Mars (Ehlmann & Edwards, 2014; Tu et al., 2021b) and other planetary bodies (Ammannito et al., 2016; Rivkin et al., 2006). Clays are also used in many different applications such as environmental remediation and protection, agriculture and manufacturing, and as additives in drilling fluids and paper (Schoonheydt, 2016). Clays are known to react with brines and there are many environments where a complex relationship exists between clays and salts/brines, including evaporitic playa environments (Rosen, 1994) and cold aqueous systems such as Don Juan Pond in Antarctica and sediments on the surface of Mars (Rapin et al., 2019; Schwenzer et al., 2012; Tu et al., 2021a; Wilson et al., 2014). In extremely cold environments, free liquid water is uncommon and increased relative humidity as a result of diurnal or seasonal variations becomes a significant factor when considering water-rock interactions (Polkko et al., 2023). The hygroscopic nature of some salts leads to salt deliquescence during periods of sufficiently elevated relative humidity resulting in interactions between the brines and clays (Brass, 1980; Dickinson & Rosen, 2003; Gough et al., 2014).

While clays, and associated cation exchange reactions, have been the focus of intense study for decades, new technology and techniques allow us to observe previously studied phenomena in new ways. One such application is Environmental Scanning Electron Microscopy (ESEM). ESEM provides a unique opportunity to observe dynamic reactions in almost real time at micrometer to nanometer scales. Fundamentally, ESEM is an extension of Scanning Electron Microscopy (SEM) in which a high level of vacuum is not required within sample chamber (Danilatos, 1988; Goldstein et al., 2018). In addition, the researcher can often control the environmental conditions experienced by the sample including precise control of water vapor

pressure and temperature in the sample chamber. Therefore, ESEM samples also do not experience desiccation as a result of high vacuum and the sample preparation requirements are substantially less complex compared to traditional SEM; in some cases no preparation is required (Baker et al., 1993). While clays are electrically insulating and typically would experience a charging effect inherent in electron microscopy applications, the presence of water vapor in ESEM applications reduces this charging effect, allowing higher resolution imaging of clays without coating. Accessories such as a Peltier cooling stage allow the researcher to modify experimental conditions in-situ. By modifying conditions inside the ESEM chamber, we can conduct dynamic experiments while obtaining high quality microscopic imaging of the reactants and products *in situ*, as the reaction is occurring.

Since the early 1990s, researchers have used ESEM to investigate the effects of relative humidity on clay swelling, including studies focused on analyzing fluid-rock interactions within hydrocarbon reservoirs (Baker et al., 1994; Mehta, 1991; Uwins et al., 1993). Additional studies have examined the effects of clay-water vapor reactions, including efforts to determine the mechanism(s) responsible for damage to ancient Egyptian sculptures stored in a museum. By subjecting sepiolite and palygorskite clays to cyclical wetting and drying cycles, with and without NaCl salt present, Rodriguez-Navarro et al. visually confirmed that swelling at elevated relative humidities was amplified in the presence of NaCl salt (Rodriguez-Navarro et al., 1998).

Most clay studies using ESEM and varying relative humidity have overwhelmingly concentrated on clay swelling (Baker et al., 1994; Carrier et al., 2013; Mehta, 1991; Sun et al., 2019; Uwins et al., 1993). However, in the presence of sorbed water or brine formed via salt deliquescence, cation exchange may also occur. Cation exchange is the process by which cations present in an aqueous solution exchange with labile cations in a clay (Grim, 1968). Acidic

leaching, cation exchange, and limited mass transport due to low water:rock volumes may have also played a significant role in the diagenetic history of Mars (Geyer et al., 2023; Vaniman et al., 2011; Yen et al., 2017). The effects of cation exchange processes on the clay and surrounding sediments largely depends on the specific conditions present. A series of previous studies examined relative humidity cycling of clay-salt mixtures in order to better understand the evolution of Ca- and Mg-sulfate hydrates like those observed on Mars (Vaniman et al., 2011; Vaniman & Chipera, 2006; Vaniman et al., 2018; Wilson & Bish, 2011). The experiments used XRD to detect sulfate mineral changes as a result of varied relative humidity and found that relative humidity cycling not only affected sulfate mineralogy but that the presence of clays also had an influence. Wilson & Bish (2011) attributed the appearance of hydrated Ca-sulfates to cation exchange between deliquesced Mg-sulfate salts and calcium bearing smectite in the absence of free liquid water. While the results of the above-mentioned studies shed light on the relationship between relative humidity and cation exchange, XRD measurements did not allow direct observation of the mechanisms driving cation exchange and subsequent secondary mineral formation at the microscopic level. A conceptual model of angstrom-thick briny films reacting with minerals at both Antarctica and on Mars has been proposed by Dickinson & Rosen (2003). By studying ground-ice which formed as pore or fracture filling in Antarctic soils, they demonstrated that the ground-ice was unlikely a product of meltwater, instead they argued that relative humidity driven deliquescence of salts was likely the source of the ground-ice seen at Dry Valleys, Antarctica. While the study performed by Dickinson & Rosen is supported by bulk chemical analysis and isotopes of ground-ice, as well as static SEM mineral images, direct evidence linking relative humidity and reactions occurring in Antarctic soils is absent (Dickinson & Rosen, 2003).

738 The purpose of this study was to investigate the physiochemical effects of relative humidity
739 on clay-salt mixtures at the microscopic scale using ESEM. Understanding the effects of brine-
740 clay interactions is important for interpreting mineral assemblages and geomorphology formed in
741 extremely cold aqueous environments, including Don Juan Pond and sedimentary systems on
742 Mars. This study addresses the dearth of microscale, in situ observations of cation exchange
743 reactions by examining the effects of relative humidity on clay-salt mixtures via ESEM during
744 temperature-driven humidity cycles.

745 ## 2. Materials & Methods

746 ### 2.1 Experimental Overview

747 In order to evaluate the effects of relative humidity (RH) on clay particles in contact with
748 salts and the potential for cation exchange, we observed samples using ESEM to collect high
749 resolution secondary electron (SE) images and elemental maps of target clay particles before,
750 during, and after a 100% relative humidity (RH) cycle. We conducted preliminary experiments
751 to determine optimal sample quantities and imaging parameters, while also defining equipment
752 limitations. During the preliminary experiments sample quantities were limited to 100 mg so that
753 we could experimentally determine the point at which free liquid water would be formed. In
754 subsequent experiments, sample quantities were increased to 2 g, and the time spent at 100% RH
755 was reduced in order to prevent the formation of free liquid water.

756 We chose montmorillonite “SAz-1” (Apache County, Arizona USA) from the Clay Mineral
757 Society as the clay substrate because it has been extensively characterized (Chipera & Bish,
758 2001; Mermut & Cano, 2001; Mermut & Lagaly, 2001) and allows direct comparison to results
759 in the previous studies (Wilson & Bish, 2011, 2012). SAz-1 is a 2:1 phyllosilicate dioctahedral

760 smectite with a relatively high cation exchange coefficient (CEC) at 123 meq/100g (Borden &
761 Giese, 2001; Essington, 2015). As with many 2:1 phyllosilicates, SAz-1 exhibits remarkable
762 swelling when exposed to water, either as free liquid or vapor. This swelling is the result of
763 water molecules sorbing between two 2:1 layers of the clay; the water molecules may contribute
764 to hydration of interlayer cations and/or be present as discrete layers of water (Grim, 1968;
765 Moore & Reynolds, 1997)

766 To create a consistent starting material, natural SAz-1 was by soaked in saturated $CaCl_2$
767 solution for >24 hours to replace all exchangeable cations with Ca^{2+}. The SAz-1 was then
768 separated from the liquid by three rounds of centrifugation for twenty minutes at 10,000 rpm and
769 rinsed with 18.2 MΩ H_2O, followed by freeze drying and gentle homogenization in a mortar and
770 pestle. The clay was mixed with ACS grade (>99.0% purity) Na_2SO_4 or $MgSO_4$ anhydrous salts
771 in a 1:10 salt:clay mass ratio. To form direct contacts between salt and clay grains as well as
772 minimize air-filled pockets within the sample, we developed a 3D printed sample press. The
773 custom sample press allowed uniform compression of the sample while conforming to the
774 dimensions of the sample cup; by pressing the air out of the sample during sample preparation,
775 minimal decompression occurred during the initial vacuum conditions inside the ESEM sample
776 chamber. In addition, the sample press produced a relatively flat surface on the sample which
777 made it significantly easier to image the sample in the microscope. After the sample was mixed
778 and pressed the sample was immediately loaded into the ESEM chamber.

779 Sodium and Mg- sulfate salts were chosen because 1) they have been observed on Mars
780 (Hecht et al., 2009) and 2) the deliquescence points of both are well known and is within the
781 range of relative humidity observed on present day mars. Therefore, they may have served an
782 important role in Martian rheological and diagenetic processes (Brass, 1980; Möhlmann &

783 Thomsen, 2011; Vaniman et al., 2004). Using two different salts also allowed us to compare the
784 effects of cation chemistry on deliquescence and cation exchange behavior. Generally, for
785 electrolyte solutions with low cation concentrations mixed with montmorillonite, cation
786 selectivity preferences of montmorillonite follow $Ca^{2+} > Mg^{2+} > Na^{+}$; where Ca^{2+} is retained in
787 the clay interlayer most strongly and Na^{+}, being the weakest is not retained in the clay (Appelo &
788 Postma, 2004; Sposito et al., 1983a; Tang & Sparks, 1993). However, when the electrolyte
789 solution is not dilute, but instead the cation in solution is in such high concentration as to be
790 considered near-infinite, clay cation selectivity plays a less significant role. Instead, the dominant
791 influence of which cation is adsorbed in the clay interlayer is controlled by the law of mass
792 action. If for example a Ca^{2+} saturated montmorillonite were mixed with a near-saturated Na_2SO_4
793 solution, then some of the adsorbed Ca^{2+} cations would exchange with the Na^{+} cations in
794 solution (Sposito et al., 1983b). Following the exchange, the Ca^{2+}, now in solution, could
795 complex with the available SO_4^{2-} potentially leading to precipitation of calcium sulfate minerals
796 such as gypsum ($CaSO_4 \cdot 2H_2O$), basanite ($CaSO_4 \cdot \frac{1}{2}H_2O$) and anhydrite ($CaSO_4$).

797 **2.2 Scanning Electron Microscopy**

798 Imaging and analysis were accomplished using a ThermoFisher Scientific Quattro S field
799 emission ESEM with a 20 kV accelerating voltage and a probe current of 4.1mA; working
800 distance varied depending on vacuum conditions. High resolution SE images were collected at a
801 chamber pressure of 70 Pa with a Gaseous Secondary Electron Detector operating in the
802 secondary electron mode. Elemental analysis and mapping were accomplished using Energy
803 Dispersive X-ray Spectroscopy (EDS) in both high vacuum and low vacuum ESEM conditions.
804 Relative humidity (RH) within the chamber was controlled by holding the chamber water vapor
805 pressure constant at 800 Pa and cooling or heating the sample to a target temperature using a

Peltier cold stage. The target temperature for a desired RH% was determined using the Antoine equation with updated parameters (NIST; Wood, 1970). Starting RH was ~3% and was increased to 100% RH over a period of thirty minutes, 100% RH was maintained for one hour followed by a ramp back to ~3% RH over thirty minutes. Three percent RH was chosen as the starting RH because this RH could be easily maintained in high vacuum mode, allowing high resolution imaging and X-ray analysis prior to and after exposure to 100% RH. In some cases, images of the clay particles are only presented after the RH ramp due to movement of the sample and loss of the original location.

3. Results

3.1 Initial Clay Characterization

The SAz-1 starting material was fine grained with aggregates of clay particles averaging between 5-12 μm in diameter (Fig. 1). EDS elemental mapping prior to reaction confirms that calcium was homogeneously distributed throughout the starting material. Magnesium is also abundant in Saz-1, likely in the octahedral layer as noted elsewhere (Essington, 2015; Mermut & Cano, 2001; Moore & Reynolds, 1997) (Fig. 2).

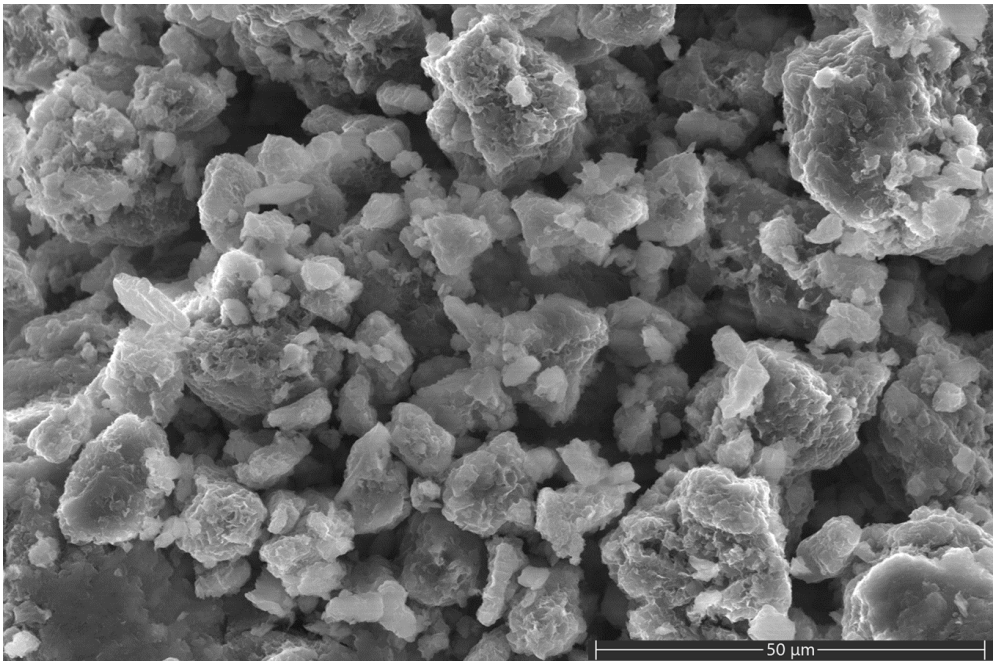

Figure 4. SE image of the unaltered montmorillonite starting material.

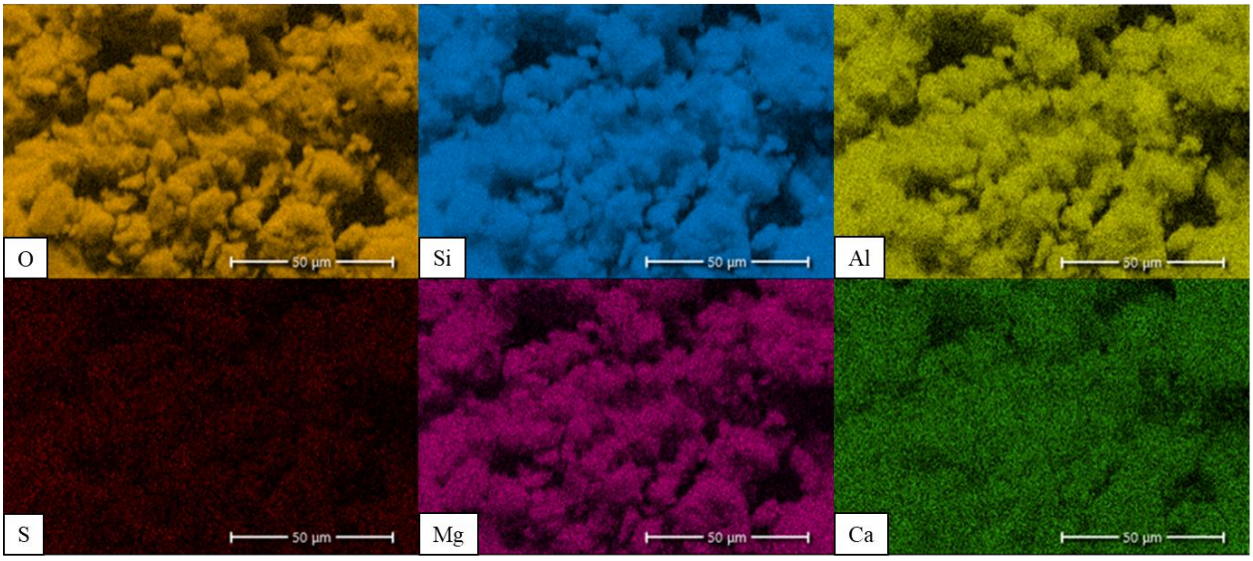

Figure 5. Colorized EDS X-ray maps of the unaltered montmorillonite under initial conditions, from the same area as Fig. 1. Color intensity is proportional to the concentration of the indicated element at each pixel (Sodium and iron also detected but not shown).

827 **3.2 Preliminary Experiment**

828 A preliminary test was conducted to determine optimal sample conditions as well as identify
829 the potential impact of equipment limitations. In the preliminary experiment we used ~100 mg of
830 Na_2SO_4 salt + clay to test the hypothesis that elevated RH within the instrument chamber would
831 produce free bulk water in contact with the sample.

832 As expected, one of the most recognizable processes observed during the relative humidity
833 cycling was clay swelling. In every experiment we conducted, Saz-1 swelled as relative humidity
834 increased and shrank as relative humidity decreased. Below 25% RH no clay volumetric changes
835 were observed; we attribute any apparent sample shifting at <25% RH to thermal equilibration.
836 Once RH increased beyond 25% clay particles began to swell and shift. While the clay particles
837 equilibrated quickly (<30 seconds) at any given RH, the salt crystals took much longer to
838 equilibrate. In many cases, it took >2 minutes for salt crystals to become visibly affected by the
839 humidity, though the time was highly dependent on the volume of the salt crystals.

840 Secondary electron images were collected throughout the hydration-dehydration cycles. In
841 Figure 3a the sample was equilibrated at 25% RH and no bulk liquid water was observed. As the
842 salt crystal equilibrates at 100% RH, roughening of the terrace surfaces becomes apparent (Fig.
843 3b), then as RH was held constant at 100% a uniform layer of liquid forms first on the Na_2SO_4
844 surfaces and eventually engulfs the clay particles as shown in Figure 3c. The bulbous, nodular
845 shapes shown on the Na_2SO_4 crystal face in Figure 3c are interpreted as a homogeneous water
846 layer rather than a solid. As the RH increased, the nodules grew laterally and vertically like a
847 film. Eventually this nodular film grew to the point where it came into visible contact with the
848 clay grains and began to cover them. Finally, as RH was brought back down to 25% the film
849 covering the surfaces shrinks in a similar manner as the growth stage, but in reverse as RH

decreased. The remaining bulk liquid water flash evaporated or co-precipitated at a point between 28% RH and 24% RH, leaving behind a network of nano- to microscale material which likely formed from widespread dissolution-precipitation (Fig. 3d).

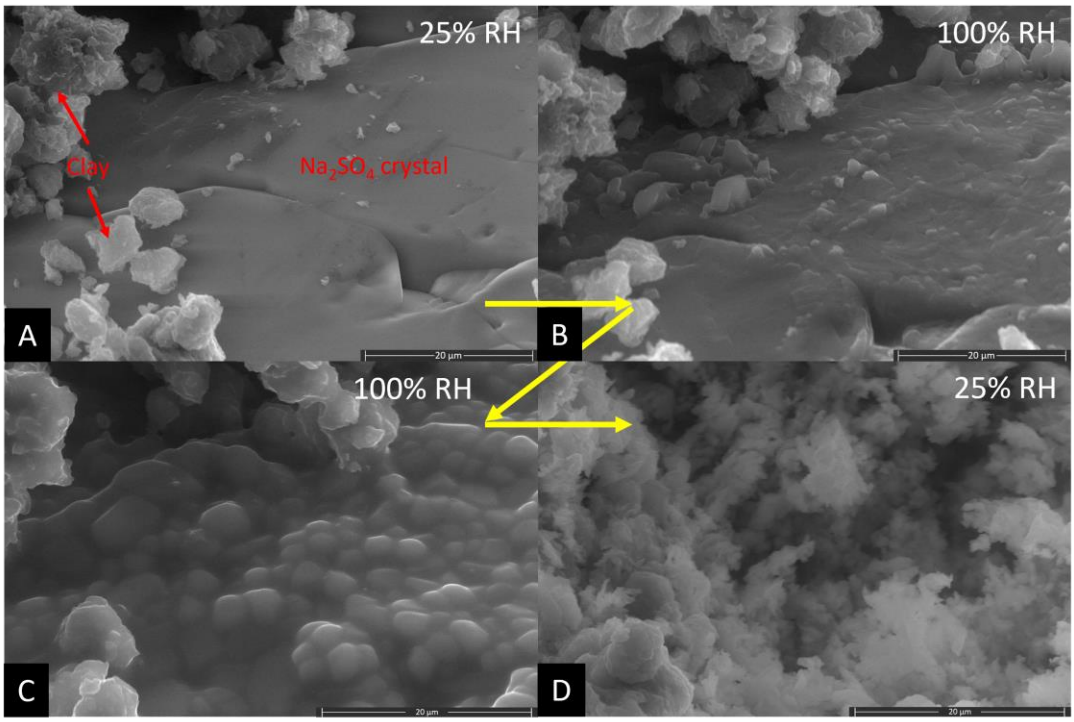

Figure 3. SAz-1 on a Na_2SO_4 crystal imaged through one humidity cycle. A) 25% RH prior to exposure to elevated RH. B) 100% RH after 30 minutes, observable clay swelling and increased surface roughness of the Na_2SO_4 crystal face. C) 100% RH after 2.5 hours, clay swelling has ceased, yet clear edges and particle shapes were maintained in the clay particles. No distinct features of the Na_2SO_4 crystal remain. Instead the salt is covered with a bulbous, nodular film. D) Return to 25% RH after 2.5 hours at 100% RH, a network of nano-micro scale crystals appeared, no further changes were observed after return to 3% RH.

It is important to note the presence of a thick layer of bulbous material, that we interpret as bulk liquid water, visible in Figure 3c. We hypothesize that the low sample volume and extended

863 time at 100% RH in the preliminary experiment allowed a layer of bulk water to accumulate.
864 However, in subsequent experiments no bulk water was observed, likely due to the larger sample
865 volumes and reduced time spent at 100% RH. These subsequent experiments were performed
866 using fresh, unreacted salt-clay mixtures.

867 **3.3 Na-Sulfate Experiments in the Absence of Bulk Water**

868 We identified a clear area with clay particles or isolated aggregates in contact with a Na_2SO_4
869 crystal to study clay-salt interactions *in situ* (Fig. 4). The Na_2SO_4 crystal and clay composition
870 were confirmed using EDS and detailed images collected before and after exposure to 100% RH
871 (Target Grain 1 - "TG1", Fig. 4, 5 & 6). As humidity increased to 100% RH, we observed
872 significant lateral and vertical motion of the sample, which we interpret as clay swelling due to
873 increasing hydration of the interlayer. However, at no point during the relative humidity cycle
874 was liquid water observed, even at 100% RH. We did observe significant alteration of both the
875 salt and clay, most notable was the formation of a salt dissolution pit which formed around a clay
876 particle shown in Figure 4b.

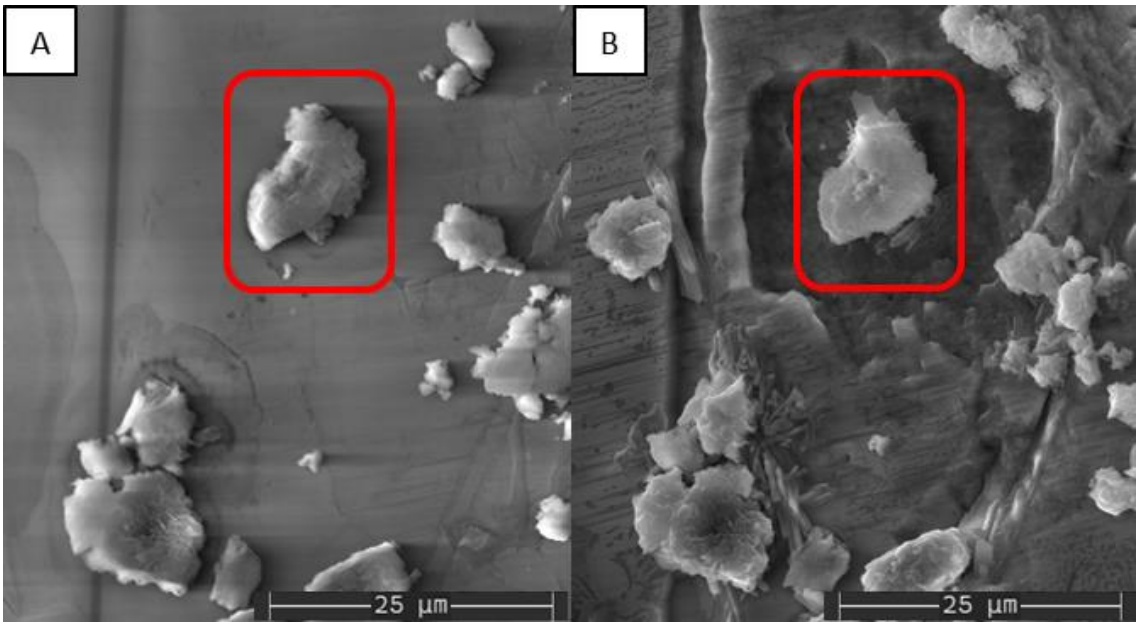

Figure 4. SE images of the target site consisting of montmorillonite clay clumps laying on top of a Na_2SO_4 crystal face, red box in both A & B highlighting TG1. A) Initial conditions. B) After exposure to 100% RH, severe dissolution etching and crystal formation were observed.

After exposing the sample to 100% RH and then reducing RH back to ~3%, new crystals appeared where montmorillonite particles were in contact with the Na_2SO_4 salt. It is worth noting that the new crystals only occurred where the montmorillonite was in direct contact with the salt; portions of the montmorillonite which were physically distant from the salt showed no signs of crystal nucleation or alteration other than residual swelling (Fig. 5). Large portions of the Na_2SO_4 crystal face also appeared to have been etched, particularly around TG1, but also around some of the other montmorillonite grains. One particularly notable dissolution pit surrounding TG1 has an indentation which mirrors the growth of the crystal attached to TG1 (just above the red rectangle in Fig. 4b). Additionally, the vertical topographic trench that crosses vertically through the field of view is visibly wider after 100% RH exposure.

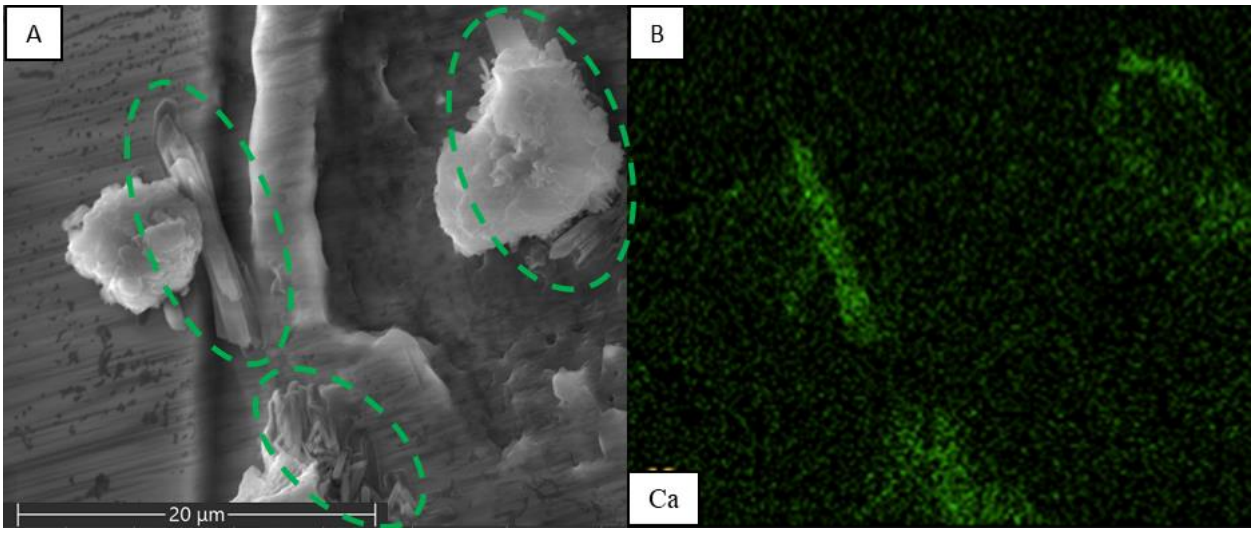

Figure 5. Close up of new crystals depicted in Fig. 4b, TG1 present at top right of both images. A) SE image, green dashed ovals indicate new crystals. B) Color EDS image of calcium for the same area as Figure 4a. Note the presence of SAz-1 grains visible in the SE image but undetectable by Ca EDS.

In addition to evidence of etching and dissolution, new crystals also appeared after exposure to 100% RH. These new crystals exhibit completely different crystal habit relative to the Na_2SO_4 salt and also have a different chemical composition. EDS elemental mapping (Fig. 6) shows before and after element maps of TG1. Prior to the 100% RH ramp calcium is homogeneously distributed in TG1, however after reaching 100% RH the calcium appears to migrate from the center of the clay to the new crystals which formed at the contact between the clay and the Na_2SO_4 crystal. Unfortunately, crystal nucleation and growth occurred too rapidly to directly capture images of growth dynamics.

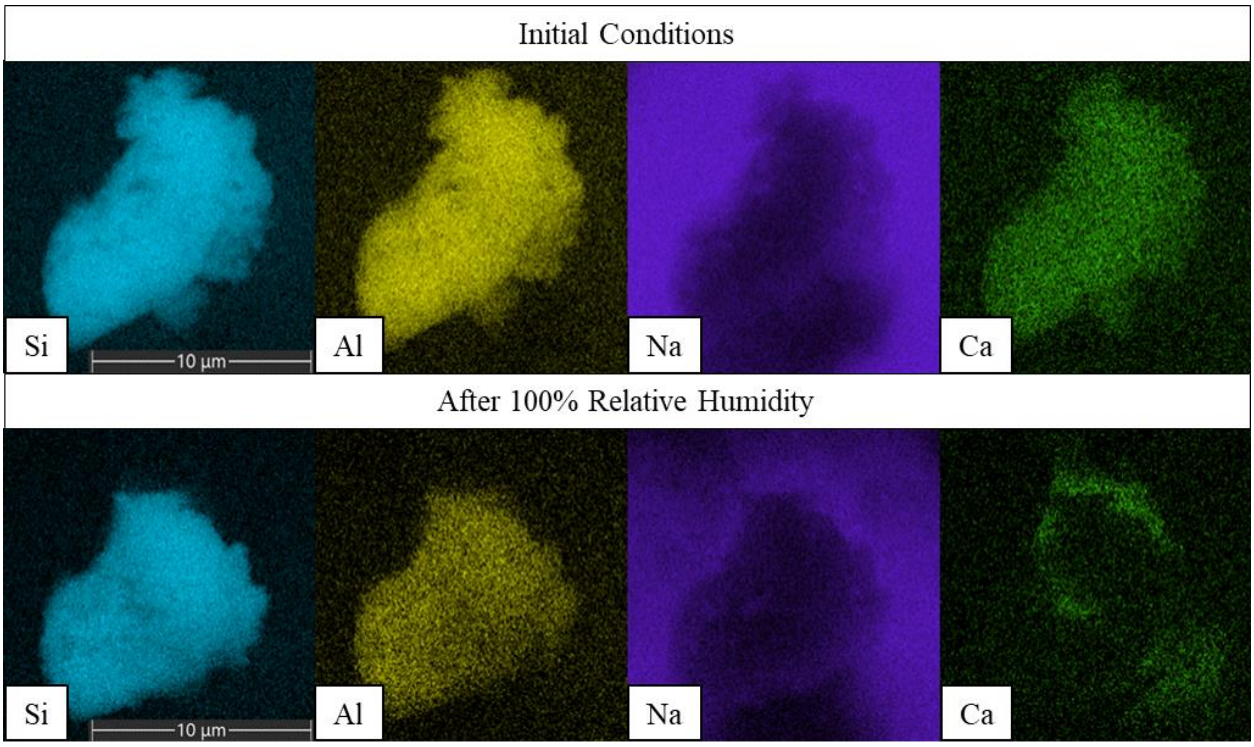

Figure 6. Calcium migration observed by comparing before and after color EDS mapping of TG1. The top row of images were collected prior to 100% RH, the bottom row images were collected after the sample was exposed to 100% RH and returned to ~3% RH.

Clay grains which were isolated away from the Na_2SO_4 did not produce new crystals and the calcium distribution remained homogenous throughout the experiment (Fig. 7). However, these isolated montmorillonite clumps also exhibited signs of swelling.

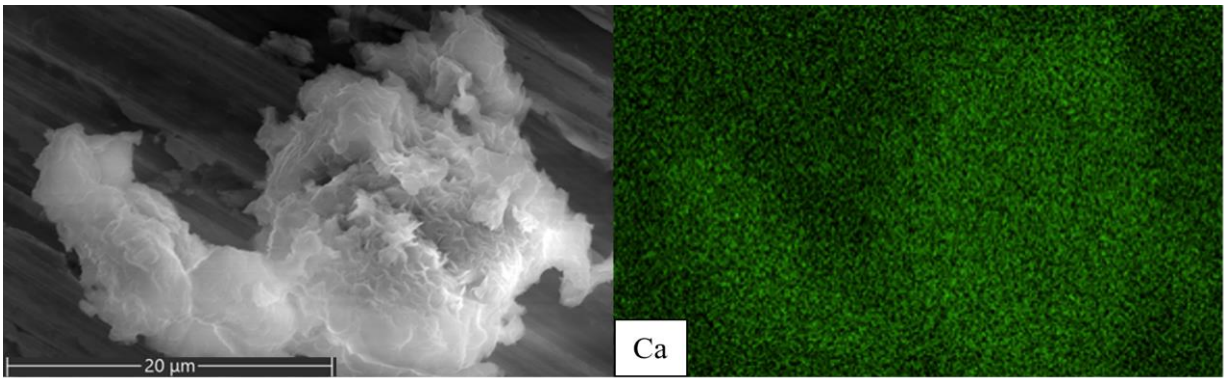

Figure 7. An isolated montmorillonite grain located on aluminum sample holder wall away from any Na_2SO_4 salt. SE image (left) and colour EDS – calcium image (right) collected after the grain was exposed to 100% RH- note the homogeneous distribution of Ca in the sample.

3.4 $MgSO_4$ -clay interactions

When the clay was mixed with $MgSO_4$, changes similar to those observed in the clay + Na_2SO_4, experiments occurred. However, in the $MgSO_4$ experiments, greater movement of the clay-salt mixture occurred as the relative humidity decreased. This prevented the collection of images and elemental maps directly comparing the same particle with initial conditions. Luckily, clay grains which had been in contact with salt crystals during the RH cycle were ubiquitous, allowing interpretation of reactions which occurred as a result of exposure to elevated relative humidity.

We again identified a study area with a target grain "TG2" which was in direct contact with the $MgSO_4$ and collected EDS elemental maps and images before and after RH cycling. Similar to the Na_2SO_4 experiments, we observed formation of blade-like crystals that contain high concentrations of Ca and S, but do not contain abundant Al or Si, indicating that newly formed calcium rich crystals are related to, but not part of, the clay matrix (Fig. 8 & Fig. 9).

928 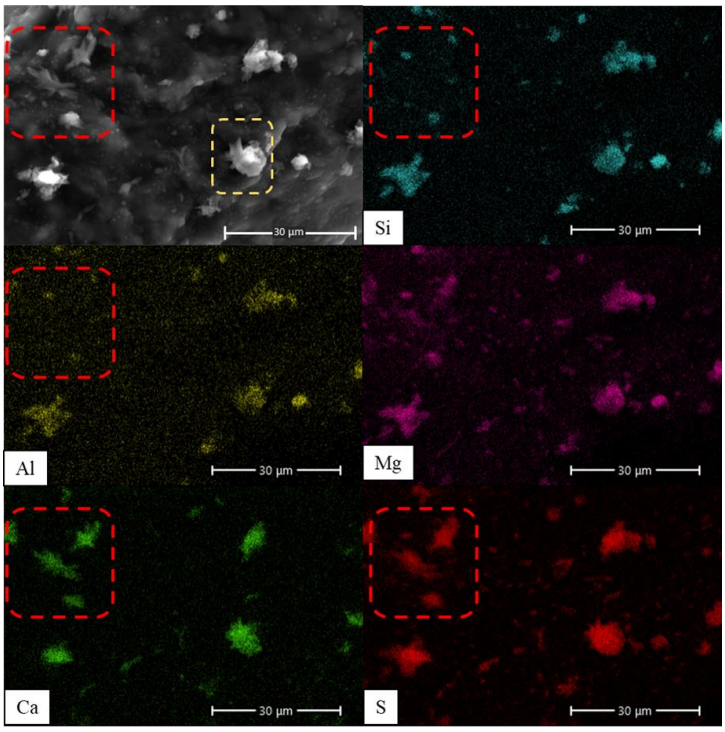

929 **Figure 8.** Elemental distributions in SAz-1 + $MgSO_4$ after one RH cycle. The red dashed boxes
930 highlight crystals which exhibit colocalized Ca and S, but are lacking in Al or Si. Yellow dashed
931 box in the SE image highlights TG2 shown in Fig. 9.

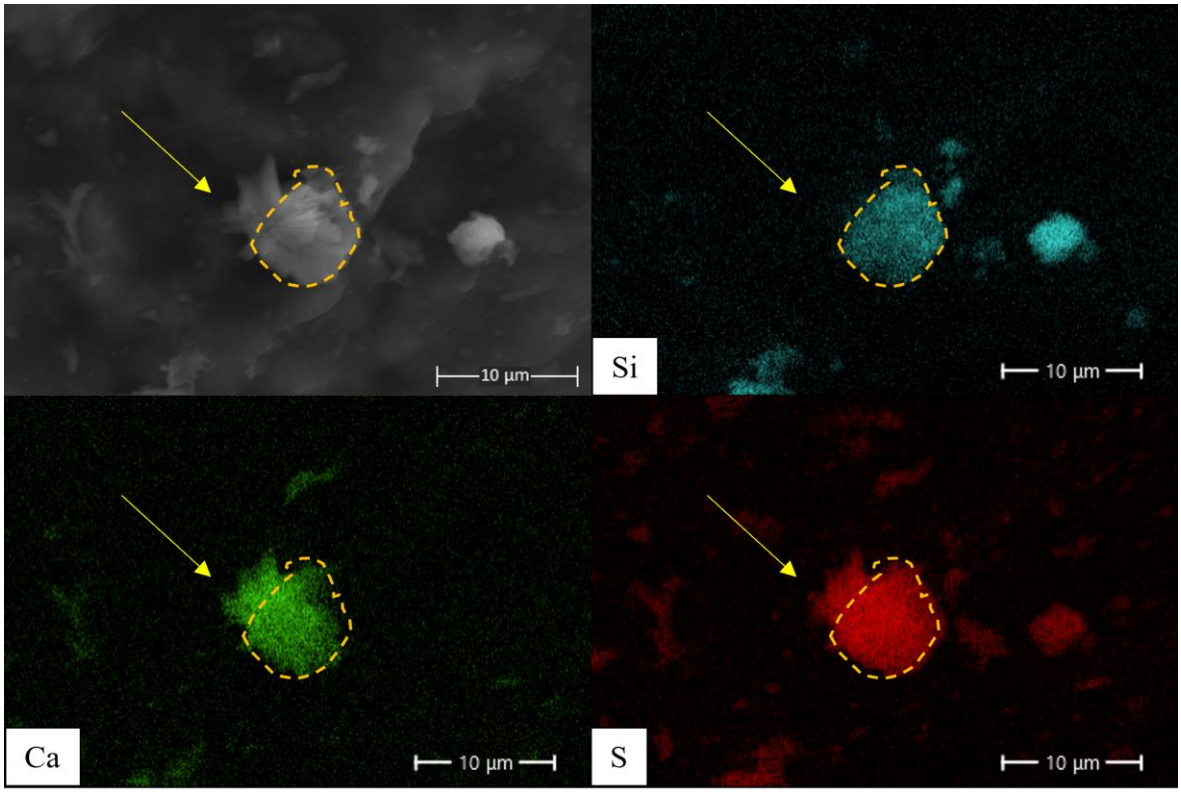

Figure 9. Close up on TG2 showing differences in elemental distribution, yellow arrows indicate the location of crystals on the upper left of the particle, visible in SE, that contain abundant Ca and S based on the EDS maps, but are absent in the Si EDS map. The yellow dashed polygon outlines the clay grain as defined by the Si EDS map.

4. Discussion

4.1 Cation Exchange & Elemental Migration

In both the Na_2SO_4 and $MgSO_4$ experiments, we observed calcium appeared to be concentrated in new crystals observed adjacent to clay grains (Fig. 5 & 9), but only when the clay grains were in contact with salt crystals. We also observed that calcium was homogeneously distributed within clay grains prior to the relative humidity cycles with salts present (Fig. 2), while after the cycle Ca was no longer homogeneously distributed within the clay grain (Fig. 6 &

9). This migration of calcium coincides with a colocalized concentration of sulfur (Fig. 8 & 9), likely due to growth of calcium sulfate crystals at the interface between the salt and the clay grains. Similar calcium sulfate precipitation has been previously observed in XRD experiments investigating clay-salt interactions during relative humidity changes (Wilson & Bish, 2011, 2012). Based on this colocalization of S and Ca, we interpret that the sulfate salts deliquesced forming a sub-micrometer layer of brine that facilitated cation exchange with the Ca^{2+} present in the clay interlayers. The release of Ca^{2+} from the clay interlayers resulted in saturation and precipitation of calcium sulfate. Element migration with no liquid water observable, even at the sub-micrometer scale, also corroborates the work of Wilson & Bish (2011) that indicated cation exchange can occur even within a molecular-scale surficial water layer.

5. Applications on Mars

Recurring slope lineae (RSL) observed on Mars as well as water tracks seen at Don Juan Pond, may not only be indicative of fluid transport but also chemical alteration, albeit on a microscopic scale. While hypotheses differ regarding the cause(s) of RSL, a common explanation is the deliquescence of salts during periods of high relative humidity (Dickson et al., 2013; Gough et al., 2017). Studies examining the water source for Don Juan Pond concluded that flows similar to recurring slope lineae (RSL) observed on Mars are likely due to the relative humidity controlled deliquescence of salts (Dickson et al., 2013; Gough et al., 2017). Tu et al. (2021) found that the presence of elevated Ca^{2+} concentrations in brines at Don Juan Pond is also likely due to cation exchange. When exposed to solutions with sufficient Na^{+} concentrations, the clay will release Ca^{2+} in exchange for Na^{+} (McBride, 1980; Toner & Sletten, 2013; Tu et al., 2021a), even though the clays present at that location would theoretically retain Ca^{2+} preferentially to Na^{+}.

A common contention to the briny RSL origin hypothesis is that RSL do not correlate perfectly with conditions conducive to the presence of liquid water (see McEwen et al., 2011; Toner et al., 2022 and references therein for a review). Toner et al (2022) argues against cation exchange as the mechanism for RSL at both Don Juan Pond and on Mars due to the preferential adsorption of Ca^{2+} by clays when exposed to dilute solutions containing the cations in question. However, as demonstrated by the result in this study, when brine formation is initiated by deliquescence of salts controlled by relative humidity, calcium can migrate out of the clay interlayer via cation exchange and even mass transport is possible, albeit on a microscopic scale.

The occurrence of cation exchange outside typical boundary conditions that assume bulk liquid water must be present, brings with it the realization that Martian sediments may in fact be undergoing active diagenesis at the microscopic scale, even under traditionally "dry" conditions. For example, hydrated salts have been detected at several RSL locations on Mars (Ojha et al., 2015). Heinz et al. (2016) observed that a Mars analogue soil, when exposed to elevated RH, would only show darkening similar to RSL if salts were present and permitted to deliquesce (Heinz et al., 2016). Thus observations of RSL on Mars suggests chemical alteration may be occurring on diurnal and seasonal time scales. Similarly, cation exchange in high salinity fluids may also have contributed to high calcium sulfate concentrations observed across Mars soils, including Ca-sulfate-rich veins (McLennan et al., 2014; Rampe et al., 2020). The elemental composition of sediments at Gale crater suggests limited chemical transport and low water:rock volumes (Bristow et al., 2015); these observations are consistent with the hypothesis that cation exchange played a major role in the formation of the Ca-sulfate minerals.

6. Conclusions

ESEM allows us to observe how minerals are altered or formed as a direct result of exposure to elevated RH. The results of this study include a before and after set of SE and elemental images which document the dissolution of salt in the absence of free liquid water which corresponds with elemental migration consistent with cation exchange between a brine and clay grains. New crystal formation observed in SE images is further distinguished by colocated concentrations of calcium and sulfur observed in elemental EDS maps, suggesting the formation of a Ca-sulfate-rich phase. In the case of both Na_2SO_4 and $MgSO_4$ salts, after a single RH cycle, clay grains which had been saturated with calcium and were in direct physical contact with salt grains no longer exhibit a homogeneous calcium distribution. Instead, calcium appears to migrate to the edge of the grain and into the newly formed crystals. The results of this study provide evidence that sub-micrometer thick layers of brine formed by salt deliquescence can facilitate cation exchange and subsequent mineral formation in extreme environments such as Antarctica or Mars.

Acknowledgements

This project was funded by the University of Oklahoma and NASA Solar System Workings grant 80NSSC23K0037.

References

Ammannito, E., DeSanctis, M., Ciarniello, M., Frigeri, A., Carrozzo, F., Combe, J.-P., . . . Raponi, A. (2016). Distribution of phyllosilicates on the surface of Ceres. *science, 353*(6303), aaf4279.

Appelo, C. A. J., & Postma, D. (2004). *Geochemistry, groundwater and pollution*: CRC press.

Baker, J., Uwins, P., & Mackinnon, I. D. (1993). ESEM study of illite/smectite freshwater sensitivity in sandstone reservoirs. *Journal of Petroleum Science and Engineering, 9*(2), 83-94.

Baker, J., Uwins, P., & Mackinnon, I. D. (1994). Freshwater sensitivity of corrensite and chlorite/smectite in hydrocarbon reservoirs—an ESEM study. *Journal of Petroleum Science and Engineering, 11*(3), 241-247.

Borden, D., & Giese, R. (2001). Baseline studies of the clay minerals society source clays: cation exchange capacity measurements by the ammonia-electrode method. *Clays and clay minerals, 49*(5), 444-445.

Brass, G. W. (1980). Stability of brines on Mars. *Icarus (New York, N.Y. 1962), 42*(1), 20-28. doi:10.1016/0019-1035(80)90237-7

Bristow, T. F., Bish, D. L., Vaniman, D. T., Morris, R. V., Blake, D. F., Grotzinger, J. P., . . . Ming, D. W. (2015). The origin and implications of clay minerals from Yellowknife Bay, Gale crater, Mars. *American Mineralogist, 100*(4), 824-836.

Carrier, B., Wang, L., Vandamme, M., Pellenq, R. J.-M., Bornert, M., Tanguy, A., & Van Damme, H. (2013). ESEM study of the humidity-induced swelling of clay film. *Langmuir, 29*(41), 12823-12833.

Chipera, S. J., & Bish, D. L. (2001). Baseline Studies of the Clay Minerals Society Source Clays: Powder X-ray Diffraction Analyses. *Clays and clay minerals, 49*(5), 398-409. doi:10.1346/CCMN.2001.0490507

Danilatos, G. (1988). Foundations of environmental scanning electron microscopy. In *Advances in electronics and electron physics* (Vol. 71, pp. 109-250): Elsevier.

Dickinson, W. W., & Rosen, M. R. (2003). Antarctic permafrost: An analogue for water and diagenetic minerals on Mars. *Geology, 31*(3), 199-202.

Dickson, J. L., Head, J. W., Levy, J. S., & Marchant, D. R. (2013). Don Juan Pond, Antarctica: near-surface CaCl2-brine feeding Earth's most saline lake and implications for Mars. *Scientific Reports, 3*(1), 1-8.

Ehlmann, B. L., & Edwards, C. S. (2014). Mineralogy of the Martian Surface. *Annual Review of Earth and Planetary Sciences, 42*(1), 291-315. doi:10.1146/annurev-earth-060313-055024

Essington, M. E. (2015). *Soil and water chemistry: an integrative approach*: CRC press.

Geyer, C., Madden, A. S. E., Rodriguez, A., Bishop, J. L., Mason, D., & Madden, M. E. (2023). The Role of Sulfate in Cation Exchange Reactions: Applications to Clay–Brine Interactions on Mars. *The Planetary Science Journal, 4*(3), 48.

Goldstein, J. I., Newbury, D. E., Michael, J. R., Ritchie, N. W., Scott, J. H. J., Joy, D. C., . . . Ritchie, N. W. (2018). Attempting Electron-Excited X-Ray Microanalysis in the Variable Pressure Scanning Electron Microscope (VPSEM). *Scanning Electron Microscopy and X-Ray Microanalysis*, 441-459.

Gough, R., Chevrier, V., & Tolbert, M. (2014). Formation of aqueous solutions on Mars via deliquescence of chloride–perchlorate binary mixtures. *Earth and Planetary Science Letters, 393*, 73-82.

Gough, R., Wong, J., Dickson, J., Levy, J., Head, J., Marchant, D., & Tolbert, M. (2017). Brine formation via deliquescence by salts found near Don Juan Pond, Antarctica: Laboratory experiments and field observational results. *Earth and Planetary Science Letters, 476*, 189-198.

Grim, R. E. (1968). *Clay Mineralogy* (2nd ed.): McGraw-Hill.

Hecht, M. H., Kounaves, S. P., Quinn, R., West, S. J., Young, S. M., Ming, D. W., . . . Hoffman, J. (2009). Detection of perchlorate and the soluble chemistry of martian soil at the Phoenix lander site. *science, 325*(5936), 64-67.

Heinz, J., Schulze-Makuch, D., & Kounaves, S. P. (2016). Deliquescence-induced wetting and RSL-like darkening of a Mars analogue soil containing various perchlorate and chloride salts. *Geophysical Research Letters, 43*(10), 4880-4884.

McBride, M. (1980). Interpretation of the variability of selectivity coefficients for exchange between ions of unequal charge on smectites. *Clays and clay minerals, 28*, 255-261.

McEwen, A. S., Ojha, L., Dundas, C. M., Mattson, S. S., Byrne, S., Wray, J. J., . . . Gulick, V. C. (2011). Seasonal flows on warm Martian slopes. *science, 333*(6043), 740-743.

McLennan, S. M., Anderson, R., Bell III, J., Bridges, J. C., Calef III, F., Campbell, J. L., . . . Cousin, A. (2014). Elemental geochemistry of sedimentary rocks at Yellowknife Bay, Gale crater, Mars. *science, 343*(6169), 1244734.

Mehta, S. (1991). *Imaging of wet specimens in their natural state using environmental scanning electron microscope (ESEM): some examples of importance to petroleum technology.* Paper presented at the SPE Annual Technical Conference and Exhibition?

Mermut, A. R., & Cano, A. F. (2001). Baseline Studies of the Clay Minerals Society Source Clays: Chemical Analyses of Major Elements. *Clays and clay minerals, 49*(5), 381-386.

Mermut, A. R., & Lagaly, G. (2001). Baseline Studies of the Clay Minerals Society Source Clays: Layer-Charge Determination and Characteristics of those Minerals Containing 2:1 Layers. *Clays and clay minerals, 49*(5), 393-397. doi:10.1346/CCMN.2001.0490506

Möhlmann, D., & Thomsen, K. (2011). Properties of cryobrines on Mars. *Icarus, 212*(1), 123-130.

Moore, D. M., & Reynolds, R. C., Jr. (1997). *X-Ray Diffraction and the Identification and Analysis of Clay Minerals* (2nd Edition ed.): Oxford University Press.

NIST. NIST Chemistry WebBook, SRD 69 - Water. Retrieved from https://webbook.nist.gov/cgi/cbook.cgi?ID=C7732185&Units=SI&Type=ANTOINE&Plot=on

Ojha, L., Wilhelm, M. B., Murchie, S. L., McEwen, A. S., Wray, J. J., Hanley, J., . . . Chojnacki, M. (2015). Spectral evidence for hydrated salts in recurring slope lineae on Mars. *Nature Geoscience, 8*(11), 829-832.

Polkko, J., Hieta, M., Harri, A. M., Tamppari, L., Martínez, G., Viúdez-Moreiras, D., . . . De La Torre Juarez, M. (2023). Initial results of the relative humidity observations by MEDA instrument onboard the Mars 2020 Perseverance Rover. *Journal of Geophysical Research: Planets, 128*(2), e2022JE007447.

Rampe, E. B., Blake, D. F., Bristow, T., Ming, D. W., Vaniman, D., Morris, R., . . . Tu, V. (2020). Mineralogy and geochemistry of sedimentary rocks and eolian sediments in Gale crater, Mars: A review after six Earth years of exploration with Curiosity. *Geochemistry, 80*(2), 125605.

Rapin, W., Ehlmann, B. L., Dromart, G., Schieber, J., Thomas, N., Fischer, W. W., . . . Clark, B. C. (2019). An interval of high salinity in ancient Gale crater lake on Mars. *Nature Geoscience, 12*(11), 889-895.

Rivkin, A., Volquardsen, E., & Clark, B. (2006). The surface composition of Ceres: Discovery of carbonates and iron-rich clays. *Icarus, 185*(2), 563-567.

Rodriguez-Navarro, C., Sebastian, E., Doehne, E., & Ginell, W. S. (1998). The role of sepiolite-palygorskite in the decay of ancient Egyptian limestone sculptures. *Clays and clay minerals, 46*, 414-422.

Rosen, M. R. (1994). The importance of groundwater in playas: a review of playa classifications and the sedimentology and hydrology of playas.

Schoonheydt, R. A. (2016). Reflections on the material science of clay minerals. *Applied Clay Science, 131*, 107-112.

Schwenzer, S., Abramov, O., Allen, C., Bridges, J., Clifford, S., Filiberto, J., . . . Newsom, H. (2012). Gale Crater: Formation and post-impact hydrous environments. *Planetary and Space Science, 70*(1), 84-95.

Sposito, G., Holtzclaw, K. M., Charlet, L., Jouany, C., & Page, A. (1983a). Sodium-calcium and sodium-magnesium exchange on Wyoming bentonite in perchlorate and chloride background ionic media. *Soil Science Society of America Journal, 47*(1), 51-56.

Sposito, G., Holtzclaw, K. M., Jouany, C., & Charlet, L. (1983b). Cation selectivity in sodium-calcium, sodium-magnesium, and calcium-magnesium exchange on Wyoming bentonite at 298 K. *Soil Science Society of America Journal, 47*(5), 917-921.

Sun, H., Mašín, D., Najser, J., Neděla, V., & Navrátilová, E. (2019). Bentonite microstructure and saturation evolution in wetting–drying cycles evaluated using ESEM, MIP and WRC measurements. *Géotechnique, 69*(8), 713-726.

Tang, L., & Sparks, D. L. (1993). Cation-exchange kinetics on montmorillonite using pressure-jump relaxation. *Soil Science Society of America Journal, 57*(1), 42-46.

Toner, J., Sletten, R., Liu, L., Catling, D., Ming, D., Mushkin, A., & Lin, P.-C. (2022). Wet streaks in the McMurdo Dry Valleys, Antarctica: Implications for Recurring Slope Lineae on Mars. *Earth and Planetary Science Letters, 589*, 117582.

Toner, J. D., & Sletten, R. S. (2013). The formation of Ca-Cl-rich groundwaters in the Dry Valleys of Antarctica: Field measurements and modeling of reactive transport. *Geochimica et cosmochimica acta, 110*, 84-105.

Tu, V. M., Ming, D., & Sletten, R. (2021a). The Mineralogy and Cation Exchange of Sediments in Don Juan Pond, Antarctica Dry Valley: Implications for Mars. *LPI Contributions, 2614*, 6021.

Tu, V. M., Rampe, E. B., Bristow, T. F., Thorpe, M. T., Clark, J. V., Castle, N., . . . Bedford, C. (2021b). A review of the phyllosilicates in Gale Crater as detected by the CheMin instrument on the Mars Science Laboratory, Curiosity rover. *Minerals, 11*(8), 847.

Uwins, P. J., Baker, J. C., & Mackinnon, I. D. (1993). Imaging fluid/solid interactions in hydrocarbon reservoir rocks. *Microscopy research and technique, 25*(5-6), 465-473.

Vaniman, D., Bish, D., Chipera, S., & Rearick, M. (2011). *Relevance to Mars of cation exchange between nontronite and Mg-sulfate brine.* Paper presented at the Lunar and Planetary Science Conference.

Vaniman, D. T., Bish, D. L., Chipera, S. J., Fialips, C. I., William Carey, J., & Feldman, W. C. (2004). Magnesium sulphate salts and the history of water on Mars. *Nature, 431*(7009), 663-665.

Vaniman, D. T., & Chipera, S. J. (2006). Transformations of Mg- and Ca-sulfate hydrates in Mars regolith. *American Mineralogist, 91*(10), 1628-1642.

Vaniman, D. T., Martínez, G. M., Rampe, E. B., Bristow, T. F., Blake, D. F., Yen, A. S., . . . Morookian, J. M. (2018). Gypsum, bassanite, and anhydrite at Gale crater, Mars. *American Mineralogist: Journal of Earth and Planetary Materials, 103*(7), 1011-1020.

Wilson, M., Wilson, L., Patey, I., & Shaw, H. (2014). The influence of individual clay minerals on formation damage of reservoir sandstones: a critical review with some new insights. *Clay Minerals, 49*(2), 147-164.

Wilson, S. A., & Bish, D. L. (2011). Formation of gypsum and bassanite by cation exchange reactions in the absence of free-liquid H2O: Implications for Mars. *Journal of Geophysical Research: Planets, 116*(E9).

Wilson, S. A., & Bish, D. L. (2012). Stability of Mg-sulfate minerals in the presence of smectites: Possible mineralogical controls on H2O cycling and biomarker preservation on Mars. *Geochimica et Cosmochimica Acta, 96*, 120-133.

Wood, L. A. (1970). The use of dew-point temperature in humidity calculations. *Journal of Research of the National Bureau of Standards–C. Engineering and Instrumentation C, 74*, 117-122.

Yen, A., Ming, D., Vaniman, D., Gellert, R., Blake, D., Morris, R., . . . Edgett, K. (2017). Multiple stages of aqueous alteration along fractures in mudstone and sandstone strata in Gale Crater, Mars. *Earth and Planetary Science Letters, 471*, 186-198.

Chapter 3. Incongruent Al-Si Release from Kaolinite-Brine Reactions

Christopher Geyer[1], Andrew S. Elwood Madden[1,2], Caitlin Hodges[1], Megan Elwood Madden[2]

[1] School of Geosciences, University of Oklahoma, Norman, OK, USA

[2] Samuel Roberts Noble Microscopy Laboratory, University of Oklahoma, Norman, OK, USA

Key Words: clay; alteration; mars; kaolinite, dissolution

Abstract

Phyllosilicates on Mars record periods of aqueous alteration when the hydrosphere was actively altering primary minerals at the surface. Unlike most terrestrial environments, both ancient and recent aqueous fluids on Mars were likely quite salty, potentially leading to aqueous alteration processes not typically observed on Earth. In this study we investigate the effects of different high salinity brines on kaolinite ($Al_2Si_2O_5(OH)_4$) alteration products to better understand the effects of salts on clay formation and diagenesis on Mars. We reacted saturated NaCl, Na_2SO_4, $CaCl_2$, $MgCl_2$, $MgSO_4$, and NH_4Cl brines as well as 10% dilutions of these saturated brines with kaolinite at 25°C and 100°C, then analyzed the reaction products using XRD, Raman spectroscopy, and ICP-OES elemental analysis of the remaining solutions. We did not observe any new secondary minerals in our XRD or Raman analyses; however, Al and Si compositions of the reacted brines indicated two different non-stoichiometric dissolution pathways. The diluted brines reacting with the kaolinite produced aqueous solutions with Al/Si ratios <1, suggesting the formation of Al-rich secondary minerals or preferential leaching of Si from the kaolinite structure. However, near-saturated brines reacted with kaolinite resulted in the opposite pattern, with Al/Si ratios >1, suggesting either the precipitation of a secondary Si-rich phase or preferential leaching of Al. The lack of XRD or Raman detectable of unambiguous alteration juxtaposed to non-stoichiometric dissolution as evidenced by elemental analysis suggests that products formed by aqueous alteration of kaolinite may be below the detection limits of current instrumentation on, or orbiting, Mars. On the other hand, these results have profound implications for the ability of near-saturated brines to mobile aluminum irrespective of brine composition or temperature up to 100°C.

1. Introduction

On Earth the presence of phyllosilicates is synonymous with aqueous chemical weathering and great effort has been made to investigate phyllosilicate weathering patterns under terrestrial conditions (Bergaya & Lagaly, 2013; Curtis, 1985; Grim, 1968). Phyllosilicate mineralogy, abundance, and unique physio-chemical characteristics differ based on several different variables that influence phyllosilicate alteration pathways, such as primary mineral/rock composition, fluid-to-rock ratio, fluid chemistry, temperature, and drainage (Bergaya & Lagaly, 2013). Due to their sensitivity to temperature- and fluid-dependent alteration pathways, phyllosilicate assemblages are often used in paleoenvironment reconstructions. For example, kaolinite is commonly the most predominant phyllosilicate in wet, warm, well-drained terrestrial settings (Bergaya & Lagaly, 2013; Khawmee et al., 2013). However, on planets such as Mars, phyllosilicate formation and alteration pathways may differ due to the presence of abundant salts. In this study we document the effects of high salinity brines on kaolinite weathering pathways by characterizing kaolinite-brine reaction products over a range of experimental conditions. This work will allow for more accurate interpretation of clay mineral assemblages observed in salty systems on Earth and other planets, including Mars.

The identification of phyllosilicates on Mars firmly established that it once had an active hydrosphere (Bishop et al., 2008a; Poulet et al., 2005). Detailed investigations of the Martian surface by remote sensing, lander, and rover analyses, backed up by Earth-based laboratory investigations, has revealed that the chemistry of fluids on Mars has changed significantly throughout the geologic past (Elwood Madden et al., 2009; Kite et al., 2021; Rapin et al., 2019; Scheller et al., 2022; Yen et al., 2017). Sedimentary units from the Noachian/Hesperian, such as those in Gale Crater which contain abundant clays, also show evidence of post depositional

aqueous alteration (Schwenzer et al., 2012). As desiccation of the Martian surface progressed, fluids in lacustrine settings would have become increasingly saltier, leading to stratigraphically discrete weathering (Bristow et al., 2021).

Salts detected on the surface of Mars today include NaCl, Na_2SO_4, $MgSO_4$ as well as other sulfate, chloride, and perchlorate salts (Clark & Van Hart, 1981; Rapin et al., 2019; Vaniman et al., 2004). Therefore, if aqueous fluids are periodically active on modern Mars, they will likely be present in the form of brines (Chevrier et al., 2020; Möhlmann & Thomsen, 2011; Zorzano et al., 2009). These modern brines may form through the deliquescence of salts during periods of sufficient relative humidity (Gough et al., 2014; Gough et al., 2017; Hecht et al., 2009). To better understand the past and present environments of Mars, a thorough understanding of the effects of different brines on phyllosilicate weathering is required.

A range of clays with varying structural and chemical complexity, including kaolinite, have been identified across the surface of Mars (Bishop, 2018; Bishop et al., 2008b; Poulet et al., 2005). The various pathways leading to neogenesis of kaolinite are diverse and include low temperature weathering of smectites, precipitation within magmatic fluids, as well as hydrothermal alteration of primary silicates (Grim, 1968; Kerr, 1952). On Mars, it has been theorized that post-depositional aqueous alteration has played a significant role in the formation and alteration of clays (Bristow et al., 2021; Bristow et al., 2015; Ehlmann et al., 2011; Ehlmann et al., 2009; Meunier et al., 2012; Michalski & Noe Dobrea, 2007). Parent materials for phyllosilicates on Mars are thought to be mafic igneous minerals including pyroxene, feldspar and olivine as well as volcanic glass (Bibring et al., 2006; Ehlmann et al., 2011; Rampe et al., 2020). Initial weathering of these minerals likely produced di- and tri-octahedral smectites such as nontronite and montmorillonite (Bristow et al., 2015; Rampe et al., 2020). In environments

with acidic fluids and adequate drainage, further weathering of the smectites and parent material may produce kaolinite. Subsequent weathering of kaolinite may either result in complete destruction of the clay via homogeneous dissolution or incongruent dissolution forming additional secondary minerals such as illite or gibbsite (Bergaya & Lagaly, 2013; Essington, 2015; Li et al., 2020).

A preponderance of research on Martian sediments has focused on parent materials and the possible alteration pathways which may have produced the currently observed distribution of phyllosilicates on Mars. However, the Martian sediments we have thus far observed merely provide a snapshot of the diverse paleoenvironments throughout Mars' history. In locations such as Mawrth Valley or Nili Fossae, kaolinite and smectite are frequently observed as "mixed-layer clays", which in a terrestrial setting indicates the alteration of smectite to kaolinite through intermediate interstratified kaolinite-smectite phases (Carter et al., 2015; Cuadros & Michalski, 2013; Milliken et al., 2010). While the discovery of mixed-layer clays provides compelling evidence for aqueous alteration, the assemblage could form via either hydrothermal or low-temperature chemical alteration pathways. If smectite to kaolinite alteration was occurring, it is likely any produced kaolinite would also continue to respond to repeated brine-driven alteration events. Thus, products of aqueous alteration of kaolinite in brines provide a missing piece of the puzzle when reconstructing Martian paleoenvironments.

By reacting brines with kaolinite at 100°C as well as lower temperatures, we aim to investigate the effects of temperature, as well as brine composition on phyllosilicate alteration pathways which may have occurred on Mars. Furthermore, no matter which processes produce kaolinite, our experiments provide insights towards understanding the mobility of Al and Si

when clays react with brines of wide-ranging compositions in a range of terrestrial and planetary settings.

2. Material & Methods

2.1 Experimental Overview

To study kaolinite alteration on Mars, two pairs of experiments were performed using a kaolinite standard reacted with twelve different aqueous solutions at both 100°C or 25°C in sealed batch reactor vessels. Kaolinite "KGa-2" was purchased from the Clay Mineral Society and has been extensively characterized in previous studies (Chipera & Bish, 2001; Keeling et al., 2000; Kogel & Lewis, 2001; Mermut & Cano, 2001). No pre-processing was performed on the KGa-2 prior to the experiments. KGa-2 was chosen for this study because kaolinite has been observed on the Martian surface (Bristow et al., 2018; Ehlmann et al., 2009), and as a reference standard, it is widely available and allows direct comparison with previous studies.

Experiments conducted at 25°C were performed in 50 mL centrifuge tubes, which were continuously shaken using an orbital shaker for 150 days. The 100°C experiments were performed in high-pressure, PTFE-lined Parr vessels (Parr model 4744) shaken manually every two days and heated in a calibrated oven. In both sets of experiments we mixed 10 mL solution with 1 g clay. Immediately prior to sealing the vessels the brine was de-oxygenated by bubbling N_2 gas at 15 mL/min through the solution for 20 min. At the end of the allotted reaction times the solid portion of the samples was separated from the liquid by four cycles of centrifugation, decanting and rinsing. Centrifugation was performed at 10,000 RPM for each 20 min cycle. The brine supernatant from the first centrifuge separation was preserved for ICP-OES elemental analysis; for the following 3 rinse steps we added 20 mL of 18.2 MΩ H_2O to the solid sample

and disaggregated the sample on a vortex mixer before further centrifugation. This rinse water was decanted, and the final rinsed solids were freeze dried using a Labconco freeze drier. Once the solid sample was completely dry it was gently homogenized by hand using an agate mortar and pestle and stored in a centrifuge tube for further XRD and Raman analysis.

2.2 Brines

The brines reacted with KGa-2 are listed in Table 1 below. For each reaction temperature both a concentrated brine (denoted with a "ns" for "near-saturated" in figures) and a dilute brine (denoted with a "10%" in figures) were reacted with the clay. Concentrated brines were created by adding ACS grade (>99.0 purity) salts to 18.2 MΩ H_2O and allowing the mixture to equilibrate for 24 hours, this was repeated until the solution was saturated at room temperature (~298K); the brine was then filtered using a 0.45 μm filter. Dilute concentrations of each brine were produced by diluting the saturated brine to 10% its saturated concentration. Additionally, 18.2 MΩ H_2O was also reacted with the clays.

Brine	Saturated Concentration (mol • kg^{-1})	Saturated Water Activity	Dilute Concentration (mol • kg^{-1})	Dilute Water Activity
NaCl	6.2	0.79_a	0.6	0.98_a
Na_2SO_4	2.0	0.94_a	0.2	0.99_a
$CaCl_2$	6.7	0.43_a	0.7	0.97_a
$MgCl_2$	5.7	0.35_c	0.6	0.97_c
$MgSO_4$	2.9	0.92_c	0.3	0.99_c
NH_4Cl	7.1	0.77_b	0.7	0.98_b

Table 4. Brines reacted with KGa-2. Water activities calculated using a: (Guendouzi et al., 2003), b: (Guendouzi et al., 2001), c: (Ha & Chan, 1999). Dilute brine concentrations were $1/10^{th}$ that of the corresponding saturated brine.

2.3 Analysis

Both the unreacted starting material and reacted clay samples were analyzed using X-Ray Diffraction (XRD) and Raman spectroscopy. A Rigaku SmartLab X-ray diffractometer (Rotating anode Cu source, 45 kV, and 200 mA) was used to perform XRD powder analysis on the clays. Mineral identification was performed using MDI Jade Pro with the ICDD PDF4+ database.

Raman analysis was performed using a Renishaw InVia Raman microscope equipped with a 500 mW 785 nm red laser and a 1200 l/cm grating, centered at 660 cm^{-1} to acquire Raman spectra between 100 and 1100 cm^{-1}. A Si wafer was used as a reference to calibrate the instrument using the crystalline Si Raman band at 520.6 cm^{-1}. Laser power was maintained at 5% to minimize sample heating and potential mineral degradation. As clays are prone to induced fluorescence, the quality of the spectra were improved when laser exposure time was limited to 1 second with 150 accumulated exposures averaged to produce the final spectra. While it is common to characterize clays using the 3000-3800 cm^{-1} range to examine the H_2O & OH vibrations, the objective of this study was to characterize changes in the silica-aluminum structure of KGa-2 as a result of brine induced weathering. Thus, analysis focused on areas known for Si-O and metal bond responses, namely <1000 cm^{-1}. To ease interpretation of the Raman data, spectra were processed by first removing baseline noise, then normalized and smoothed using a Savitzky-Golay filter. Spectra processing was accomplished using the ChemoSpec package in R (Hanson, 2014). Unsmoothed versions of all Raman spectra used in this study are provided in the supplemental materials (S1).

Elemental silicon and aluminum concentrations in the reacted brines were quantified using a Thermo Fisher Scientific iCap Pro Inductively Coupled Plasma – Optical Emission Spectrometer (ICP-OES). Initial brine Si and Al compositions were also determined and were subtracted from

the reported values for all samples. During processing of the reacted brines, the sample of concentrated NH_4Cl brine reacted at 25°C was lost, therefore this experimental data is missing from the results reported here.

3. Results & Discussion

3.1 Raman Spectra

As can be seen in both the 100°C and 25°C Raman spectra shown in Fig. 1, the characteristic peaks associated with kaolinite (Wang et al., 2015) are discernable in each of the reacted samples.

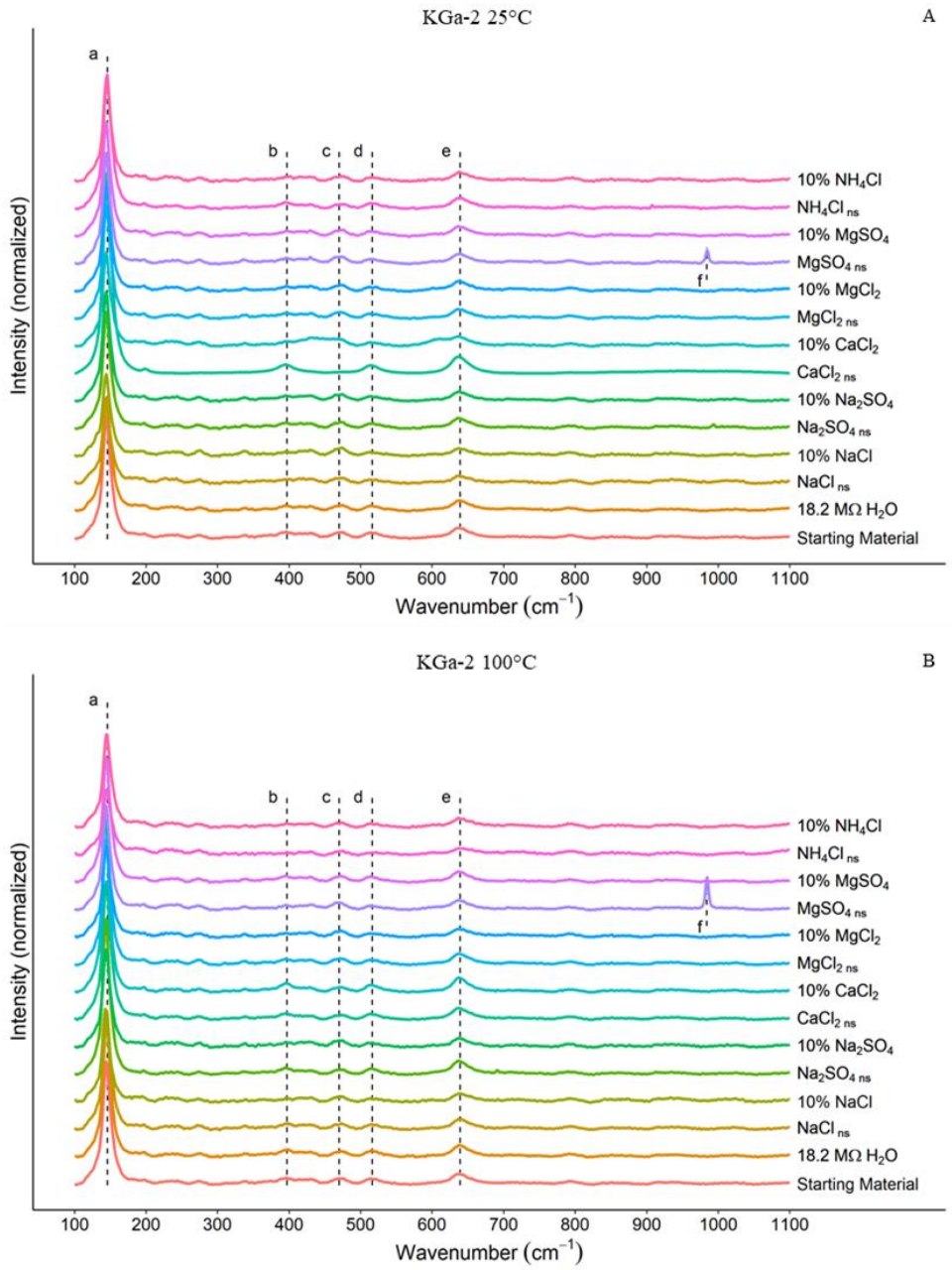

1326

1327 **Figure 6.** Raman spectra for KGa-2 experiments. A) KGa-2 + brines reacted at 25°C. B) KGa-2

1328 + brines reacted at 100°C. Dashed lines highlighting specific wavenumbers: "a" ~146 cm^{-1}, "b"

1329 ~397 cm^{-1}, "c" ~470 cm-1, "d" ~512 cm-1, "e" ~639 cm-1, and "f" ~984 cm^{-1}. Intensities at lines

1330 a-e are typical for KGa-2 (Frost et al., 1997; Wang et al., 2015). Intensity at line f is attributed to

1331 SO_4^{2-} (Ben Mabrouk et al., 2013). Unsmoothed Raman spectra are shown in Fig. A1. Near
1332 saturated brines are denoted with 'ns' and dilute brines denoted with '10%', respectively.

1333 In both Fig. 1A & 1B line a (~146 cm^{-1}) is the highest intensity peak, commonly assigned to
1334 v_2 of the AlO_6 octahedra in kaolinite; a peak at ~146 cm^{-1} is also associated with TiO_2 which is a
1335 known contaminant in KGa-2 (Chipera & Bish, 2001; Frost et al., 1997; Shoval et al., 2008).
1336 Lines b and d in Fig. 1 highlight the secondary and tertiary intensities for TiO_2 at 397 cm^{-1} and
1337 516 cm^{-1}, respectively (Kernazhitsky et al., 2014; Shoval et al., 2008). Line c at ~470 cm^{-1} in Fig.
1338 1 can be attributed to Si-O stretching modes found in both the SiO_4 tetrahedron of kaolinite as
1339 well as silica (SiO_2), another known contaminant in KGa-2 (Chipera & Bish, 2001; Frost et al.,
1340 1997). Line e in Fig.1 at 639 cm^{-1} is likely the result of the Al-O bonds in AlO6 octahedra in a
1341 sheet formation (Frost et al., 1997; Tarte, 1967; Thomas et al., 1989). A singular peak at ~984
1342 cm^{-1} highlighted by line f found in both 25°C $MgSO_{4\ ns}$ and 100°C $MgSO_{4\ ns}$ is assigned to SO_4
1343 (Mason & Madden, 2022; Wang et al., 2006). The presence of SO_4 in both the 25°C and 100°C
1344 $MgSO_{4\ ns}$ Raman spectra indicates that, at least for those samples, not all the brine was removed
1345 by the triple rinsing procedure that was performed on the sample prior to drying.

1346 While the broad Raman spectra in Fig. 1 clearly contain peaks commonly associated with
1347 kaolinite, to acquire a detailed understanding a closer look is required. Figure 2 shows a close-
1348 up of the 100-200 cm^{-1} region in the Raman spectra, which is useful for differentiating kaolinite
1349 from its polymorphs: dickite, halloysite, and nacrite.

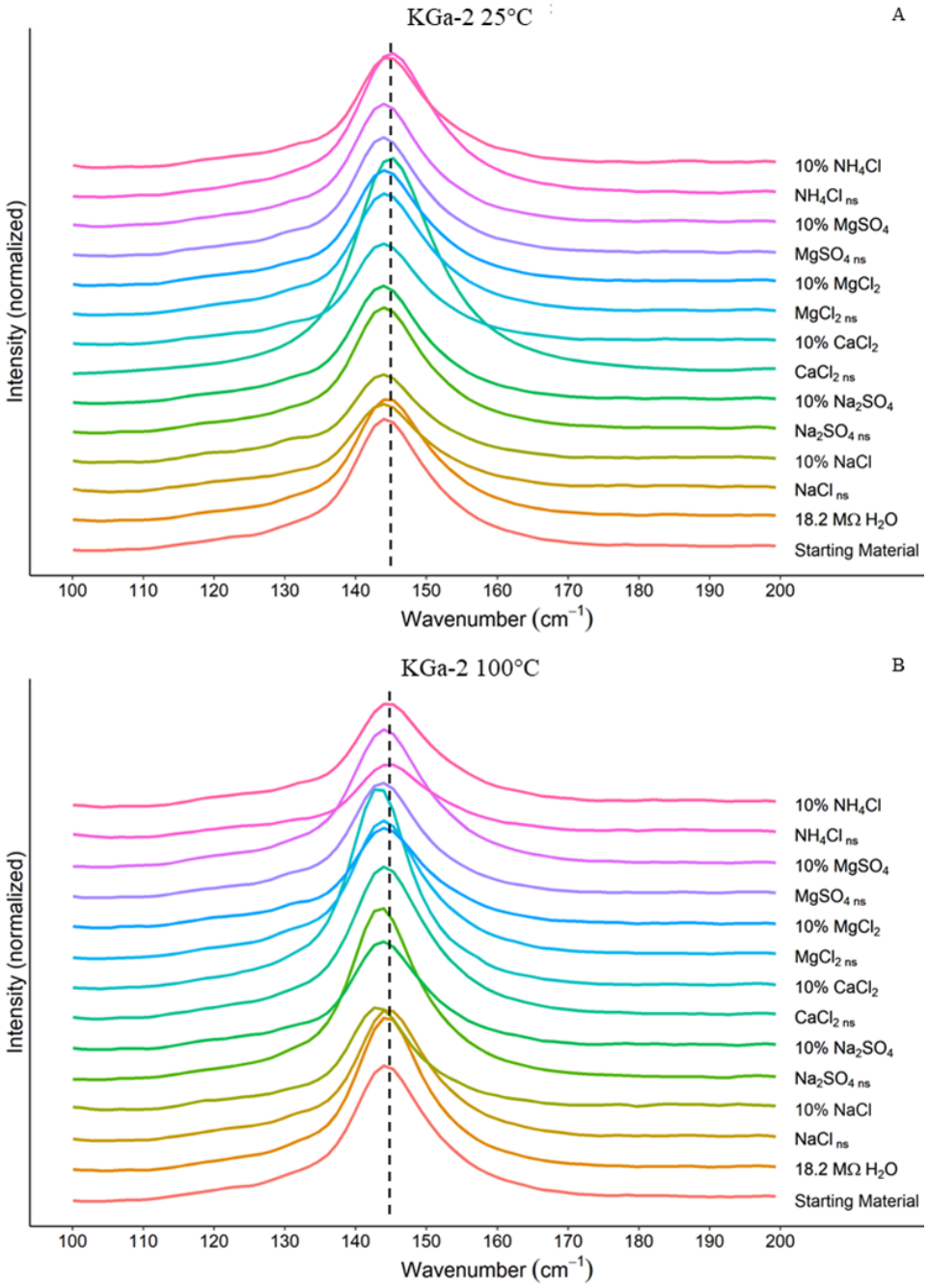

1350

1351 **Figure 7.** Close-up of 100-200 cm^{-1} region of Raman spectra for KGa-2 experiments. A) KGa-2

1352 + brines reacted at 25°C. B) KGa-2 + brines reacted at 100°C. Dashed line in both A & B

1353 indicates the 145 cm^{-1} peak position for unreacted kaolinite. Some reacted clays produced shifts

to lower wavenumbers which could be the result of intercalation or the formation of halloysite, whereas intensities associated with dickite are absent.

Three peak positions commonly associated with dickite are 118, 131, and 141 cm^{-1}; in dickite analyses reported in the literature where 131 and 141 were present, they were roughly equivalent in intensities with each other, however KGa-2 also has a minor response at 132 (Frost, 1997). As can be seen in Fig. 2 A & B, no peaks are present at sufficient intensities in the ~130 cm^{-1} region to indicate the presence of dickite. Nacrite has two intense bands at 179 and 198 cm^{-1}, neither of which are present (Frost & Kloprogge, 2000). Whereas dickite and nacrite formation may be easily ruled out, halloysite is a more complicated matter; some halloysites have an intense peak at 141 cm^{-1} which may be responsible for the shift toward lower wavenumbers seen in some samples (Fig. 2). Of the clay-brine 25°C experiments only 18.2 MΩ H_2O, saturated $CaCl_2$ and both the dilute and saturated NH_4Cl reacted kaolinite exhibited no negative shift in wavenumbers. The majority of the 100°C experiments also exhibited a negative wavenumber shift, with the exception of 18.2 MΩ H_2O, saturated NaCl and both the dilute and saturated NH_4Cl reactions.

To establish the presence of halloysite it is helpful to look at other regions in the Raman spectra, namely 325-425 cm^{-1} as shown in Fig 3. First, a visual phenomenon is present in Fig. 3A must be addressed, the high signal to noise ratio seen in 25°C near saturated $CaCl_2$. It is known that clay grain orientation significantly impacts Raman intensities as scattering will reduce signal intensity (Wang et al., 2015). The high signal to noise ratio seen in Fig. 3A for 25°C near saturated $CaCl_2$ may be the result of a serendipitously oriented sample as no particular effort was made to orient the samples prior to Raman analysis. An alternate hypothesis for the exceptionally high signal to noise ratio of 25°C near saturated $CaCl_2$ could be the prevalence of long-range

ordering (if a mixed-layer is present) and reduced stacking disorder; this could be tested by further analysis by Transmission Electron Microscopy. Typically, halloysite has only one peak in this region, at 335 cm^{-1}, whereas kaolinite typically has strong responses at 335, 355, and 397 cm^{-1} (Frost & Shurvell, 1997; Frost et al., 1997). However, as demonstrated by the noise-dominated spectra in Fig. 3, the complexity of the spectra preclude any concrete identification. One alternative hypothesis which would account for the complexity of the 325-425 cm^{-1} region as well as the shifts observed in the ~145 cm^{-1} peak would be that the clay had become intercalated or "doped" with the cation provided in the reacting brine. Intercalation of kaolinite in this context would involve insertion of a cation supplied by the reacting brine between the individual sheets of the kaolinite, altering some but not all of the OH bonds present in the $Si\text{-}O_4$ tetrahedra and $Al\text{-}O_6$ octahedra (Fu & Yang, 2017). Our results are consistent with a study by Frost (1997), who reported that intercalation of kaolinite caused a negative shift of the 145 cm^{-1} peak to 143 cm^{-1} as well as increased complexity in the 325-425 cm^{-1} region of the Raman spectra.

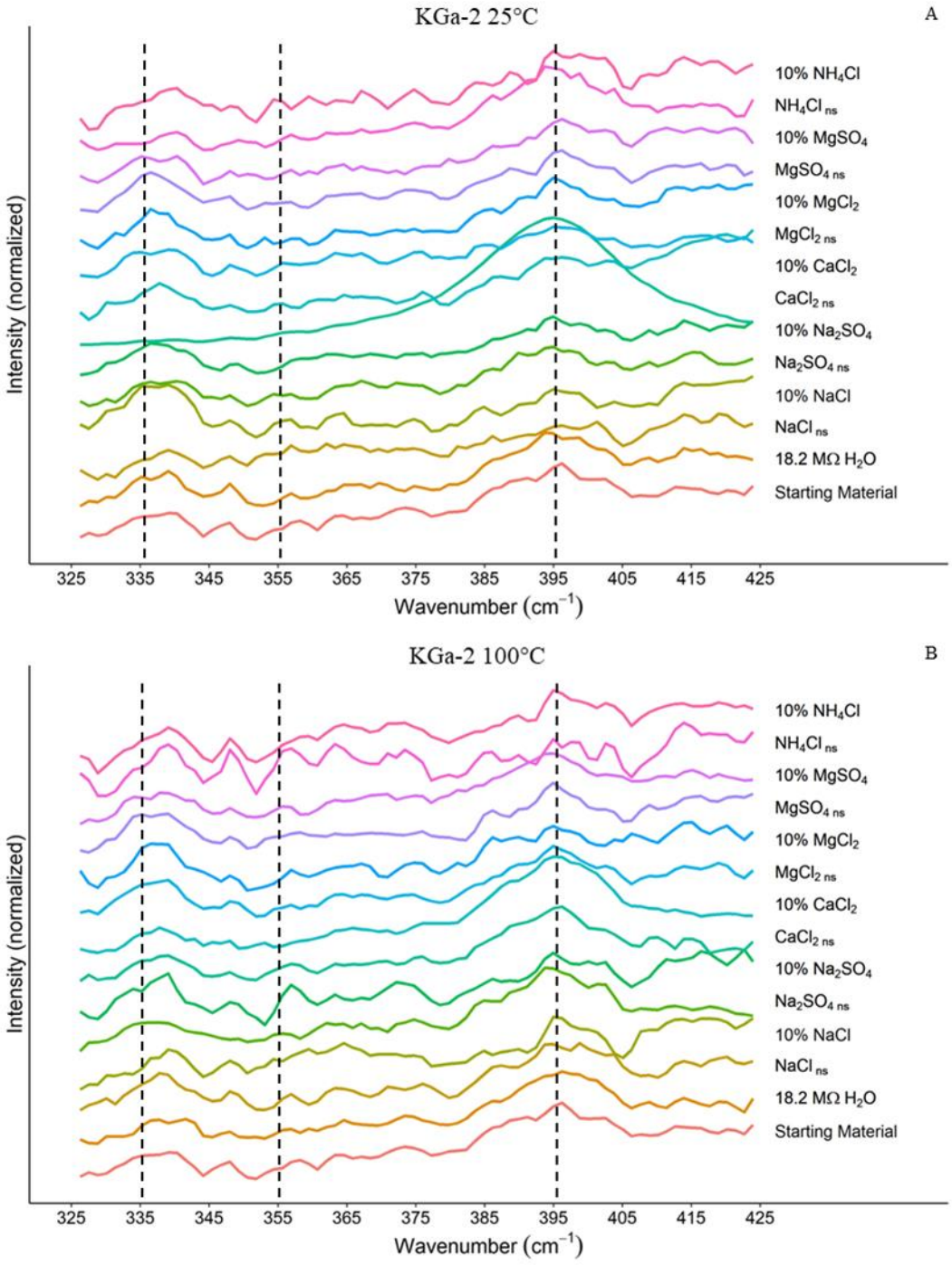

Figure 8. Close-up of 325-425 cm^{-1} region of Raman spectra for KGa-2 experiments. A) KGa-2 + brines reacted at 25°C. B) KGa-2 + brines reacted at 100°C. Dashed lines indicate wavenumbers where peaks are common for kaolinite.

3.2 Mineralogy by XRD

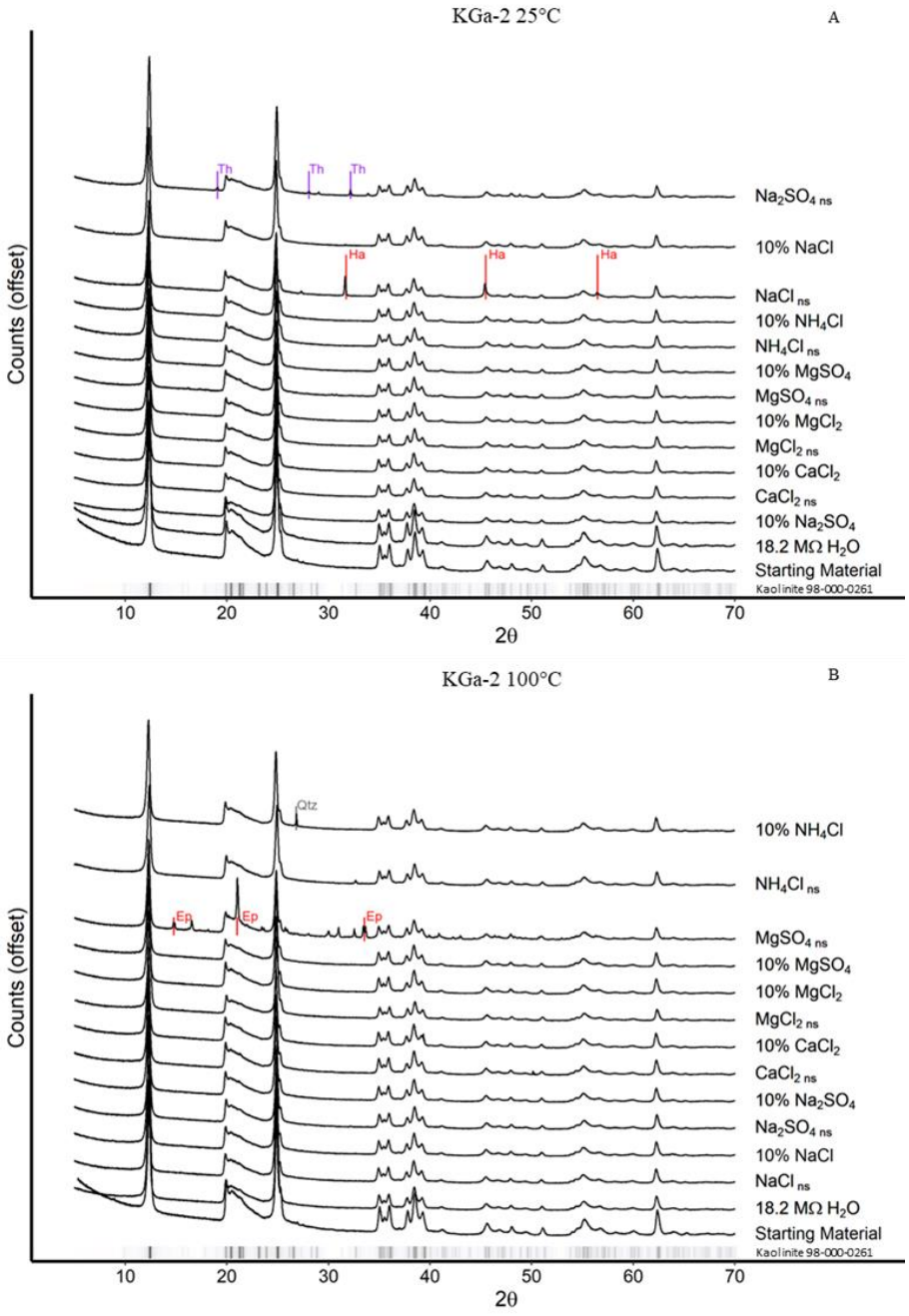

Figure 9. XRD Patterns for KGa-2 experiments. The ribbon at the base of each graph is for the primary intensities taken from the ICDD PDF4+ card for Kaolinite (98-000-0261). A) KGa-2 + brines reacted at 25°C; "Th" = Thenardite, "Ha" = Halite. B) KGa-2 + brines reacted at 100°C; "Qtz" = Quartz, "Ep" = Epsomite.

XRD patterns for the 25°C and 100°C clay-brine reaction presented in Fig.4 reflect the characteristic trace of kaolinite, with little to no deviation in key intensities as compared to the ribbon from the ICDD PDF4+ standard kaolinite. Several of the brine-clay reactions exhibit minor trace minerals. In the 25°C experiments thenardite (Na_2SO_4) was found in the KGa-2 reacted with $Na_2SO_{4\ ns}$ brine and halite (NaCl) was found in KGa-2 reacted with $NaCl_{\ ns}$ brine (Fig. 2a), despite the triple rinse procedure. For the 100°C experiments epsomite ($MgSO_4$) was detected in KGa-2 reacted with $MgSO_{4\ ns}$ brine, and quartz (SiO_2) was detected in KGa-2 reacted with 10% NH_4Cl brine (Fig. 2b). While the presence of minor contamination from residual brine is evident, the lack of evidence for kaolinite alteration is equally conspicuous.

The kaolinite polymorph dickite is of particular interest when investigating whether hydrothermal processes or low temperature aqueous alteration reactions were the principal mechanisms responsible for clay formation on Mars. Dickite is commonly associated with hydrothermal alteration of kaolinite at temperatures between 80-160°C (Bergaya & Lagaly, 2013; Cuadros et al., 2014; Palinkaš et al., 2009). While dickite shares many of the characteristic kaolinite XRD peaks, a triplet at 20-24° 2θ with a high intensity peak at ~23.4° 2θ are distinguishing features in dickite's XRD pattern (Chen et al., 2001). As can be seen in Fig. 2, neither the 25°C experiments, nor the 100°C experiments produced detectable peaks indicative of dickite.

While it is unsurprising that the 25°C experiments did not produce dickite, the 100°C experiments were well within the 80-160°C temperature window where alteration of kaolinite to dickite is expected. Possible explanations for the lack of dickite formation are: 1) the reaction period used in this study (50 days for the 100°C experiments) was not sufficient or 2) dickite is frequently, though not always, a product of both elevated temperatures and pressures. The

pressure maintained in the Parr vessels was generated by water vapor (<10 atm) and thus orders of magnitude lower than the pressure reported by some for dickite formation (Chen et al., 2001; Palinkaš et al., 2009).

Similar to the alteration of kaolinite to dickite, illitization of kaolinite is a well-known aqueous alteration pathway which provides useful information regarding burial history of kaolinite (Lanson et al., 1996). However, the telltale ~9° 2θ and 17° 2θ of illite are also absent in the XRD patterns of both the 25°C and 100°C experiments (Fig. 2) (Moore & Reynolds Jr, 1989). This is due to the lack of K^+ in our experiments, as well as the lack of elevated pressure, as both are often required for illitization to occur (Bentabol et al., 2003; Mantovani & Becerro, 2010). Fluids on Mars contain(ed) abundant K^+ and thus, while illite formation was not observed in this study, it is nevertheless a plausible reaction pathway on Mars (Thompson et al., 2016).

3.3 Silicon and Aluminum Concentrations in Reacted Brines

While additional secondary phases were not detected by XRD or Raman analysis, elemental analyses of the reacted fluids show elevated concentrations of Al and Si beyond the concentrations observed in the unreacted fluids in all the experiments, indicating that some dissolution of kaolinite occurred (Fig. 5).

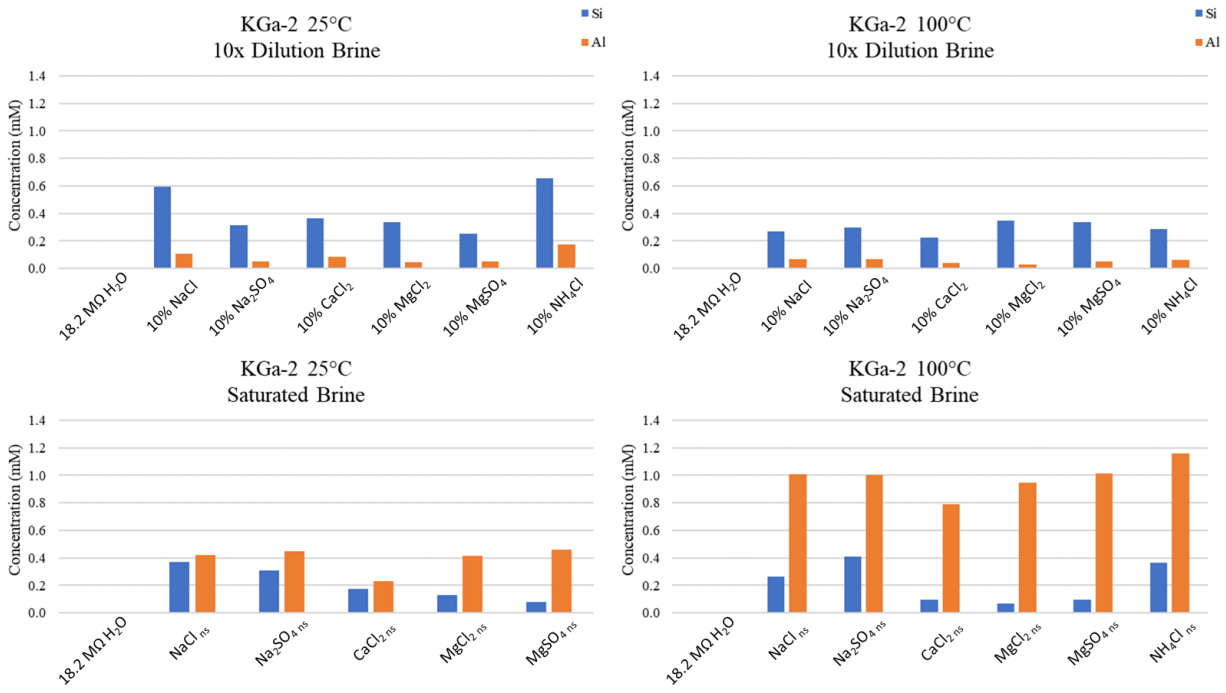

Figure 10. Si and Al concentrations observed in the reacted brines. Si and Al concentrations within the unreacted, initial brine have been subtracted from these values, allowing us to directly compare the amount of Al and Si added to solutions as a result of the reaction with kaolinite. Reactions involving 18.2 MΩ H_2O yielded Al & Si concentrations below 35 ppb, which is not visible in the graph above. Concentrated brines are denoted using a "$_{ns}$" suffix, dilute brines are noted with a "10%" prefix.

In both the 25°C and 100° reaction conditions, the saturated brines exhibited Al/Si ratios >1 after reaction with the kaolinite, whereas the more dilute (10% of saturated) reacted brines had Al/Si ratios <1 (Fig. 3 & Table A1). If stoichiometric dissolution of kaolinite were taking place, an Al/Si =1 would be expected given the composition of kaolinite - $Al_2Si_2O_5(OH)_4$. Only two of the reactions yielded Al/Si ratios indicative of homogeneous, stoichiometric dissolution: saturated NaCl and saturated $CaCl_2$, both reacted at 25°C.

Instead, it appears that heterogeneous dissolution and precipitation of new secondary phases, or incongruent dissolution that preferentially leaches either Si or Al are occurring in the remaining experiments. Gong et. al. (2019) found that for solutions near equilibrium with respect to kaolinite at neutral pH, kaolinite dissolution did occur, but the experimental solutions exhibited erratic Al:Si ratios due to the precipitation of secondary phases such as gibbsite ($Al(OH)_3$) (Gong et al., 2019). When modeling the aqueous alteration of Martian parent material into clay minerals, Bridges et al. (2015) found it necessary to incorporate heterogeneous dissolution mechanisms to constrain conditions required for secondary mineral precipitation. Heterogenous dissolution and precipitation reactions, such as kaolinite alteration to gibbsite and/or illite, result in excess Si in the reacted brine and Al sequestered in the solid phase, yielding aqueous Al/Si ratios <1, similar to those observed in the 10x diluted solutions.

One possible explanation for the discrepancy between the <1 Al/Si ratios seen in the reacted diluted brines and the absence of new Al or Si minerals observed in powder XRD data is the small volume of material that would have precipitated. Typical detection limits for XRD are reported at around 0.1 – 1 wt% for most minerals; however, the detection limit of the ICP-OES in this study is ~35 ppb. In the context of our experiments, diluted NaCl reacted at 25°C had a Si:Al ratio of ~6 with an Si-Al discrepancy of ~15 ppm; if all of absent Al had coprecipitated as gibbsite the expected quantity of gibbsite formed would be 0.04 weight % of the reacted clay, a value significantly lower than typical XRD detection limits. Likewise, secondary gibbsite is likely also difficult to detect in such small quantities in the Raman analyses, as the only significant Raman peak for gibbsite is at ~465 cm^{-1} which at 0.04 wt% would likely be swamped by the 470 cm^{-1} Si-O response (Lafuente et al., 2015). Therefore, we posit that the elevated

Si:Al ratios observed in the dilute brine experiments may indicate formation of an Al-rich phase, despite the lack of new solid reaction products detected by XRD or Raman.

While precipitation of new mineral phases may explain the results for reactions involving diluted brines, the same cannot be said for the concentrated brine reactions. Considering only the Si and Al concentrations observed in the reacted fluids, one might reasonably infer that silica may have precipitated as a secondary product of kaolinite dissolution, since the average Al/Si ratio observed in concentrated brines is 2.5 for reactions at 25°C and 6.8 for reactions at 100°C. If precipitation of secondary Si-rich phases were invoked to explain this deviation from the idealized 2:2 Al:Si ratio then we might consider quartz or amorphous silica as the most likely phases. However, calculated saturation indices for quartz and amorphous silica (modelled using PHREEQC with the pitzer database) indicate that while the saturated reacted brines are supersaturated with respect to quartz, they are undersaturated with respect to amorphous silica (Messer et al., 1981; Parkhurst & Appelo, 2013), making quartz the most likely secondary precipitate.

If quartz had precipitated during the experiment, we would expect to detect the reaction products in the XRD data, since quartz produces relatively intense XRD peaks even at low wt%. For example: saturated $MgCl_2$ reacted at 100°C had an Al-Si discrepancy of ~17 ppm; if all of the absent Si had coprecipitated as quartz (SiO_2) the expected yield would be 0.36 weight% of the reacted clay, which is well within the detection capabilities of XRD (Tomaino, 1994). However, none of the XRD patterns for the concentrated brines show a detectable increase in quartz intensities at the expected positions (20.8°, 26.7° , and 50.2° 2θ) (Moore & Reynolds Jr, 1989) (Fig. 2). If silica tetrahedra were breaking down and forming silica, either as quartz or amorphous silica, we would also expect to see a Raman peak at ~470 cm^{-1}. However, comparing

1498 the relative intensity of the peaks observed at ~470 cm^{-1} to the starting material, there is no
1499 significant increase in the intensity of the Si-O peak observed (Fig. 1), indicating that no
1500 additional quartz precipitated.

1501 Instead, the Al/Si ratios >1 resulting from kaolinite dissolution in concentrated brines may be
1502 the product not of the precipitation of secondary phases, but rather the effect of incongruent
1503 dissolution, where Al is preferentially leached from the kaolinite structure. Of particular note,
1504 concentrated brines reacted at 100°C produced significantly higher Al/Si ratios, as well as higher
1505 total Al abundances than their 25° counterparts. This significant temperature effect indicates that
1506 the non-stoichiometric alteration process is influenced by temperature. Non-stoichiometric
1507 dissolution of phyllosilicates is well documented, and in the case of kaolinite the Al ion is
1508 released preferentially over Si during the initial stages of dissolution when the pH of the reacting
1509 fluid is below 6 and (Carroll-Webb & Walther, 1988; Gong et al., 2019; Khawmee et al., 2013;
1510 Mulders et al., 2018). A possible reason Al-rich secondary minerals in XRD and Al-rich
1511 amorphous signatures in Raman are not observed is that the abundant Al preferentially released
1512 did not form a solid product. Rather, Al complexation with anions provided by the brine (SO_4^{2-}
1513 and Cl^-) may have formed highly soluble Al-anion aqueous complexes such as $Al(SO_4)_2^-$ and
1514 $AlCl_3$ (Driscoll et al., 1989). For both the 25°C and 100°C reacted near saturated brines Al
1515 content was significantly higher than their dilute counterparts.

1516 ## 4. Applications to Mars

1517 As the Martian climate progressed from wet to dry the composition of the fluids at the
1518 surface would have become increasingly concentrated brines. The results of this study indicate
1519 that salty fluids, either dilute or concentrated, would have been capable of altering kaolinite in

Mars' past or present. All brines used in this study demonstrated some degree of kaolinite dissolution, even at low temperatures and high concentrations.

As demonstrated by this study, aqueous alteration of kaolinite by dilute brines results in different reaction pathways as compared to kaolinite alteration by concentrated brines. During Mars' early wetter climate, kaolinite weathering likely formed Al-rich phases with Si rich fluids. As the Martian climate dried, the remaining fluid would have become saturated with respect to Si and precipitated Si rich phases, which may be reflected in CRISM observations in which hydrated silica was found co-located with kaolinite (Mustard et al., 2008). In environments where higher salinity fluids were dominant, incongruent dissolution would be more pronounced, with additional Al preferentially released relative to Si into the weathering fluid. If the system were open, Al rich fluids would have then migrated to the subsurface and as the planet desiccated the fluids would have become saturated with respect to Al. This is consistent with models produced by Fairén et al. which predict the formation of gibbsite ($Al(OH)_3$) in the subsurface (Fairén et al., 2017). While the departure of Al/Si ratios from near unity suggest that equilibrium had not been reached for the closed system experiments in this study, on Mars the extent of reaction may be expected to be greater due to an open system.

Trace minerals formed *in situ* by aqueous alteration of kaolinite may be beyond the detection of instrumentation currently on ground-based rovers and orbiting spectrometers. Investigation into the 100-200 cm^{-1} and 325-425 cm^{-1} Raman spectral regions generated in this study demonstrates that it is difficult to differentiate between alteration of kaolinite into halloysite, or kaolinite intercalation. Orbital and rover based spectral analysis is fraught with interferences which would likewise make interpretation of such minor intensities difficult. Thus, when

interpreting Martian environments with sediments rich in phyllosilicates, consideration should be given to trace minerals that are likely present but beyond our ability to detect.

One difference between this study and likely real-world conditions is the absence of K^+ in the brines reacted with kaolinite, as brines on Mars are likely to contain some K^+ from igneous parent materials. The availability of K^+ rich brines concurrent with high temperature hydrothermal conditions would potentially allow for illitization of kaolinite, whereas in the brines used in this study K^+ was not present, thus preventing illitization. Future experiments that incorporate K^+ are needed to further study the effects of high salinity brines on the kaolinite-illite transitions.

5. Conclusions

The results of this study provide a firm foundation for understanding the progression of kaolinite alteration in salty solutions on Mars. Aside from residual contamination from the brines reacted with the kaolinite, no alteration or secondary minerals were detected using Raman or XRD, likely due to the small volume of material produced during the 50 day reactions. It is possible that negative shifts observed in the ~145 cm^{-1} Raman peak may be due to alteration of kaolinite to halloysite. However, given the complexity of the Raman spectra it is equally possible that the observed negative shift can be attributed to kaolinite intercalation by cations present in the reacting brines.

While neither the low-temperature (25°C) nor elevated temperature (100°C) clay-brine reactions produced secondary minerals detectable with XRD or Raman, elemental analysis of the reacted brines did reveal evidence of incongruent kaolinite dissolution at both temperature conditions. In both temperature conditions dilute brine reactions produce Al/Si ratios <1

indicating precipitation of Al-rich phase such as gibbsite likely occurred, but in such small volume that the secondary phases could not be detected in XRD or Raman analyses. In contrast, the concentrated brine reactions produced aqueous Al:Si ratios >1, with sufficient Si missing from the brine that any precipitates should have been detectable in XRD and/or Raman. Thus, the absence of any evidence of silica suggests that kaolinite instead followed a non-stoichiometric dissolution pathway whereby Al was preferentially released over Si. Additionally, this incongruent dissolution was more pronounced in 100°C reactions relative to 25°C reactions, suggesting accelerated kaolinite dissolution in hydrothermal conditions for all the brines we tested. As demonstrated in this study, incongruent dissolution of kaolinite with the potential for trace amounts of secondary mineral precipitation is difficult to detect with typical Raman and XRD bulk analytical methods and must be paired with other techniques such as ICP for a thorough understanding of the alteration processes.

Acknowledgements

This project was funded by NASA PDART grants 80NSSC18K0512 & 80NSSC23K0037. XRD data collection was performed at the Samuel Roberts Noble Microscopy Laboratory, an OU core facility supported by the Vice President for Research and Partnerships. The authors would like to thank Itunu T. Apalara for her assistance analyzing samples and Steve J. Chipera for his guidance on XRD interpretation.

References

Ben Mabrouk, K., Kauffmann, T. H., Aroui, H., & Fontana, M. D. (2013). Raman study of cation effect on sulfate vibration modes in solid state and in aqueous solutions. *Journal of Raman spectroscopy, 44*(11), 1603-1608.

Bentabol, M., Ruiz Cruz, M., Huertas, F., & Linares, J. (2003). Hydrothermal transformation of kaolinite to illite at 200 and 300° C. *Clay Minerals, 38*(2), 161-172.

Bergaya, F., & Lagaly, G. (2013). *Handbook of Clay Science*: Elsevier.

Bibring, J.-P., Langevin, Y., Mustard, J. F., Poulet, F., Arvidson, R., Gendrin, A., . . . Forget, F. (2006). Global mineralogical and aqueous Mars history derived from OMEGA/Mars Express data. *Science, 312*(5772), 400-404.

Bishop, J. L. (2018). Remote detection of phyllosilicates on Mars and implications for climate and habitability. In *From habitability to life on Mars* (pp. 37-75): Elsevier.

Bishop, J. L., Dobrea, E. Z. N., McKeown, N. K., Parente, M., Ehlmann, B. L., Michalski, J. R., . . . Mustard, J. F. (2008a). Phyllosilicate diversity and past aqueous activity revealed at Mawrth Vallis, Mars. *Science, 321*(5890), 830-833.

Bishop, J. L., Noe Dobrea, E. Z., McKeown, N. K., Parente, M., Ehlmann, B. L., Michalski, J. R., . . . Bibring, J.-P. (2008b). Phyllosilicate diversity and past aqueous activity revealed at Mawrth Vallis, Mars. *Science (American Association for the Advancement of Science), 321*(5890), 830-833. doi:10.1126/science.1159699

Bridges, J. C., Schwenzer, S., Leveille, R., Westall, F., Wiens, R., Mangold, N., . . . Berger, G. (2015). Diagenesis and clay mineral formation at Gale Crater, Mars. *Journal of Geophysical Research: Planets, 120*(1), 1-19.

Bristow, T., Grotzinger, J. P., Rampe, E., Cuadros, J., Chipera, S., Downs, G., . . . Morris, R. (2021). Brine-driven destruction of clay minerals in Gale crater, Mars. *Science, 373*(6551), 198-204.

Bristow, T. F., Bish, D. L., Vaniman, D. T., Morris, R. V., Blake, D. F., Grotzinger, J. P., . . . Ming, D. W. (2015). The origin and implications of clay minerals from Yellowknife Bay, Gale crater, Mars. *American Mineralogist, 100*(4), 824-836.

Bristow, T. F., Rampe, E. B., Achilles, C. N., Blake, D. F., Chipera, S. J., Craig, P., . . . Gellert, R. (2018). Clay mineral diversity and abundance in sedimentary rocks of Gale crater, Mars. *Science advances, 4*(6), eaar3330.

Carroll-Webb, S. A., & Walther, J. V. (1988). A surface complex reaction model for the pH-dependence of corundum and kaolinite dissolution rates. *Geochimica et cosmochimica acta, 52*(11), 2609-2623.

Carter, J., Loizeau, D., Mangold, N., Poulet, F., & Bibring, J.-P. (2015). Widespread surface weathering on early Mars: A case for a warmer and wetter climate. *Icarus, 248*, 373-382.

Chen, P. Y., Wang, M. K., & Yang, D. S. (2001). Mineralogy of dickite and nacrite from northern Taiwan. *Clays and clay minerals, 49*(6), 586-595.

Chevrier, V. F., Rivera-Valentín, E. G., Soto, A., & Altheide, T. S. (2020). Global temporal and geographic stability of brines on present-day Mars. *The planetary science journal, 1*(3), 64.

Chipera, S. J., & Bish, D. L. (2001). Baseline Studies of the Clay Minerals Society Source Clays: Powder X-ray Diffraction Analyses. *Clays and clay minerals, 49*(5), 398-409. doi:10.1346/CCMN.2001.0490507

Clark, B. C., & Van Hart, D. C. (1981). The salts of Mars. *Icarus, 45*(2), 370-378.

Cuadros, J., & Michalski, J. R. (2013). Investigation of Al-rich clays on Mars: Evidence for kaolinite–smectite mixed-layer versus mixture of end-member phases. *Icarus, 222*(1), 296-306.

Cuadros, J., Vega, R., Toscano, A., & Arroyo, X. (2014). Kaolinite transformation into dickite during burial diagenesis. *American Mineralogist, 99*(4), 681-695.

Curtis, C. D. (1985). Clay mineral precipitation and transformation during burial diagenesis. *Philosophical Transactions of the Royal Society of London. Series A, Mathematical and Physical Sciences, 315*(1531), 91-105.

Driscoll, C., Schecher, W., & Gitelman, H. (1989). Aluminum and health–A critical review. In: New York: Marcel Dekker.

Ehlmann, B. L., Mustard, J. F., Murchie, S. L., Bibring, J.-P., Meunier, A., Fraeman, A. A., & Langevin, Y. (2011). Subsurface water and clay mineral formation during the early history of Mars. *Nature, 479*(7371), 53-60.

Ehlmann, B. L., Mustard, J. F., Swayze, G. A., Clark, R. N., Bishop, J. L., Poulet, F., . . . Wray, J. J. (2009). Identification of hydrated silicate minerals on Mars using MRO-CRISM: Geologic context near Nili Fossae and implications for aqueous alteration. *Journal of Geophysical Research: Planets, 114*(E2).

Elwood Madden, M. E., Madden, A. S., & Rimstidt, J. D. (2009). How long was Meridiani Planum wet? Applying a jarosite stopwatch to determine the duration of aqueous diagenesis. *Geology, 37*(7), 635-638.

Essington, M. E. (2015). *Soil and water chemistry: an integrative approach*: CRC press.

Fairén, A. G., Gil-Lozano, C., Uceda, E. R., Losa-Adams, E., Davila, A. F., & Gago-Duport, L. (2017). Mineral paragenesis on Mars: The roles of reactive surface area and diffusion. *Journal of Geophysical Research: Planets, 122*(9), 1855-1879.

Frost, R. (1997). The structure of the kaolinite minerals—a FT-Raman study. *Clay Minerals, 32*(1), 65-77.

Frost, R., & Shurvell, H. (1997). Raman microprobe spectroscopy of halloysite. *Clays and clay minerals, 45*, 68-72.

Frost, R. L., Ha, T. T., & Kristof, J. (1997). FT-Raman spectroscopy of the lattice region of kaolinite and its intercalates. *Vibrational Spectroscopy, 13*(2), 175-186.

Frost, R. L., & Kloprogge, J. T. (2000). Raman spectroscopy of nacrite single crystals at 298 and 77 K. *Spectrochimica Acta Part A: Molecular and Biomolecular Spectroscopy, 56*(5), 931-939.

Fu, L., & Yang, H. (2017). Structure and electronic properties of transition metal doped kaolinite nanoclay. *Nanoscale Research Letters, 12*, 1-7.

Gong, L., Rimstidt, J. D., Zhang, Y., Chen, K., & Zhu, C. (2019). Unidirectional kaolinite dissolution rates at near-equilibrium and near-neutral pH conditions. *Applied Clay Science, 182*, 105284.

Gough, R., Chevrier, V., & Tolbert, M. (2014). Formation of aqueous solutions on Mars via deliquescence of chloride–perchlorate binary mixtures. *Earth and Planetary Science Letters, 393*, 73-82.

Gough, R., Wong, J., Dickson, J., Levy, J., Head, J., Marchant, D., & Tolbert, M. (2017). Brine formation via deliquescence by salts found near Don Juan Pond, Antarctica: Laboratory experiments and field observational results. *Earth and Planetary Science Letters, 476*, 189-198.

Grim, R. E. (1968). *Clay Mineralogy* (2nd ed.): McGraw-Hill.

Guendouzi, M. E., Dinane, A., & Mounir, A. (2001). Water activities, osmotic and activity coefficients in aqueous chloride solutions at T= 298.15 K by the hygrometric method. *The Journal of Chemical Thermodynamics, 33*(9), 1059-1072.

Guendouzi, M. E., Mounir, A., & Dinane, A. (2003). Water activity, osmotic and activity coefficients of aqueous solutions of Li2SO4, Na2SO4, K2SO4,(NH4) 2SO4, MgSO4, MnSO4, NiSO4, CuSO4, and ZnSO4 at T= 298.15 K. *The Journal of Chemical Thermodynamics, 35*(2), 209-220.

Ha, Z., & Chan, C. K. (1999). The water activities of MgCl2, Mg (NO3) 2, MgSO4, and their mixtures. *Aerosol Science & Technology, 31*(2-3), 154-169.

Hanson, B. A. (2014). ChemoSpec: an R package for the chemometric analysis of spectroscopic data. *Package Version*, 2.0-2.

Hecht, M. H., Kounaves, S. P., Quinn, R., West, S. J., Young, S. M., Ming, D. W., . . . Hoffman, J. (2009). Detection of perchlorate and the soluble chemistry of martian soil at the Phoenix lander site. *Science, 325*(5936), 64-67.

Keeling, J. L., Raven, M. D., & Gates, W. P. (2000). Geology and characterization of two hydrothermal nontronites from weathered metamorphic rocks at the Uley graphite mine, South Australia. *Clays and clay minerals, 48*, 537-548.

Kernazhitsky, L., Shymanovska, V., Gavrilko, T., Naumov, V., Fedorenko, L., Kshnyakin, V., & Baran, J. (2014). Laser-excited excitonic luminescence of nanocrystalline TiO2 powder. *Український фізичний журнал*(59,№ 3), 248-255.

Kerr, P. F. (1952). Formation and occurrence of clay minerals. *Clays and clay minerals, 1*, 19-32.

Khawmee, K., Suddhiprakarn, A., Kheoruenromne, I., Bibi, I., & Singh, B. (2013). Dissolution behaviour of soil kaolinites in acidic solutions. *Clay Minerals, 48*(3), 447-461.

Kite, E. S., Steele, L. J., Mischna, M. A., & Richardson, M. I. (2021). Warm early Mars surface enabled by high-altitude water ice clouds. *Proceedings of the National Academy of Sciences, 118*(18), e2101959118.

Kogel, J. E., & Lewis, S. A. (2001). Baseline studies of the clay minerals society source clays: Chemical analysis by inductively coupled plasma-mass spectroscopy (ICP-MS). *Clays and clay minerals, 49*(5), 387-392.

Lafuente, B., Downs, R. T., Yang, H., & Stone, N. (2015). The power of databases: The RRUFF project. In (pp. 1-30). Berlin, MГjnchen, Boston: Berlin, MГjnchen, Boston: DE GRUYTER.

Lanson, B., Beaufort, D., Berger, G., Baradat, J., & Lacharpagne, J.-C. (1996). Illitization of diagenetic kaolinite-to-dickite conversion series; late-stage diagenesis of the Lower Permian Rotliegend Sandstone reservoir, offshore of the Netherlands. *Journal of Sedimentary Research, 66*(3), 501-518.

Li, S., He, H., Tao, Q., Zhu, J., Tan, W., Ji, S., . . . Zhang, C. (2020). Kaolinization of 2: 1 type clay minerals with different swelling properties. *American Mineralogist, 105*(5), 687-696.

Mantovani, M., & Becerro, A. I. (2010). Illitization of kaolinite: The effect of pressure on the reaction rate. *Clays and clay minerals, 58*(6), 766-771.

Mason, D. P., & Madden, M. E. E. (2022). Raman spectroscopy of high salinity brines and ices. *Icarus, 372*, 114759.

Mermut, A. R., & Cano, A. F. (2001). Baseline Studies of the Clay Minerals Society Source Clays: Chemical Analyses of Major Elements. *Clays and clay minerals, 49*(5), 381-386.

Messer, J. J., Israelsen, E. K., & Adams, V. D. (1981). Natural salinity removal processes in reservoirs.

Meunier, A., Petit, S., Ehlmann, B. L., Dudoignon, P., Westall, F., Mas, A., . . . Ferrage, E. (2012). Magmatic precipitation as a possible origin of Noachian clays on Mars. *Nature Geoscience, 5*(10), 739-743.

Michalski, J. R., & Noe Dobrea, E. Z. (2007). Evidence for a sedimentary origin of clay minerals in the Mawrth Vallis region, Mars. *Geology, 35*(10), 951-954.

Milliken, R. E., Bish, D. L., Bristow, T., & Mustard, J. F. (2010). *The Case for Mixed-layered Clays on Mars*. https://ui.adsabs.harvard.edu/abs/2010LPI....41.2030M

Möhlmann, D., & Thomsen, K. (2011). Properties of cryobrines on Mars. *Icarus, 212*(1), 123-130.

Moore, D. M., & Reynolds Jr, R. C. (1989). *X-ray Diffraction and the Identification and Analysis of Clay Minerals*: Oxford University Press (OUP).

Mulders, J. J., Harrison, A. L., Christ, J., & Oelkers, E. H. (2018). Non-stoichiometric dissolution of sepiolite. *Energy procedia, 146*, 74-80.

Mustard, J. F., Murchie, S. L., Pelkey, S., Ehlmann, B., Milliken, R., Grant, J. A., . . . Dobrea, E. N. (2008). Hydrated silicate minerals on Mars observed by the Mars Reconnaissance Orbiter CRISM instrument. *Nature, 454*(7202), 305-309.

Palinkaš, S. S., Šoštarić, S. B., Bermanec, V., Palinkaš, L., Prochaska, W., Furić, K., & Smajlović, J. (2009). Dickite and kaolinite in the Pb-Zn-Ag sulphide deposits of northern Kosovo (Trepča and Crnac). *Clay Minerals, 44*(1), 67-79.

Parkhurst, D. L., & Appelo, C. (2013). Description of input and examples for PHREEQC version 3—a computer program for speciation, batch-reaction, one-dimensional transport, and

inverse geochemical calculations. *US geological survey techniques and methods, 6*(A43), 497.

Poulet, F., Bibring, J.-P., Mustard, J., Gendrin, A., Mangold, N., Langevin, Y., . . . Gomez, C. (2005). Phyllosilicates on Mars and implications for early Martian climate. *Nature, 438*(7068), 623-627.

Rampe, E. B., Blake, D. F., Bristow, T., Ming, D. W., Vaniman, D., Morris, R., . . . Tu, V. (2020). Mineralogy and geochemistry of sedimentary rocks and eolian sediments in Gale crater, Mars: A review after six Earth years of exploration with Curiosity. *Geochemistry, 80*(2), 125605.

Rapin, W., Ehlmann, B. L., Dromart, G., Schieber, J., Thomas, N., Fischer, W. W., . . . Clark, B. C. (2019). An interval of high salinity in ancient Gale crater lake on Mars. *Nature Geoscience, 12*(11), 889-895.

Scheller, E. L., Hollis, J. R., Cardarelli, E. L., Steele, A., Beegle, L. W., Bhartia, R., . . . Ehlmann, B. L. (2022). Aqueous alteration processes in Jezero crater, Mars− implications for organic geochemistry. *science*, eabo5204.

Schwenzer, S., Abramov, O., Allen, C., Bridges, J., Clifford, S., Filiberto, J., . . . Newsom, H. (2012). Gale Crater: Formation and post-impact hydrous environments. *Planetary and Space Science, 70*(1), 84-95.

Shoval, S., Panczer, G., & Boudeulle, M. (2008). Study of the occurrence of titanium in kaolinites by micro-Raman spectroscopy. *Optical Materials, 30*(11), 1699-1705.

Tarte, P. (1967). Infra-red spectra of inorganic aluminates and characteristic vibrational frequencies of AlO4 tetrahedra and AlO6 octahedra. *Spectrochimica Acta Part A: Molecular Spectroscopy, 23*(7), 2127-2143.

Thomas, P., Ramakrishnan, V., & Vaidyan, V. (1989). Oxidation studies of aluminum thin films by Raman spectroscopy. Thin Solid Films, 170(1), 35-40.

Thompson, L., Schmidt, M., Spray, J., Berger, J., Fairén, A., Campbell, J., . . . Pradler, I. (2016). Potassium-rich sandstones within the Gale impact crater, Mars: The APXS perspective. *Journal of Geophysical Research: Planets, 121*(10), 1981-2003.

Tomaino, G. P. (1994). Qauntitative determination of quartz in calcite, dolomite, and talc by powder x-ray diffraction analysis. *Analytica chimica acta, 286*(1), 75-80.

Vaniman, D. T., Bish, D. L., Chipera, S. J., Fialips, C. I., William Carey, J., & Feldman, W. C. (2004). Magnesium sulphate salts and the history of water on Mars. *Nature, 431*(7009), 663-665.

Wang, A., Freeman, J. J., & Jolliff, B. L. (2015). Understanding the Raman spectral features of phyllosilicates. *Journal of Raman spectroscopy, 46*(10), 829-845. doi:10.1002/jrs.4680

Wang, A., Freeman, J. J., Jolliff, B. L., & Chou, I.-M. (2006). Sulfates on Mars: A systematic Raman spectroscopic study of hydration states of magnesium sulfates. *Geochimica et cosmochimica acta, 70*(24), 6118-6135.

Yen, A., Ming, D., Vaniman, D., Gellert, R., Blake, D., Morris, R., . . . Edgett, K. (2017). Multiple stages of aqueous alteration along fractures in mudstone and sandstone strata in Gale Crater, Mars. *Earth and Planetary Science Letters, 471*, 186-198.

Zorzano, M. P., Mateo-Martí, E., Prieto-Ballesteros, O., Osuna, S., & Renno, N. (2009). Stability of liquid saline water on present day Mars. *Geophysical Research Letters, 36*(20).

Supplementary Materials

	KGa-2 25°C		KGa-2 100°C	
Fluid	Si	Al	Si	Al
18.2 MΩ H_2O	31.72	13.21	9.25	24.64
NaCl $_{ns}$	10,406	11,389	7,382	27,114
10% NaCl	16,691	2,920	7,640	1,829
$Na_2SO_{4\ ns}$	8,731	12,133	11,427	26,987
10% Na_2SO_4	8,800	1,460	8,309	1,923
$CaCl_{2\ ns}$	4,926	6,178	2,645	21,363
10% $CaCl_2$	10,233	2,271	6,294	1,115
$MgCl_{2\ ns}$	3,598	11,175	1,894	25,586
10% $MgCl_2$	9,452	1,229	9,769	789
$MgSO_{4\ ns}$	2,200	12,465	2,680	27,361
10% $MgSO_4$	7,046	1,431	9,405	1,468
$NH_4Cl_{\ ns}$	Lost	Lost	10,175	31,241
10% NH_4Cl	18,444	4,691	8,084	1,769

Table A1. Silicon and Aluminum concentrations in ppb of the reacted brines for both low and high temperature experiments.

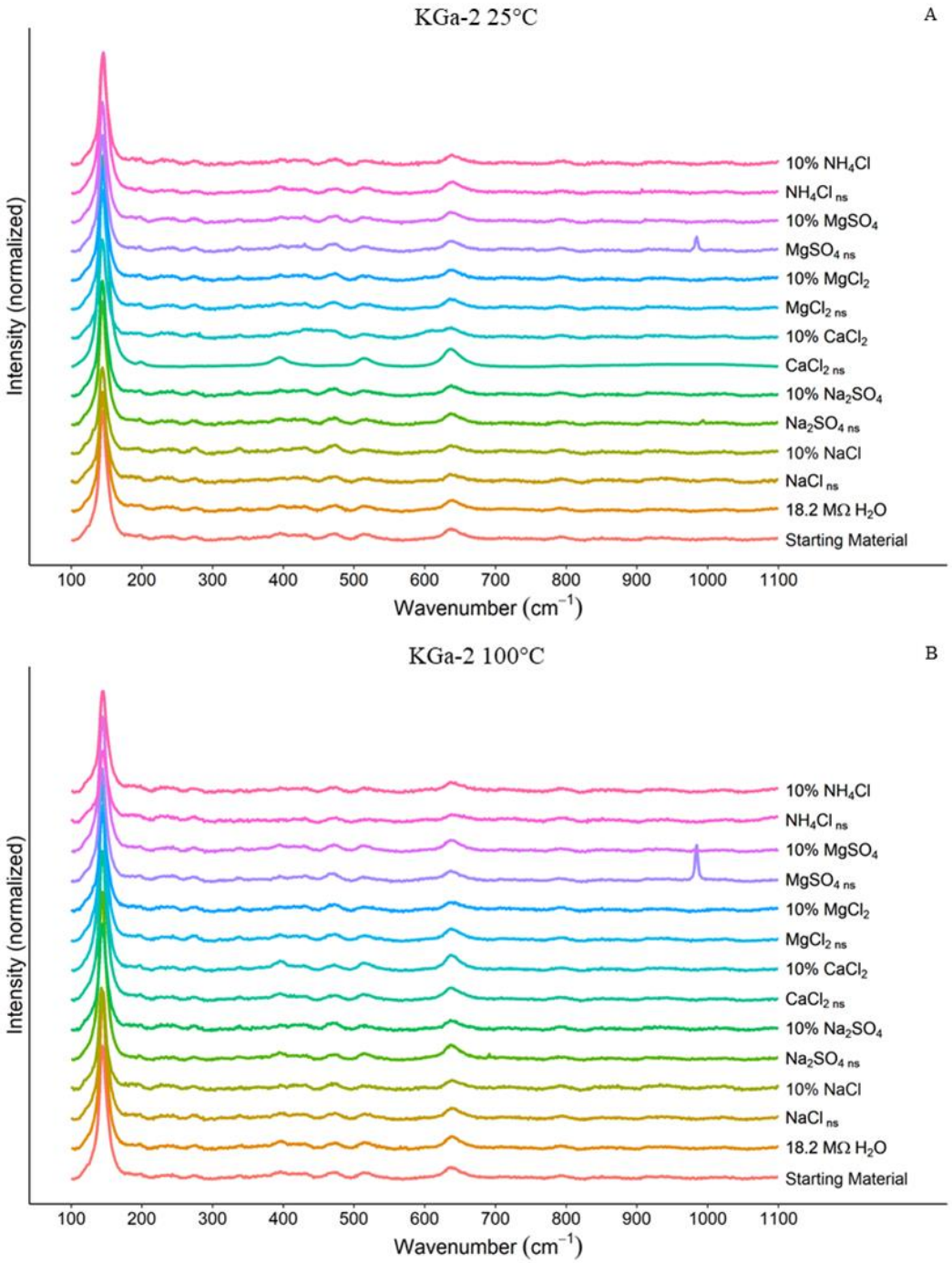

1786

1787 **Figure A1.** Raman spectra for KGa-2 experiments without a smoothing Savitzky-Golay filter. A)

1788 KGa-2 + brines reacted at 25°C. B) KGa-2 + brines reacted at 100°C.

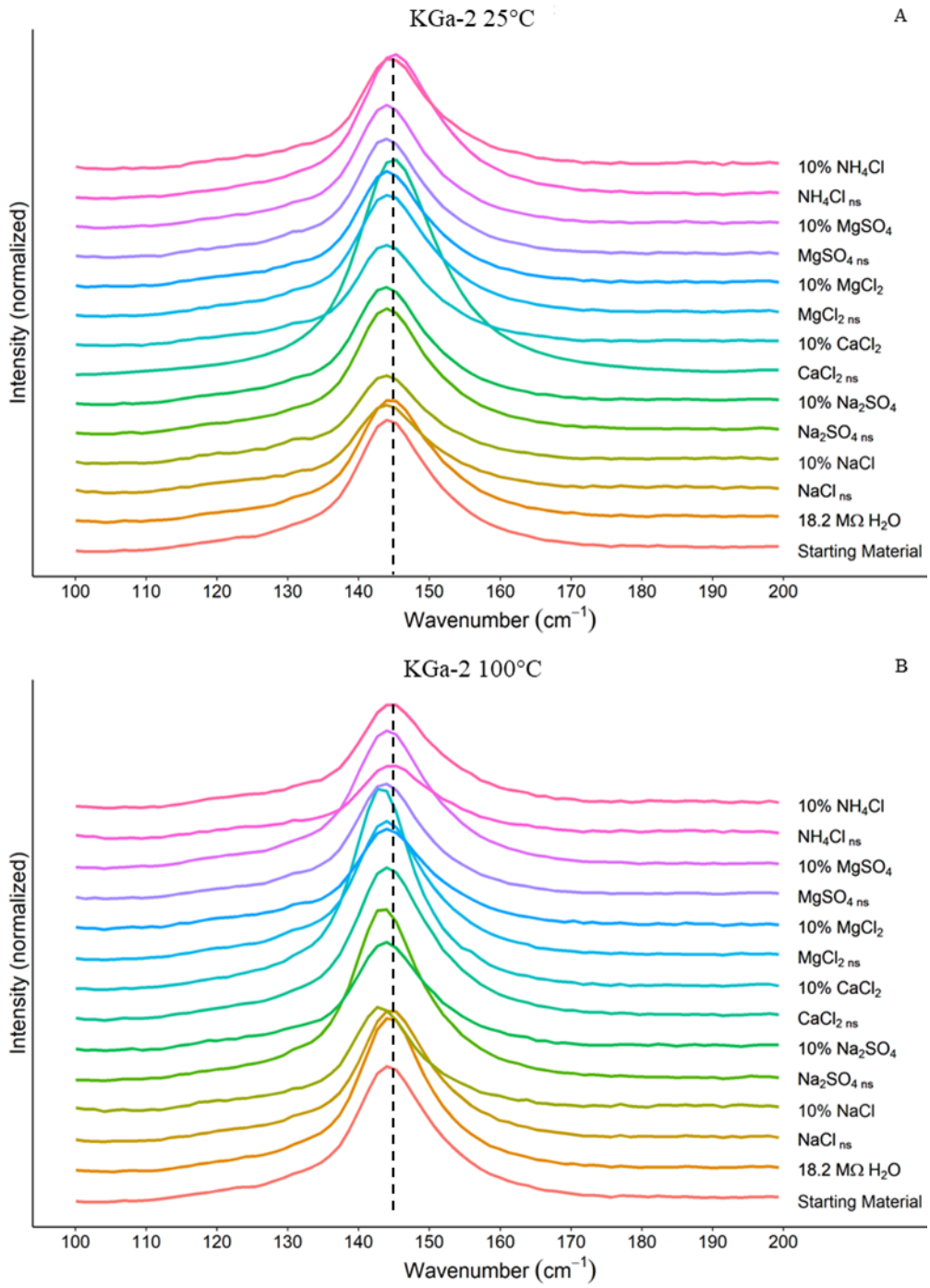

Figure A2. Close-up of 100-200 cm^{-1} region of Raman spectra for KGa-2 experiments without a smoothing Savitzky-Golay filter. A) KGa-2 + brines reacted at 25°C. B) KGa-2 + brines reacted at 100°C.

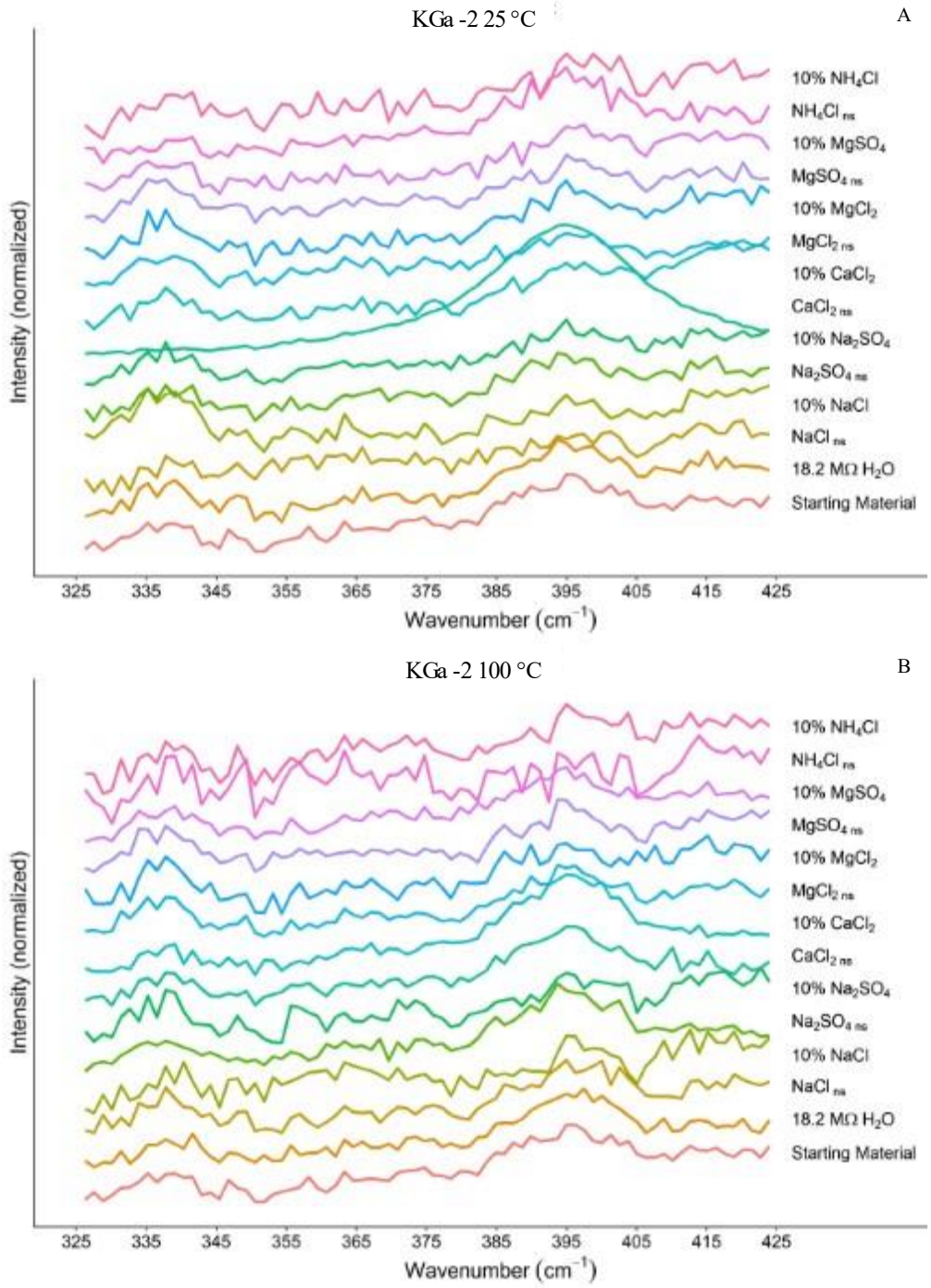

1793

1794 **Figure A3.** Close-up of 325-425 cm^{-1} region of Raman spectra for KGa-2 experiments without a

1795 smoothing Savitzky-Golay filter.. A) KGa-2 + brines reacted at 25°C. B) KGa-2 + brines reacted

1796 at 100°C.

Chapter 4. The Influence of Brines on Smectite Aqueous Alteration

Christopher Geyer[1], Andrew S. Elwood Madden[1,2], Caitlin Hodges[1], Janice L. Bishop[3], Megan Elwood Madden[1]

[1] School of Geosciences, University of Oklahoma, Norman, OK, USA

[2] Samuel Roberts Noble Microscopy Laboratory, University of Oklahoma, Norman, OK, USA

[3] SETI Institute and NASA Ames, Mountain View, CA, USA

Key Words: clay; alteration; mars; smectite, dissolution

Abstract

The interconnected evolution of brines and sediments on Mars have created a convoluted narrative in which smectites act as a main character. Aqueous alteration of Martian smectites by high salinity brines may have resulted in elemental partitioning or changes in secondary mineral formation not typically seen on Earth. This study investigated the aqueous alteration of two smectites, nontronite and montmorillonite, by a near-saturated as well as dilute NaCl, Na_2SO_4, $CaCl_2$, $MgSO_4$, $MgCl_2$ and NH_4Cl brines at 25°C and 100°C. Solid reaction products were analyzed using XRD and Raman spectroscopy, liquid samples were analyzed for elemental concentrations using ICP-OES. The results of this study indicate that both brine composition and concentration influence incongruent dissolution in smectites. Al/Si stoichiometric ratios for both nontronite and montmorillonite dissolution had moderate to strong correlation to H_2O activity. Patterns in Al/Si stoichiometric ratios were observed between the same brine reacted at different temperatures as well as between near-saturated/dilute brines reacted at the same temperature. The interdependence of brine composition, concentration, and temperature agree with similar studies that an ion pairing effect strongly influences incongruent dissolution of smectites. Disparate smectite dissolution pathways influenced by brines would have had an impact on Martian sediments, and as such should be taken into account when attempting to interpret Mars' paleoenvironments.

1. Introduction

Clay minerals, including smectites, provide critical clues informing our understanding of the Martian paleoclimate (Ehlmann et al., 2011). On Earth, clay alteration pathways and the factors which influence them are fairly well understood in dilute to saline waters. However, on planets and planetary bodies where the aqueous geochemical history significantly differs, additional alteration pathways may also be important (Grim, 1968; Wilson, 1999).

The identification of smectites in sedimentary contexts on Mars strongly implies that at some point the Martian hydrosphere was actively altering minerals (Bishop et al., 2008; Michalski & Noe Dobrea, 2007; Poulet et al., 2005). However, the Martian hydrosphere is complex, with a history of acidic and alkaline fluids, cyclical wetting and drying cycles, as well as geographically isolated depositional environments (Elwood Madden et al., 2009; Hurowitz et al., 2023; Rapin et al., 2019; Scheller et al., 2022; Squyres & Knoll, 2005; Yen et al., 2017). For example, sediments found in Gale Crater have abundant clays, likely deposited in a lacustrine environment and subsequently subjected to post-depositional aqueous alteration under acidic and arid conditions (Bristow et al., 2015; Bristow et al., 2021; Grotzinger et al., 2014; Schwenzer et al., 2012). Whereas, at Jezero crater, it has been inferred that carbonates may have been the result of alkaline fluids in a lacustrine environment (Horgan et al., 2020; Hurowitz et al., 2023).

Salts are also commonly observed in sediments and soils on Mars, including NaCl, Na_2SO_4, $MgSO_4$ as well as other sulfate, chloride, and perchlorate salts which have been detected on the Martian surface (Clark & Van Hart, 1981; Thomas et al., 2019; Vaniman et al., 2004). These salts are likely remnants of past aqueous systems. As the Martian hydrosphere shrank due to freezing and/or evaporation and fluids became more saline, their influence on aqueous alteration of clays would likewise have changed, a progression of alteration likely reflected in smectite

distribution and composition. In addition, periodic aqueous alteration by active aqueous fluids may still be occurring on Mars today (Chevrier et al., 2020; Möhlmann & Thomsen, 2011; Zorzano et al., 2009) via brines formed through the deliquescence of salts during periods of elevated relative humidity (Gough et al., 2014; Gough et al., 2017; Hecht et al., 2009).

Smectites, including saponite, nontronite, and montmorillonite as well as beidellite and hectorite, are the most common of several phyllosilicate phases observed on the surface of Mars and are thought to have formed due to in-situ aqueous alteration of Mars' basaltic crust (Bibring et al., 2006; Bishop, 2018; Bristow et al., 2015; Ehlmann et al., 2009; Rampe et al., 2020). Nontronite and montmorillonite were chosen for this study because they are useful in the interpretation of paleoenvironments as they are sensitive to the geochemical conditions in which they formed and/or were subsequently exposed to. For example, in well drained environments, montmorillonite will weather to kaolinite as soluble silica and base cations are leached from the soil, whereas in in dryer environments smectites tend to be stable, but slightly acidic soil conditions will ultimately alter to hydroxyl-interlayered smectite (Bergaya & Lagaly, 2013; McKinley et al., 1999). Aqueous alteration of smectites is complex, particularly considering that smectites exhibit high cation exchange capacity, where hydrated cations in the interlayer may exchange with cations in the fluids the clays are exposed to. For example, brines initially poor in Ca^{2+} content may have exchanged cations with clay-bound Ca^{2+} as the fluid percolated downwards, ultimately leading to gypsum precipitation on Mars (Nachon et al., 2014; Schwenzer et al., 2016).

The interaction between clays and brines is not straightforward, therefore spatially and temporally variable fluid chemistry may have left a complicated story imprinted within the sediments of Mars, partially decipherable through the alteration of smectites. For example, Al-

rich clays such as kaolinite and montmorillonite are frequently observed overlaying Fe-bearing nontronite in areas such as Mawrth Vallis (Bishop et al., 2008; Loizeau et al., 2007; Poulet et al., 2005), a stratigraphic relationship that could be the result of aqueous alteration by fluids with changing chemistry as the fluid percolated downwards. Previous studies suggest that the relatively fast dissolution rate of nontronite would result in preferential enrichment of montmorillonite and kaolinite in overlying units which had originally contained all three clays (Gainey et al., 2014).

In addition to the effects of evolving Martian fluid chemistry is the complex nature of smectite alteration itself. On Earth alteration of smectites and parent material typically produce secondary minerals such as illite and/or kaolinite during initial stages of incongruent dissolution and eventually progress towards more congruent dissolution (Cama et al., 2000; Li et al., 2020; Marty et al., 2011; Steiner et al., 2016). However, Miller et al. (2012) reported that nontronite dissolution in a KCl brine at temperatures up to 300°C produced celadonite rather than the expected illite and hypothesized that abundant Al relative to Fe is required for the formation of illite (Miller et al., 2012). Gorrepati et al. (2009) reported that brine composition and concentration influenced silica precipitation, which would influence smectite stability in those brines (Gorrepati et al., 2010).

Clearly, aqueous alteration of smectites is multifaceted, particularly in the context of Mars. However, the tools available to study clays on Mars are somewhat constrained compared to the wealth of analytical techniques available on Earth. Therefore, using a synthesis of analytical techniques currently available on Mars to analyze clay alteration products, paired with elemental analyses of brines reacted with smectites is needed to provide comparable data linking experimental studies and Martian paleoenvironments. This study characterizes secondary

reaction products formed via aqueous alteration of smectites in near-saturated and more dilute brines, then analyzes the products with Raman spectroscopy and XRD to better understand clay diagenesis and preservation on Mars and other salty planetary bodies using techniques currently available on Mars. By reacting concentrated and dilute brines with smectites at both low and elevated temperatures and characterizing both the resulting fluid and clay products, we aim to better understand of how phyllosilicates may have evolved on Mars, informing interpretations of paleoenvironments and the fate of water on Mars.

2. Materials & Methods

2.1 Experimental Overview

Two sets of experiments were performed using two different dioctahedral smectite standards purchased from the Clay Mineral Society (CMS), NAu-2 and SAz-1, each reacted with twelve brines. Nontronite "NAu-2" has been previously characterized as containing less than 6 weight percent of contaminants including anorthite, quartz, biotite, talc, and ilmenite (Keeling et al., 2000). We reduced the particle size by crushing the sample received from CMS in a mortar & pestle, then micronizing and sieving to obtain particles ≤0.63 μm for the experiments. The montmorillonite clay used in this study was "SAz-1" has been characterized elsewhere and contains contaminants including feldspar, quartz, and mica accounting for up to 2 weight percent (Chipera & Bish, 2001; Mermut & Cano, 2001; Mermut & Lagaly, 2001). Minimal processing of the SAz-1 standard was performed, only sieving to ≤0.63 μm to ensure particle sizes were uniform between the clays used. NAu-2 and SAz-1 were chosen for this study because both are well characterized and readily available, and as discussed previously, montmorillonite and nontronite are present on Mars. Both nontronite and montmorillonite are dioctahedral smectites which exhibit characteristic swelling and the ability to exchange interlayer cations. Their main

difference being the cation substituted for Al^{3+} in the octahedral layer; for nontronite it is Fe3+ whereas for montmorillonite it is Mg^{2+} (Essington, 2015).

Each clay-brine pairing was reacted at two different temperatures for different periods of time. Room temperature (25°C) experiments took place in 50 mL polypropylene centrifuge tubes, continuously shaken by an orbital shaker for 150 days. Experiments at 100°C were performed in high pressure PTFE lined vessels (Parr model 4744) and were shaken once every other day for 150 days and heated in a calibrated oven. We monitored the mass of all the experiments and noted no loss of material from any of the reactors. In both sets of experiments, we mixed 20 mL of de-oxygenated fluid with 2 g of clay. We de-oxygenated the fluids immediately prior to loading the reactors by bubbling N_2 gas through the brine at a rate of 15 mL/min for 20 min. At the end of each experiment set, the solid portion of the samples was separated from the liquid by four cycles of centrifugation (10,000 RPM for 20 min each), decanting, and rinsing with ultrapure water. The brine supernatant from the first centrifuge separation was acidified and refrigerated for elemental analysis. For the subsequent 3 rinse steps, 20 mL of 18.2 MΩ H_2O was added to the solid sample, the sample was disaggregated on a vortex mixer, then centrifuged. This rinse water was decanted, and the final rinsed solid sample was freeze dried using a Labconco freeze drier overnight. Once the solid sample was completely dry it was gently homogenized by hand using an agate mortar and pestle and stored for later analysis.

2.2 Brines

The brines reacted with each of the clay standards, NAu-2 and SAz-1, are listed in Table 1. For each reaction temperature both a concentrated brine (denoted with a “ns” for “near-saturated” in figures) and a dilute brine (denoted with a “10%” in figures) were reacted with each clay. Concentrated brines were created by adding ACS grade (>99.0 purity) salts to 18.2 MΩ

H_2O and allowing the mixture to equilibrate for 24 hours at room temperature; this was repeated until the solution was saturated and the salt no longer dissolved. Once the brine reached saturation, we filtered the solution using a 0.45 μm filter. Dilute concentrations of each brine were created by diluting the saturated brine to 10% its saturated concentration. Additionally, 18.2 MΩ H_2O was also reacted with the clays.

Brine	Near-Saturated Concentration (mol • kg^{-1})	Near-Saturated H_2O Activity	Dilute Concentration (mol • kg^{-1})	Dilute H_2O Activity
NaCl	6.2	0.79_a	0.6	0.98_a
Na_2SO_4	2.0	0.94_a	0.2	0.99_a
$CaCl_2$	6.7	0.43_a	0.7	0.97_a
$MgCl_2$	5.7	0.35_b	0.6	0.97_b
$MgSO_4$	2.9	0.92_b	0.3	0.99_b
NH_4Cl	7.1	0.77_c	0.7	0.98_c

Table 5. List of brines reacted with SAz-1 and NAu-2. Water activities calculated using a: (Guendouzi et al., 2003), b: (Ha & Chan, 1999), c: (Guendouzi et al., 2001). It is pertinent to note that all dilute brines have a H_2O activity >0.95, while all near-saturated brines have H_2O activities <0.95.

2.3 Analysis

Powder X-Ray Diffraction (XRD) and Raman spectroscopy were used to analyze the starting material and the reacted clay samples. Elemental compositions of the unreacted and reacted brines were also measured by Inductively Coupled Plasma – Optical Emission Spectrometry (ICP-OES).

XRD analyses were performed using a Rigaku SmartLab X-ray Diffractometer (Rotating anode Cu source, 45 kV, and 200 mA) with XRD data subsequently processed using MDI Jade Pro with the ICDD PDF4+ database. XRD patterns of both the starting material and brine-reacted SAz-1 and NAu-2 were acquired between 5-70 °2θ on oriented samples. For selected

clay-brine solid reaction products additional scans were collected between 2-35 °2θ for an ethylene glycol solvated and heat-treated (375°C for 24hr) subsample. XRD sample preparations followed methods described in Moore & Reynolds (1989). XRD patterns presented in this study are shown with normalized intensities, but no further processing was required.

For Raman analysis, a Renishaw InVia Raman microscope with a 500 mW 785 nm red laser and a 1200 l/cm grating, centered at 660 cm^{-1} was used to acquire spectra between 100 and 1100 cm^{-1}. Calibration was performed using an Si wafer producing a sharp band for Si at 520.6 cm^{-1}. Laser power was maintained at 5% to minimize sample heating and potential mineral degradation. For each sample, a repeat scan was acquired to ensure potential laser induced damage did not occur. Clay fluorescence was minimized by averaging 150 accumulated exposures of 1 second each to produce the final spectra. While clay hydration and interlayer chemistry are commonly characterized by Raman using the 3000-3800 cm^{-1} range of H_2O and OH vibrations, the focus of this study was to characterize alteration of the SAz-1 and NAu-1 such as changes in the octahedral silicate sheets, therefore we focused our Raman analyses on a range ≤1100 cm^{-1}, where the peaks are indicative of Si-O and metal bonds. Additionally, typically x-ray amorphous phases containing Al, Fe or Si commonly have peaks in the <1000 cm^{-1} regions. To facilitate interpretation of the Raman data, we processed the spectra by first removing baseline noise, then normalized and smoothed using a Savitzky-Golay filter. The ChemoSpec package in R was used for all spectra processing (Hanson, 2014). Unsmoothed versions of all Raman spectra used in this study are provided in the supplemental materials (S1).

Elemental magnesium, silicon, aluminum, and iron content within the reacted brines were quantified using a Thermo Fisher Scientific iCap Pro ICP-OES. Initial brine compositions were

also determined and were subtracted from the reported values for all samples to determine the solutes changes resulting from clay alteration within the fluid.

3. Results & Discussion

3.1 NAu-2-brine Experiments

Raman spectra produced by NAu-2-brine reactions are shown in Fig. 1. A duplicate figure that contains the raw spectra without smoothing is also provided in the supplemental material - Fig. A1. Previous studies characterizing the Raman spectra of nontronite, including NAu-2 specifically in some cases, have identified many of the peaks observable in Fig. 1 (Demaret et al., 2023; Frost & Kloprogge, 2000a, 2000b; Gibbons et al., 2020) (and references therein). Within the 25°C reactions two clay-brine reaction products contain significant intensities absent in the starting material. These reaction products were observed in the near-saturated Na_2SO_4 and dilute Na_2SO_4. Strong peaks at 459, 619/638, and 994/1008 cm^{-1} were observed in both of these experiments, which can be assigned v_2, v_4, and v_1/v_3 vibrations from residual SO_4^{2-} present in the reacted clay (Ben Mabrouk et al., 2013). In the 100°C spectra for NAu-2 reacted with saturated Na_2SO_4, an intense peak at 994 cm^{-1} can be attributed to v_2 vibrations of SO_4^{2-} (Ben Mabrouk et al., 2013). The presence of a triplet at ~600 cm^{-1} in both the 25°C and 100°C near-saturated Na_2SO_4 reacted NAu-2 samples is indictive of thenardite (Fig. 1).For convenience, RRUFF reference spectra for minerals of interest in this paper are provided in Fig. 2. As can be seen in Fig. 2, gypsum, thenardite and anhydrite have their most intense peak at ~1000 cm^{-1} as well as minor peaks in the 400-600 cm^{-1} range similar to near-saturated and dilute Na_2SO_4 reacted at 25°C and near-saturated Na_2SO_4 reacted at 100°C (Figs. 1 & 2). While some of the SO_4^{2-} peaks in the NAu-2 samples do not fall exactly on the same line as the reference sulfate minerals, it is

known that the cation present in the sulfate mineral will alter the peak location, with decreasing line position as the cation radius increases (Ben Mabrouk et al., 2013).

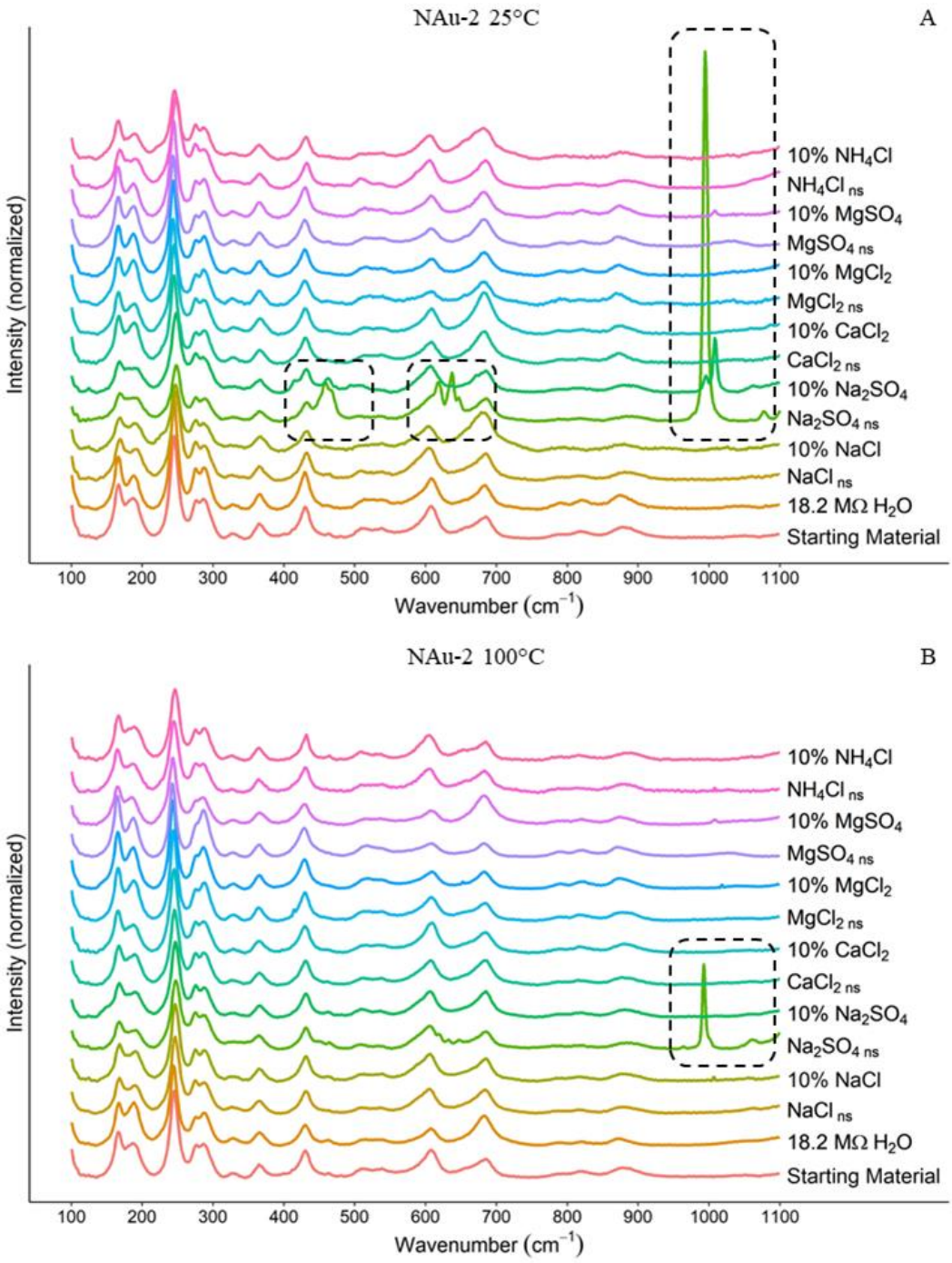

2003

2004 **Figure 11.** Raman spectra for NAu-2 experiments. A) NAu-2 + brines reacted at 25°C. B) NAu-

2005 2 + brines reacted at 100°C. Dashed boxes highlight specific peaks which are not characteristic

2006 of NAu-2; 459, 619, 638 cm^{-1}, and the 994 – 1008 cm^{-1} range which are all characteristic of

2007 SO_4^{2-}. For convenience, RRUFF reference Raman spectra for minerals of interest in this paper

are provided in the supplementary material Fig. 2. Major peaks for goethite (~450 cm^{-1}) and gibbsite (1050 cm^{-1}) are absent. We also did not observe any significant increase in the peaks indicative of SiO_2 (~200-500 and 800-1000 cm^{-1}) as a result of alteration.

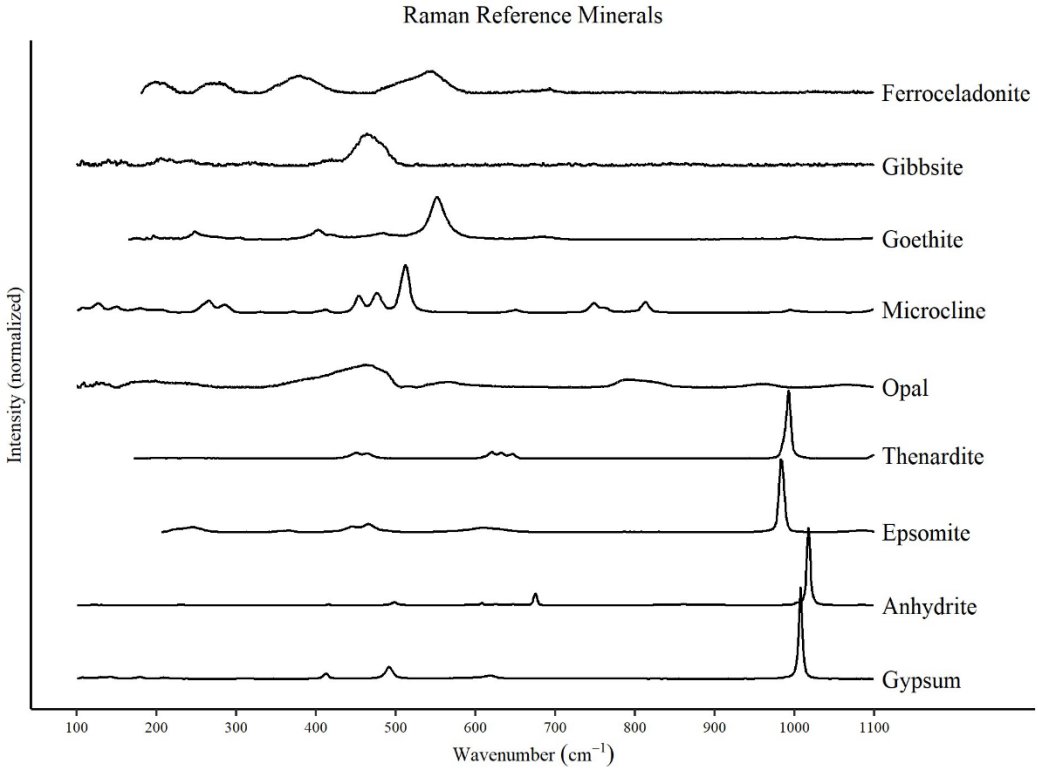

Figure 2. Raman spectra of some minerals discussed in this study. All spectra were retrieved from the RRUFF database (Lafuente et al., 2015). Opal is used in this instance to represent amorphous silica.

Analysis of the broad 5-70 °2θ NAu-2 25°C and 100°C XRD patterns confirms the presence of secondary minerals, notably sulfates (Fig. 3). Secondary minerals present include gypsum ($CaSO_4•2H_2O$), anhydrite ($CaSO_4$), hexahydrate ($MgSO_4•6H_2O$), thenardite ($Na_2SO)_4$, and halite (NaCl). The presence of hexahydrate, thenardite, and halite in samples reacted with $MgSO_4$, Na_2SO_4, and NaCl brines, respectively, indicates that the triple rinsing procedure was not entirely successful in removing the brine from the sample. However, the presence of Ca-sulfate

2021 secondary minerals in samples that were reacted with $MgSO_4$ and Na_2SO_4 brines indicates that
2022 calcium was present during the reaction. In the 25°C and 100° NAu-2 experiments Ca-sulfates
2023 were observed in both near-saturated and dilute $MgSO_4$ and Na_2SO_4 clay-brine reactions, The
2024 presence of Ca-sulfate secondary minerals can be explained by cation exchange between the
2025 reacting brine and NAu-2 (Geyer et al., 2023).

2026 The conspicuous absence of a diffraction peak at ~12.4 °2θ or 25 °2θ in Fig. 3 rules out the
2027 possibility of kaolinite formation as a result of the clay-brine weathering at the temperatures and
2028 timescales tested here. Steiner et al also identified goethite (FeO(OH)) as a likely secondary
2029 mineral resulting from incongruent nontronite dissolution (Steiner et al., 2016). However, for this
2030 study, we did not observe any evidence of goethite in either the Raman spectra (goethite peaks
2031 expected ~400 cm^{-1} and ~450 cm^{-1}, Fig. 1) or the XRD patterns (goethite peaks expected at
2032 21.26, 36.68, and 33.24 °2θ, Fig. 3) (Demaret et al., 2023).

2033 NAu-2 is a natural sample and may have some Ca^{2+} in the interlayer as well as known
2034 contaminants including anorthite ($CaAl_2Si_2O_8$- ~10 wt%) and calcite ($CaCO_3$- ~1 wt%))
2035 (Gibbons et al., 2020; Keeling et al., 2000). The conspicuous peak shifts observed in the low
2036 angle <15 °2θ region of the diffraction data for both the 25°C and 100°C reactions (Fig. 3) are
2037 due to changes in the d(001) basal spacings and are likely the result of cation exchange. The 001
2038 basal reflection is significantly influenced by the hydration state of the clay as well as the
2039 specific interlayer cation present. The NAu-2 clays were prepared identically and were exposed
2040 to the same level of relative humidity during analysis, thus the differences in the 001 peak °2θ
2041 positions are more likely indicative of differences in interlayer cations than changes in the
2042 interlayer spacing due to hydration alone (Chipera & Bish, 2001; Moore & Reynolds Jr, 1989).
2043 Generally speaking, d-spacings of the 001 basal reflection decrease (increasing °2θ) as the

hydrated radii of the interlayer cation decreases; with generalized °2θ peak positions for a smectite with a particular interlayer cation as follows: Ca^{2+} ≈ 5.7 Å, Mg^{2+} ≈ 6.0 Å, Na^{+} ≈ 7.2 Å, and NH_4^{+} ≈ 7.3 Å (Ayari et al., 2007). The location of the starting material 001 peak suggests the dominance of Ca^{2+} in the interlayer whereas the 001 peak locations observed in the reacted samples typically reflect cation exchange with the brine it was reacted with (Fig. 3). In the 20-30 °2θ range, complexity arises from varying intensities of peaks typical of contaminant minerals present in the starting material. Known contaminants in NAu-2 such as anorthite, quartz, mica, and others are notoriously difficult to remove, and some samples exhibit increased intensities of peaks associated with these minerals. The increased presence of the contaminant minerals for some samples and not others may be a result of particle size fractionation during crushing and weighing out of the individual samples.

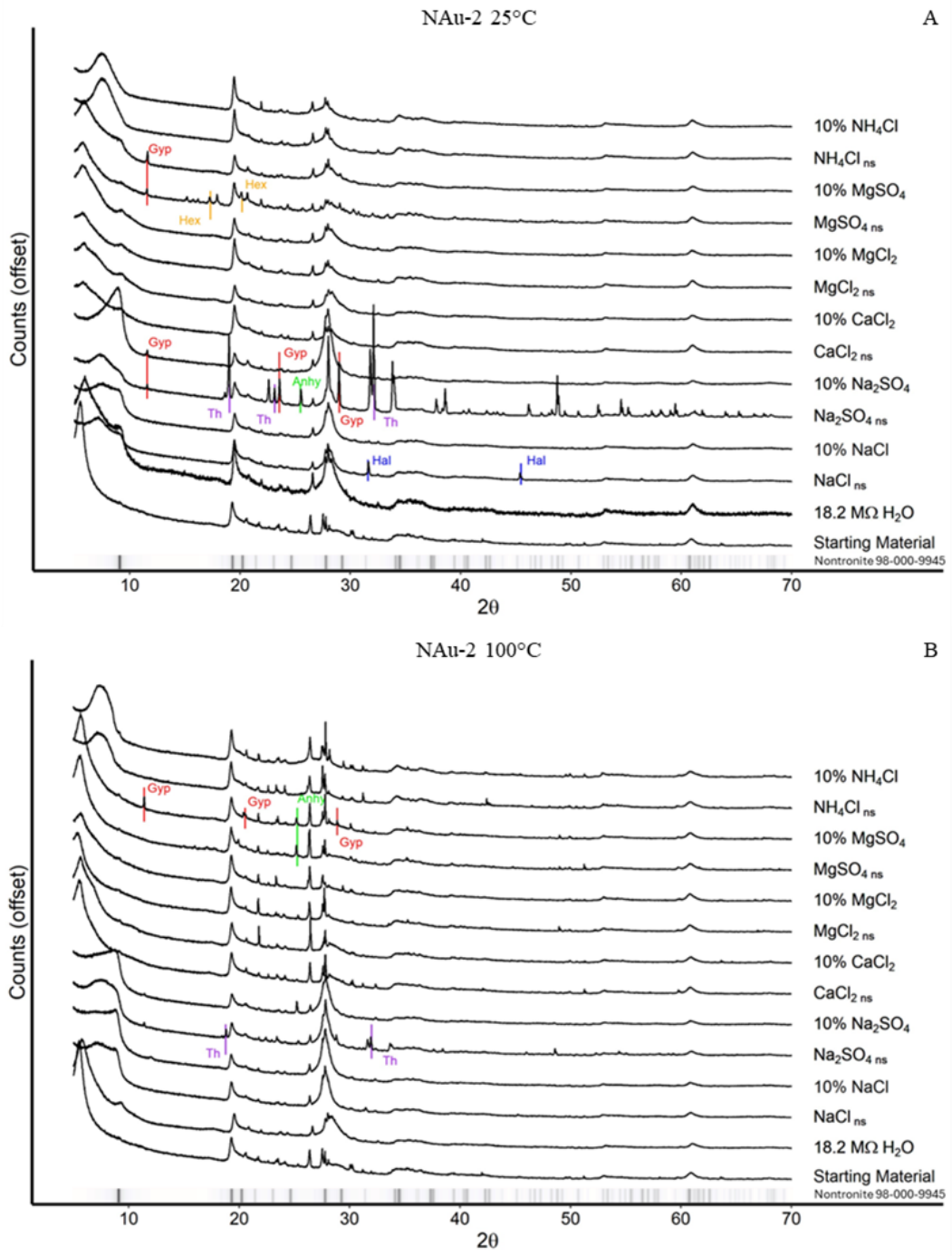

2055

2056 **Figure 3.** XRD Patterns for NAu-2 experiments. The ribbon at the base of each graph represents

2057 the primary intensities for nontronite (98-000-9945). A) NAu-2 + brines reacted at 25°C. B)

2058 NAu-2 + brines reacted at 100°C. Shifts in the 5-12 °2θ are attributed to changes in the interlayer

2059 spacing as a result of cation exchange. Changes observed in the 20-30 °2θ are attributed to either

evaporative minerals from residual brine or heterogenous inclusion of trace phases typically found in NAu-2. The most intense peaks for the minerals resulting from residual brine evaporation are indicated with vertical lines. “Gyp” = Gypsum, “Hex” = Hexahydrate, “Th” = Thenardite, “Anhy” = Anhydrite, “Hal” = Halite, and “An” = Anorthite

Not all the low angle <15 °2θ peaks observable in Fig. 3 are clear cut examples of simple cation exchange-- many exhibit severe peak broadening or double peaks. To elucidate the cause, several samples underwent ethylene glycol solvation and heat treatment to identify potentially interstratified clay minerals (Figs. 4 & 5).

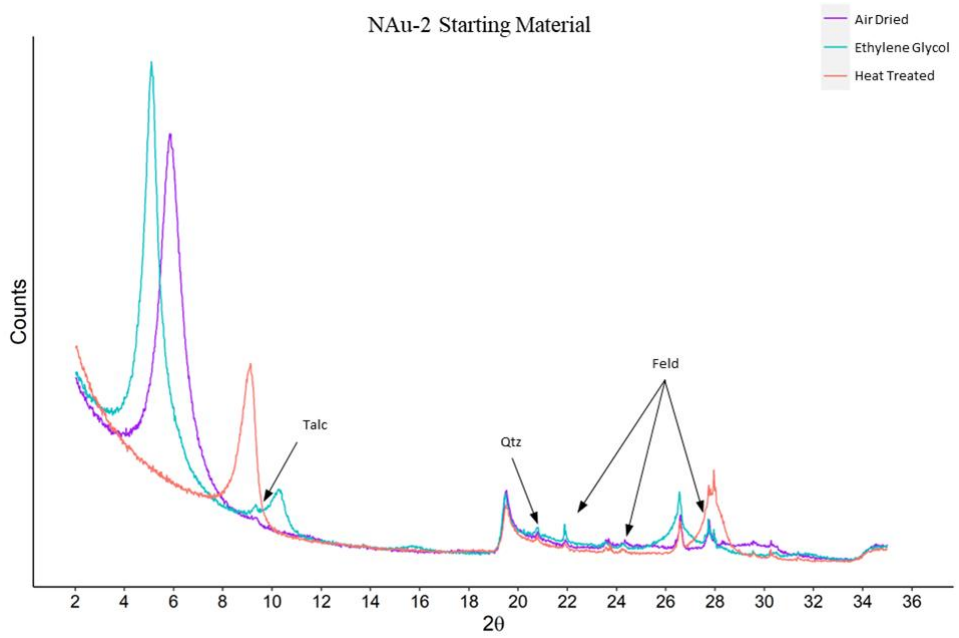

Figure 4. Air Dried, Ethylene Glycol, and Heat Treated XRD patterns for NAu-2 starting material. Known contaminants feldspar (“Feld”), talc and quartz (“Qtz”) indicated by arrows. The basal 001 reflection exhibits a d-spacing decrease (shift in peak from 4.5 to 9 °2θ) due to removal of H_2O in the interlayers in the heated sample. No illite or kaolinite was detected in the starting material.

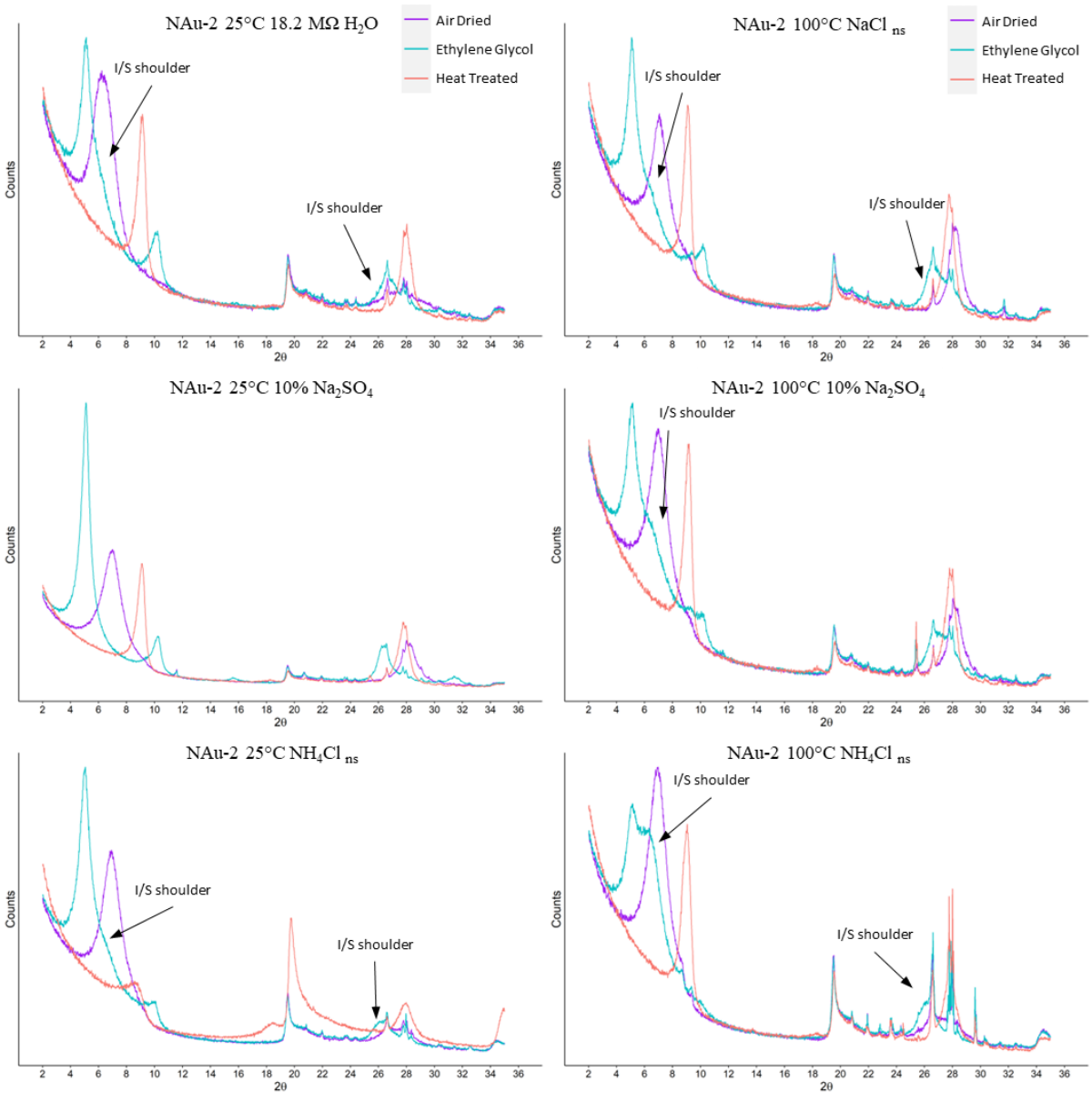

Figure 5. Air Dried, Ethylene Glycol, and Heat Treated XRD patterns for select NAu-2 clay-brine reaction products. "I/S" illite/smectite shoulders indicated with arrows for all samples except 25°C 10% Na_2SO_4, which showed no indication of I/S. In general, 100°C samples exhibited more intense I/S shoulders than samples reacted at 25°C.

While the 2-35 °2θ XRD patterns for ethylene glycol and heat treated NAu-2 starting material contained evidence of talc, feldspar, and quartz, known impurities within the clay

standard, it did not contain other expected impurities- neither illite nor kaolinite were detected in the starting material (Fig. 4). Of the 25°C NAu-2-brine experiments, 18.2 MΩ H_2O, dilute Na_2SO_4 and near-saturated NH_4Cl received ethylene glycol solvation and heat treatment. Of the 100°C experiments near-saturated NaCl, dilute Na_2SO_4 and near-saturated NH_4Cl received ethylene glycol solvation and heat treatment. The presence of shoulders at ~6.6 °2θ and ~26.3 °2θ in the ethylene glycol treated samples and a peak at ~18.6 °2θ in the heat treated samples provides evidence of illite in several of the reaction products (Moore & Reynolds Jr, 1989; Środoń, 1980). Of the 25°C samples which underwent ethylene glycol solvation and heat treatment, both the 18.2 MΩ H_2O and near-saturated NH_4Cl experiments produced mixed-layer illite/smectite, however, dilute Na_2SO_4 did not. All three of the 100°C samples which underwent ethylene glycol solvation and heat treatment (near-saturated NaCl, dilute Na_2SO_4 and near-saturated NH_4Cl) produced diffraction patterns indicative of mixed-layer illite/smectite. Moore & Reynolds Jr (1989) suggest using the reflections at ~10 °2θ and ~16.5 °2θ and their difference (°Δ2θ) to calculate the percent illite. Unfortunately, the reflections at ~16.5 °2θ for these samples are of such low intensity the accuracy of such a calculation would be questionable. However, the extremely low response at ~16.5 °2θ suggests that the portion of illite in the mixed-layer portion of illite/smectite is significantly lower than 10%. The significance of temperature is apparent when comparing the 25°C and 100°C ethylene glycol solvated XRD patterns of dilute Na_2SO_4 reacted clays, where illite formed in the higher temperature experiment, but is undetectable in the lower temperature experiment (Fig. 5).

We also monitored smectite dissolution and/or alteration by comparing the Si, Al and other cations released to solution (Cappelli et al., 2018). Examining the elemental abundances in the reacted brines confirms that incongruent dissolution is occurring, including alteration of

nontronite to illite $(K,H_3O)(Al,Mg,Fe)_2(Si,Al)_4O_{10}[(OH)_2,(H_2O)]$ as evidenced by the glycolated and heat treated XRD analyses. Previous studies have compared the ratios of Fe/Si in the reacted fluids to their stoichiometric ratio in the clay to determine dissolution rates (Gainey et al., 2014; Steiner et al., 2016). While we did not collect time series data needed to quantify alteration rates, these comparisons can help us elucidate different dissolution mechanisms and processes that may be occurring in the different solutions. To simplify interpretation of elemental ratios we calculated the "stoichiometric ratio" which is the ratio of two elements in the reacted brine compared to their stoichiometric ratio in the clay (Eqn. 1), the results of these calculations for NAu-2, using the structural formula $M^+_{0.72}(Si_{7.55}Al_{0.45})(Fe_{3.83}Mg_{0.05})O_{20}(OH)_4$ from Keeling et al (2000), where Si/Al = 16.8, are presented in Table 2. 'M^+' represents cations such as K^+, Na^+, or Ca^{2+} present in the interlayer. Keeling et al. (2000) reported a minor K^+ component in NAu-2 which may provide a source of K^+ required if illitization were occurring.

Equation 1: $$Stoichiometric\ ratio = \frac{A_{aq}/B_{aq}}{A_{clay}/B_{clay}}$$

Brine	25°C Fe/Si	25°C Fe/Al	25°C Al/Si	100°C Fe/Si	100°C Fe/Al	100°C Al/Si	H_2O Activity
18.2 MΩ H_2O	0.72	0.73	0.99	0.03	0.63	0.05	1
NaCl $_{ns}$	0.04	0.01	5.52	0.08	0.00	30.51	0.79
NaCl $_{dilute}$	0.01	0.01	1.01	0.02	0.01	2.57	0.98
Na_2SO_4 $_{ns}$	0.04	0.01	7.50	0.29	0.03	11.22	0.94
Na_2SO_4 $_{dilute}$	0.13	0.07	1.72	0.03	0.03	0.85	0.99
$CaCl_2$ $_{ns}$	0.08	0.01	11.68	0.06	0.01	9.79	0.43
$CaCl_2$ $_{dilute}$	0.01	0.00	1.87	0.03	0.07	0.42	0.97
$MgCl_2$ $_{ns}$	0.09	0.01	16.64	0.08	0.00	19.14	0.35
$MgCl_2$ $_{dilute}$	0.01	0.00	1.83	0.00	0.01	0.62	0.97
$MgSO_4$ $_{ns}$	0.24	0.01	17.91	0.02	0.00	5.50	0.92
$MgSO_4$ $_{dilute}$	0.01	0.00	1.99	0.00	0.00	0.33	0.99
NH_4Cl $_{ns}$	0.03	0.01	6.40	0.02	0.00	4.63	0.77
NH_4Cl $_{dilute}$	0.05	0.03	1.37	0.00	0.00	0.35	0.98
Spearman's Coefficient	0.01	0.37	-0.82	-0.44	0.50	-0.82	

Table 6. Stoichiometric ratios calculated using Fe, Si, and Al abundances in brines reacted with NAu-2 at 25°C and 100°C. Green highlighted values are below the stoichiometric ratio, gold highlighted values are above the stoichiometric ratio, and blue highlighted values are within 5% of the stoichiometric ratio for NAu-2 raw aqueous concentrations. The Spearman's coefficients for each stoichiometric ratio compared to the H_2O activity of the reacting brine indicate the degree of correlation with respect to the activity of water in the initial brine.

Stoichiometric ratios that deviate from 1 indicate either incongruent dissolution or non-stoichiometric dissolution, or a combination of both. Incongruent dissolution here is defined as the dissolution of one mineral with the concurrent precipitation of a secondary mineral; non-stoichiometric dissolution is defined here as the preferential leaching of one element over another from the mineral structure during dissolution. Stoichiometric ratio values less than 1 indicate either the formation of secondary minerals incorporating element A, or preferential leaching of element B; while values over 1 indicate formation of secondary minerals containing

B or preferential leaching of A. All reacted brines for both the 25°C and 100°C NAu-2 reactions had Fe/Si and Fe/Al stoichiometric ratios less than 1 (Table 2) indicating either the precipitation of a secondary Fe-rich phase or the preferential leaching of Si and Al over Fe for NAu-2. Similarly, Steiner et al. (2016) also reported Fe/Si ratios in solution below the Fe/Si nontronite stoichiometric ratio when reacting nontronite with chloride brines. They interpreted these lower than stoichiometric ratios as indicating incongruent dissolution and precipitation of Fe-bearing secondary minerals, as confirmed via synchrotron XRD analyses that found goethite in addition to nontronite in their reacted samples. However, iron oxide phases were not observed in any of the reacted clay solids produced in this study with either Raman (226, 292, and 413 cm^{-1}) or bulk powder XRD analyses (21.3, 36.7 and 33.2 °2θ). Thus, regardless of temperature, brine composition or concentration, Fe is preferentially retained by NAu-2 over Si and Al during dissolution in the experiments performed in this study. In addition, Fe/Si or Fe/Al stoichiometric ratios also appear to be independent of the activity of water, as indicated by the low Spearman's coefficients reported in Table 2. Steiner et al. (2016) also observe a linear, negative relationship between dissolution rates and the activity of water within the brines tested (Steiner et al., 2016).

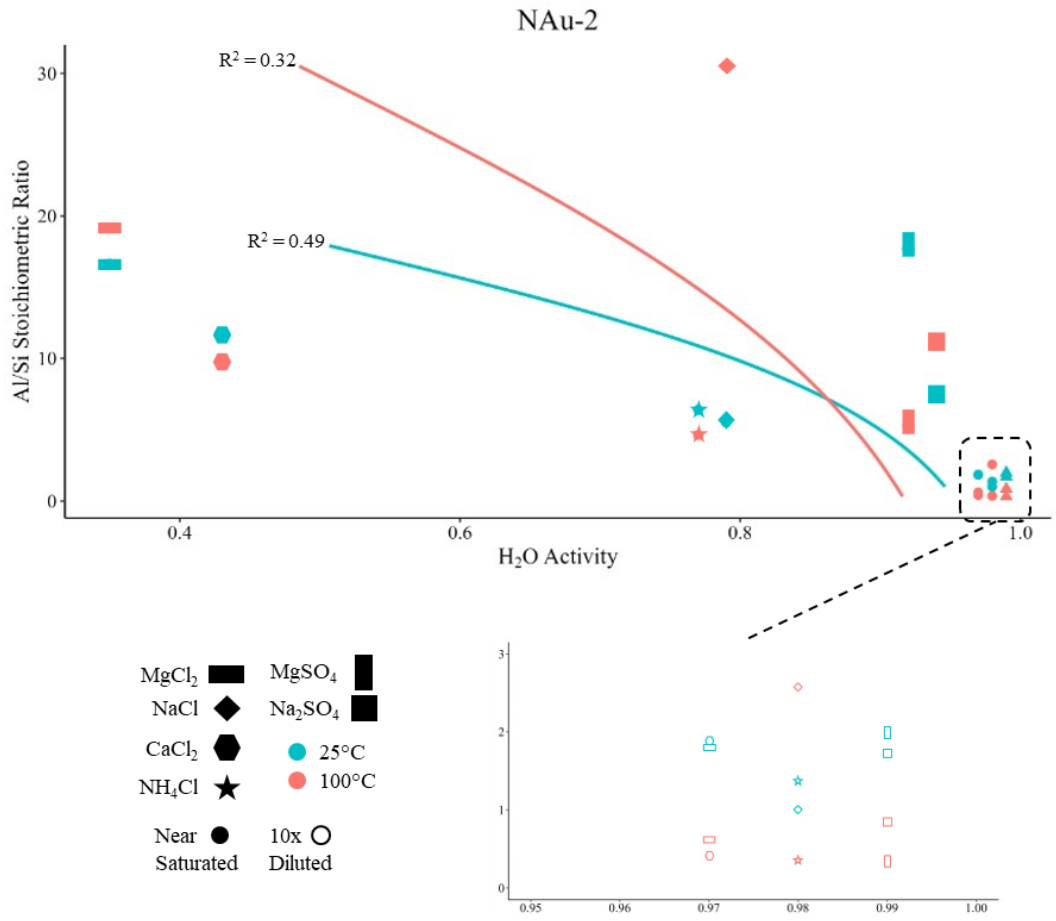

2145

2146 **Figure 6**. Al/Si stoichiometric ratio vs H_2O Activity for NAu-2 25°C and 100°C experiments;
2147 blue triangles represent brines reacted at 25°C and orange circles indicate brines reacted at
2148 100°C. The dashed box highlights the range corresponding to the 0.9-1.0 activity of water.
2149 McFadden pseudo R^2 = 0.49 for samples reacted at 25°C (blue dashed line). McFadden pseudo
2150 R^2 = 0.32 for samples reacted at 100°C (orange dashed line).

2151 While Fe stoichiometric ratios are uniformly below 1 for all brines reacted with NAu-2 at
2152 25°C and 100°C, the Al/Si stoichiometric ratio was either near 1 or significantly above 1 for all
2153 brines reacted at 25°C and all near-saturated brines reacted at 100°C. Al/Si stoichiometric ratios
2154 above 1 indicate either preferential leaching of Al from NAu-2, or Si removal due to
2155 precipitation of secondary phases. Preliminary modeling using PHREEQC (phreeqc database,

25°C/100°C, pH = 7, balance on Cl^-) predicts that all 25°C reacted brines were saturated with respect to quartz, but undersaturated with respect to amorphous silica, and all 100°C reacted brines were undersaturated with respect to quartz and amorphous silica (supplementary material Table A3.) (Parkhurst & Appelo, 2013). However, none of the clays reacted at 25°C had significantly increased intensities for peaks associated with quartz in either the Raman (~470 cm^{-1}) or XRD patterns (20.8°, 26.7°, and 50.2° 2θ) relative to the starting material.

Incongruent dissolution of nontronite with precipitation of illite, as indicated by the glycolated and heat treated XRD analyses (Fig. 5), would lead to excess Si in the remaining solids. Indeed, Al/Si stoichiometric ratios for almost all the 25°C experiments, and all the near-saturated 100°C experiments are greater than 1, indicating preferential release of Al to solution and/or precipitation of Si-rich solids. However, a previous study examined smectite dissolution in 1M KCl solutions at 200°C and found that as illitization occurred Si concentrations in the reacting fluid also increased, however they did not report Al concentrations (Mills et al., 2023). Mills et al. (2023) postulated that edge dissolution of the octahedral and tetrahedral layers was occurring, producing $SiO_{2(aq)}$ as illite was forming. While Mills et al. (2023) did not report aqueous Al concentrations, precluding a stoichiometric ratio analysis, the $SiO_{2(aq)}$ concentrations reported in their 200°C experiments are at least two orders of magnitude higher than those observed in the 100°C experiments reported here. Therefore, as indicated by the Al/Si stoichiometric ratios, the reaction mechanism for NAu-2 incongruent dissolution may not be consistent with respect to brines of different compositions and concentrations.

While illite is a common alteration product formed from smectite alteration, ferroceladonite $K(Al, Fe^{3+})(Fe^{2+}, Mg)Si_4O_{10}(OH)_2$ has also been observed forming as a result of dissolution of nontronite in KCl brines at 250°C and 100°C (Miller et al., 2012). The formation of

ferroceladonite rather than illite would explain why, in the reacted brines, Fe/Si and Fe/Al stoichiometric ratios were less than 1 while Al/Si ratios were greater than 1. In ferroceladonite, considerable Fe substitution for Al in the octahedral layer occurs whereas the tetrahedral layer consists of Si almost exclusively; therefore, if ferroceladonite were forming we would expect lower Fe/Al stoichiometric ratios as Fe from the nontronite substitutes for Al in the forming 10 Å clay. The presence of ferroceladonite rather than illite would also explain the rather low intensity XRD response at ~16.5 °2θ as ferroceladonite exhibits a weak 002 reflection owing to the presence of octahedral iron (Moore & Reynolds Jr, 1989).

Ferroceladonite is traditionally thought to be a product of hydrothermal alteration of basalt and is occasionally observed with nontronite; however, there is evidence that ferroceladonite may precipitate directly from solution or transformation of an Fe-smectite such as nontronite (Meunier et al., 2010; Miller et al., 2012; Polgári et al., 2013) However, the mechanism of ferroceladonite genesis as well as the methods used for its detection are ambiguous. For instance, in ferroceladonite XRD patterns, the 060 reflection is typically given as 1.51 Å (61.4 °2θ) and is linearly correlated with the Fe^{3+} octahedral content, however the use of 060 as an identifying characteristic of ferroceladonite has been disputed (Buckley et al., 1978; Weiszburg et al., 2004). Additionally, the characteristic Raman spectrum of ferroceladonite (Fig. 2) exhibits three primary broad peaks around 300, 400, and 520 cm^{-1}. Neither the 25°C nor the 100°C brines reacted with NAu-2 exhibited significant increases in Raman signal at the aforementioned wavenumbers with respect to the NAu-2 starting material. Similarly, the low intensity seen at ~16.5 °2θ may be the result of ferroceladonite or a result of illite in such small quantities that its 002 intensity is negligible in the XRD patterns acquired in this study. Thus, if ferroceladonite

rather than illite is present in the reacted NAu-2 solids, additional analyses such as infra-red spectrometry or electron microscopy would be required for definitive resolution.

The activity of water appears to directly affect Al/Si ratios observed in the solid and aqueous reaction products for both the 25°C and 100°C reacted NAu-2 brines. Across both temperatures, the aqueous Al/Si stoichiometric ratios observed in the near-saturated brines are consistently higher than their diluted counterparts. The significant differences between near-saturated and dilute Al/Si stoichiometric ratios suggests that preferential Al leaching or Si precipitation is more intense in concentrated brines. A significantly different reaction pathway may be responsible for producing the striking difference in Al/Si stoichiometric ratios. The effects of ionic strength on Al-containing mineral solubilities have been previously studied, and found that Al^{3+} mobility increases with increasing ionic strength NaCl brines (Palmer et al., 2001). On the other hand, silica precipitation was also found to accelerate in brines, thus removing Si from solution, and that different salts impacted silica precipitation to differing extents (Gorrepati et al., 2010). Both Palmer et al (2001) and Gorrepati et al. (2010) posited that ion pairing effects were responsible for enhanced Al^{3+} mobility and silica precipitation in high ionic strength solutions. In our experiments which produced incongruent dissolution of NAu-2, ion pairing effects could explain the increased Al/Si stoichiometric ratios in near-saturated brines as well as the complicated effects of temperature, along with brine composition and concentration on aqueous solute composition.

In addition, the variations we observed in Al/Si with brine composition and concentration are also noteworthy. While the linear relationships observed between Al/Si ratios and H_2O activity were found to be statistically significant ($\alpha = 0.05$) based on the Spearman's coefficient, the composition of the brine also appears to play an important role beyond the activity of water

(Figure 6). If incongruent dissolution and illite precipitation were only dependent on activity of water and independent of brine composition, then we would expect similar Al/Si stoichiometric values between brines with comparable H_2O activities at the same temperature. In the 25°C reaction, brines with divalent cations had higher Al/Si stoichiometric ratios than brines with monovalent cations. However, in the 100°C reaction no clear pattern was apparent between divalent and monovalent cation brines. The correlation between H_2O activity and Al/Si stoichiometric ratios as well as the presence of illite in some of the subsamples suggests that brine composition and concentration, possibly through ion pair effects, strongly influence incongruent dissolution of NAu-2.

3.2 SAz-1-brine Experiments

Raman spectra produced by the SAz-1–brine reactions are shown in Fig. 7; a duplicate figure showing the results without smoothing is provided in the supplemental material (Fig. A2). These spectra (Fig. 7) share many of the peaks (~190, 250-300, ~420, and ~700 cm^{-1}) associated with SAz-1 in other studies (Bishop & Murad, 2004; Demaret et al., 2023; Wang et al., 2015). Of the 25°C reactions, only the sample reacted with near-saturated $CaCl_2$ contains peaks not typically attributed to montmorillonite; a peak at 218 cm^{-1} which is commonly attributed to Ca-Cl vibrations as well as a shifted peak and increase in intensity at 283 cm^{-1} associated with Ca-O vibrations (Uriarte et al., 2015). Of the 100°C reactions, samples reacted with near-saturated Na_2SO_4, near-saturated $MgSO_4$, and dilute $MgSO_4$ had strong peaks at 415 – 495 cm^{-1}, 619 – 638 cm^{-1}, and 994 – 1008 cm^{-1} which can be attributed to *v2*, *v4*, and *v1/v3* vibrations from residual SO_4^{2-} present in the reacted clay (Ben Mabrouk et al., 2013; Wang et al., 2006). The peaks indicative of Ca–Cl bonds in the 25°C near-saturated $CaCl_2$ reacted SAz-1 as well as the hydrated SO_4^{2-} peaks in the 100°C near-saturated Na_2SO_4, near-saturated $MgSO_4$, and dilute

2247 $MgSO_4$ reacted SAz-1 suggest that the triple rinse procedure was not effective at removing all of
2248 the excess brines prior to drying the sample. Additionally, a small peak at ~513 cm^{-1} can be
2249 assigned to potassium feldspar which is a known contaminant in SAz-1 (microcline is provided
2250 as the reference potassium feldspar in Fig. 2).

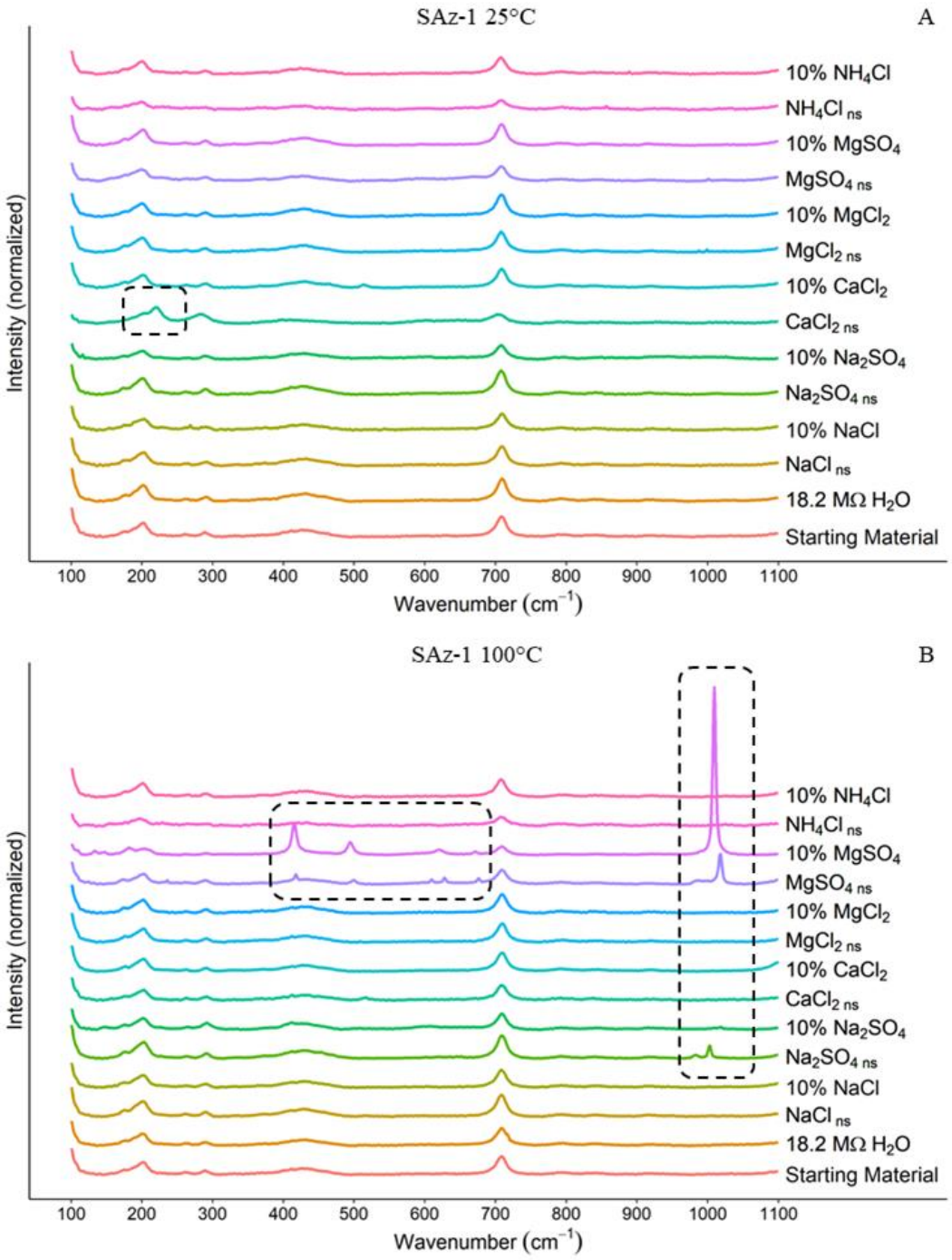

2251

2252 **Figure 7.** Raman spectra for SAz-1 experiments. A) SAz-1 + brines reacted at 25°C. B) SAz-1 +

2253 brines reacted at 100°C. Dashed boxes highlight specific peaks which are not characteristic of

2254 SAz-1: in Fig. 7A 218 cm^{-1} (Ca-Cl), in Fig. 7B 459, 619 – 638 cm^{-1} (SO_4^{2-}), and the 994 – 1008

2255 cm^{-1} range (also SO_4^{2-}). For convenience, RRUFF reference spectra for minerals discussed in this

paper are provided in Fig. 2. Major peaks for goethite (~450 cm^{-1}) and gibbsite (1050 cm^{-1}) are absent. We also did not observe any significant increases in the intensity in the peaks indicative of SiO_2 (~200-500 and 800-1000 cm^{-1}).

The 5-70 °2θ XRD patterns for the 25°C and 100°C SAz-1 brine reacted SAz-1 samples are presented in Fig. 8. The unreacted SAz-1 "starting material" strongly resembles patterns obtained in previous studies of SAz-1, with the notable exception being that the smectite 001 basal reflection in this study is at 16.0 Å (5.52 °2θ) compared to the typical 13.3 Å (6.63 °2θ) for SAz-1 (Fi. 6)(Chipera & Bish, 2001). As discussed above in our interpretation of the NAu-2 experiments, the smectite basal spacing is highly sensitive to the interlayer cation present as well as the relative humidity at the time of analysis. Within the reacted samples, sulfate phases observed in the Raman spectra are confirmed by several secondary minerals evident in the XRD patterns, including gypsum ($CaSO_4•2H_2O$), anhydrite ($CaSO_4$), and thenardite (Na_2SO_4). Secondary sulfate minerals were only observed in the Na_2SO_4 experiments at 25°C, which contained traces of gypsum. However, reactions carried out at 100°C produced considerably more complex secondary mineral assemblages. Both the near-saturated and dilute Na_2SO_4 brine experiments at 100°C contain gypsum. Near-saturated Na_2SO_4 also contained thenardite, whereas the dilute Na_2SO_4 products contained anhydrite in addition to gypsum. The presence of thenardite in SAz-1 reacted with Na_2SO_4 brine indicates that the triple rinse procedure was not successful at removing all of the excess brine from the sample. Ca-sulfate secondary minerals observed in samples of SAz-1 reacted with Na_2SO_4 and $MgSO_4$ brines likely formed as the result of cation exchange. SAz-1 has a relatively high cation exchange capacity of ~120 meq/100 g with the major exchange cation being Ca^{2+} (Borden & Giese, 2001).

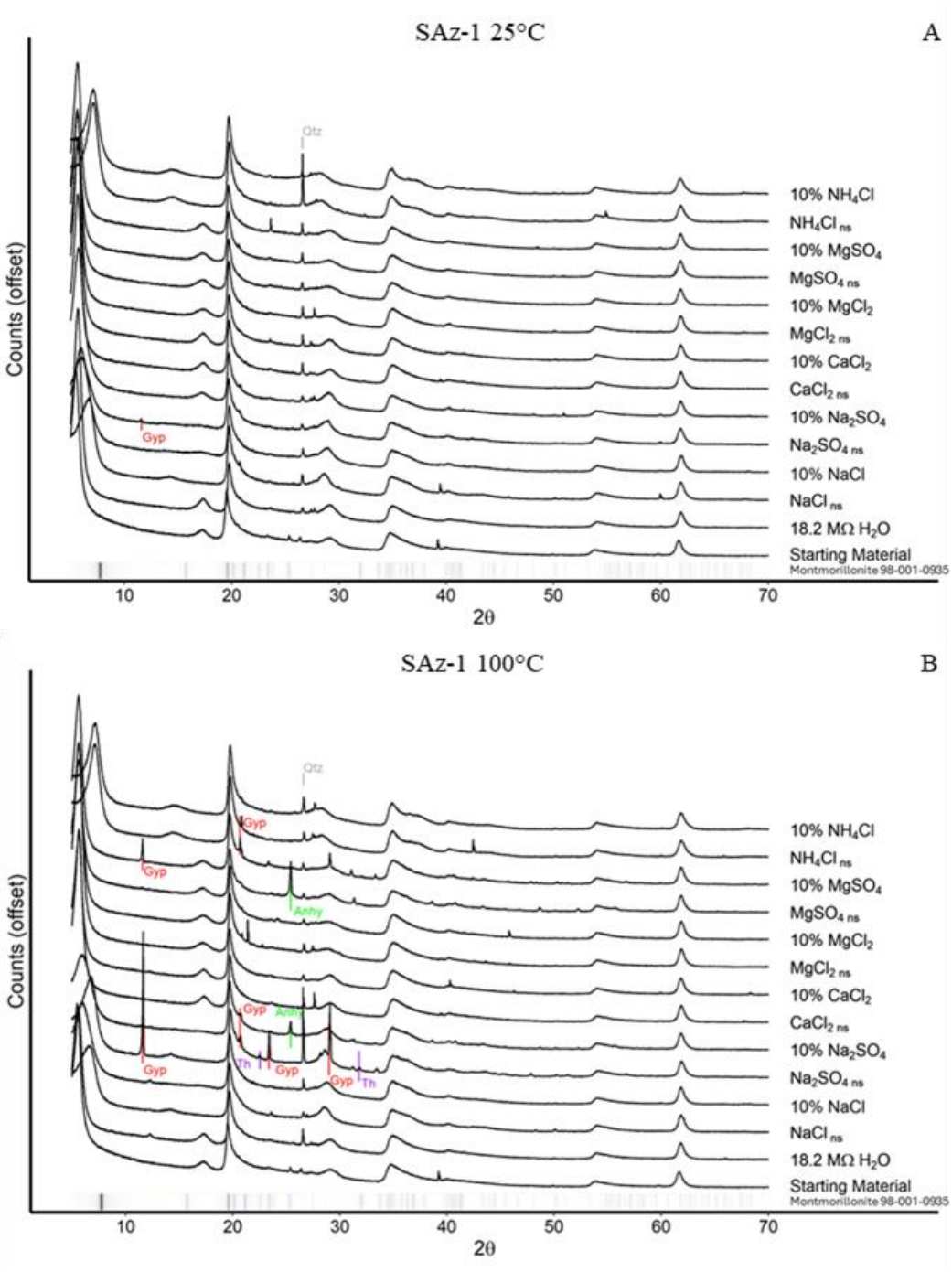

2278

2279 **Figure 8.** XRD Patterns for SAz-1 experiments. The ribbon at the base of each graph shows the

2280 primary intensities for montmorillonite (98-001-0935). A) SAz-1 + brines reacted at 25°C. B)

2281 SAz-1 + brines reacted at 100°C. A peak shift from ~6.2 °2θ towards ~9 °2θ, indicative of

2282 changes in the interlayer spacing, can be observed for near-saturated NaCl, near-saturated NH_4Cl

and dilute NH_4Cl in both the 25°C and 100°C experiments. Changes observed in the 20-30 °2θ are attributed to either contaminant minerals from residual brine or heterogenous inclusion of contamination phases typically found in NAu-2. “Gyp” = Gypsum, “Th” = Thenardite, “Anhy” = Anhydrite, “Qtz” = Quartz.

When comparing the low angle <20 °2θ XRD patterns for SAz-1 (Fig. 8) with the data collected for NAu-2 (Fig.3), two observations stand out: 1) shifts in the 001 basal reflection at ~7°2θ observed in the NaCl, Na_2SO_4, and NH_4Cl brines at both 25°C and 100°C, are similar to those observed in NAu-2, and 2) whereas NAu-2 did not have any appreciable peaks in the 14-18°2θ space (6.3-4.9 Å d-spacings), SAz-1 does have a peak which appears to shift from lower d-spacing to higher d-spacing (~18°2θ in the ethylene glycol sample to ~14.5°2θ in the heat treated sample) for both near-saturated and dilute NH_4Cl reacted with SAz-1 at 25°C and 100°C. Additionally, a weak peak in the same 14-18°2θ range appears in both the 25°C and 100°C near-saturated NaCl and 100°C near-saturated Na_2SO_4 experiments. The broad peaks observed in the 14-18 °2θ range are the 003 reflection for smectite. Therefore, we selected several of the reacted SAz-1 samples for additional ethylene glycol solvation and heat treatment prior to supplementary XRD scans to further investigate possible interstratification (Figs. 9 & 10).

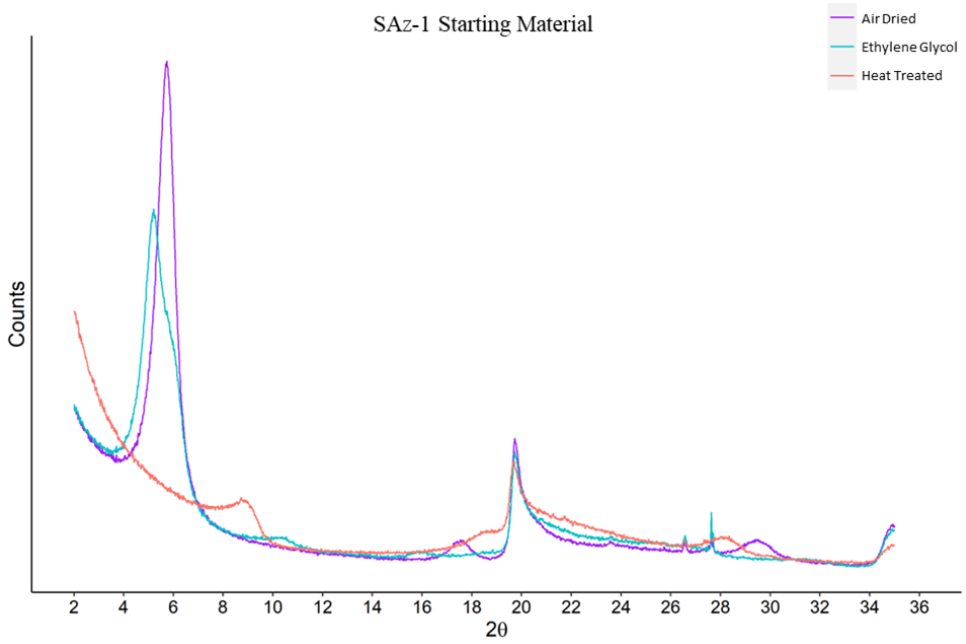

Figure 9. Air Dried, Ethylene Glycol, and Heat Treated XRD patterns for SAz-1 starting material. In the ethylene glycol pattern, peak broadening at ~6 °2θ may be the result of more than one cation present in the interlayer, intermixed illite/smectite layers or partial expansion from ethylene glycol. Kaolinite was not observed in the SAz-1 starting material.

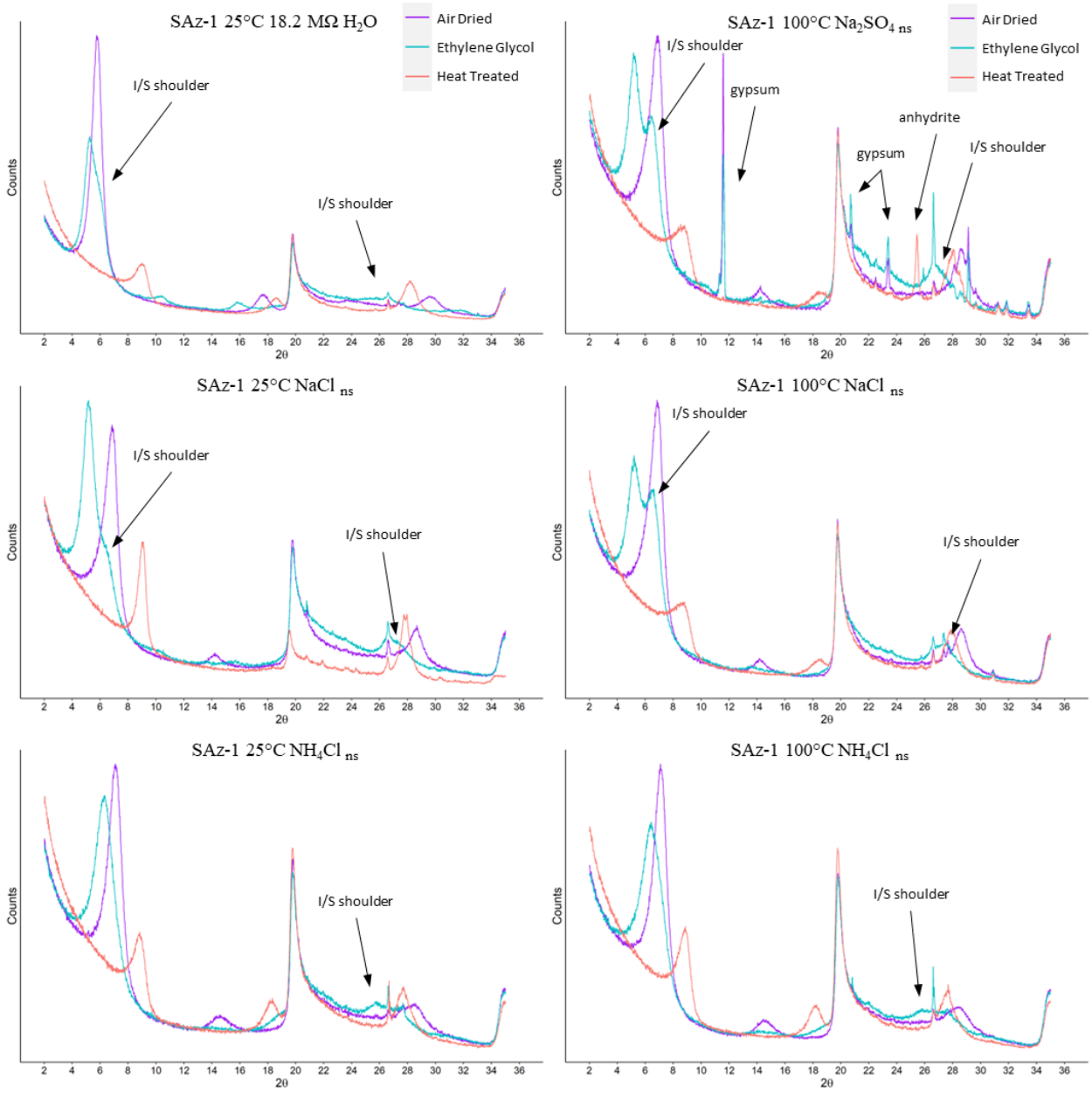

2304

2305 **Figure 10.** Air Dried, Ethylene Glycol, and Heat Treated XRD patterns for select SAz-1 clay-

2306 brine reaction products. "I/S" illite/smectite shoulders indicated with arrows for all samples. In

2307 SAz-1 reacted with Na_2SO_4 at 100°C, gypsum dehydrates to anhydrite in the heat-treated sample.

2308 The results of ethylene glycol and heat treatment on the unreacted SAz-1 starting material are

2309 presented in Fig. 9 and select SAz-1 subsamples which underwent ethylene glycol and heat

2310 treatment are presented in Fig. 10. All ethylene glycol solvated samples exhibit a illite/smectite
2311 shoulder at ~26.4 °2θ. When comparing the influence of temperature, 100°C near-saturated NaCl
2312 produced much more intense I/S shoulders at ~6.5 and ~26.4 °2θ relative to its 25°C counterpart.
2313 For near-saturated NH_4Cl the intensity of the 25°C ~6.5 °2θ peak appears similar to its 100°C
2314 counterpart, while the ~26.4 °2θ I/S shoulder appears only marginally more intense in the 100°C
2315 sample, in contrast to the behavior of NAu-2. Of the six subsamples chosen for ethylene glycol
2316 treatment, only 25°C 18.2 MΩ H_2O reacted SAz-1 had peaks at ~10 °2θ and ~16 °2θ of
2317 sufficient intensity above background to calculate a percent illite. Using the criteria of °Δ2θ
2318 between the 001/002 and the 002/003 peaks (illite/EG-smectite) established by Moore &
2319 Reynolds Jr (1989) the 25°C 18.2 MΩ H_2O reacted SAz-1 contains up to 6.9% illite.

2320 Similar to the incongruent dissolution observed in the NAu-2 experiments, secondary illite
2321 formation in the SAz-1 experiments is not exclusively dependent on either temperature or brine
2322 concentration. For example, the I/S shoulders for near-saturated NaCl reacted at 25°C are
2323 significantly less intense than for the same brine reacted at 100°C; whereas, when comparing
2324 25°C to 100°C reacted NH_4Cl the I/S shoulders are similar in magnitude. Thus, while
2325 temperature clearly influences SAz-1 alteration, brine composition also plays a role. The
2326 persistence of Ca-sulfate minerals is also evident in the ethylene glycol and heat treated XRD
2327 patterns for near-saturated Na_2SO_4 reacted with SAz-1 at 100°C (Fig. 10); in the ethylene glycol
2328 solvated sample gypsum peaks are clearly visible at ~11.6, 20.7, 23.4, and 29.2 °2θ, however
2329 upon heating the sample to 375°C, gypsum dehydrates to anhydrite.

Brine	25°C Al/Si	100°C Al/Si	H_2O Activity
18.2 MΩ H_2O	1.34	0.09	1
NaCl $_{ns}$	4.19	1.76	0.79
NaCl $_{dilute}$	0.17	0.10	0.98
Na_2SO_4 $_{ns}$	1.87	0.45	0.94
Na_2SO_4 $_{dilute}$	0.39	0.08	0.99
$CaCl_2$ $_{ns}$	2.45	1.99	0.43
$CaCl_2$ $_{dilute}$	0.15	0.06	0.97
$MgCl_2$ $_{ns}$	2.61	4.33	0.35
$MgCl_2$ $_{dilute}$	0.26	0.14	0.97
$MgSO_4$ $_{ns}$	3.10	1.20	0.92
$MgSO_4$ $_{dilute}$	0.20	0.08	0.99
NH_4Cl $_{ns}$	1.88	1.01	0.77
NH_4Cl $_{dilute}$	0.19	0.06	0.98
Spearman's Coefficient	-0.66	-0.83	

Table 7. Stoichiometric ratios calculated using Si and Al abundances in brines reacted with SAz-1 at 25°C and 100°C using Eqn. 1. Green highlighted values are below the stoichiometric ratio, gold highlighted values are above the stoichiometric ratio, and blue highlighted values are within 5% of the stoichiometric ratio for SAz-1. Elemental aqueous concentrations are provided in the supplementary material Table A1. Spearman's coefficients for each stoichiometric ratio indicate a correlation to the activity of water for each brine prior to reaction.

The formation of secondary illite, as observed in the XRD data, indicates that incongruent dissolution of SAz-1 is occurring, which is also evident based on the concentrations of Mg, Al, and Si observed in the experimental fluids. Table 3 details the stoichiometric ratios of Al/Si for both the 25°C and 100°C reacted SAz-1, as well as the Spearman's coefficient of each of the ratios compared to the H_2O activity within the initial solution. Stoichiometric ratios were calculated using Eqn. 1, based on the formula unit for SAz-1:

2342 $(Ca_{0.39}Na_{0.36}K_{0.02})(Al_{2.71}Mg_{1.11}Fe_{0.12}Mn_{0.01}Ti_{0.03})(Si_8)O_{20}(OH)_4$ yielding Al/Si = 0.34 (Van

2343 Olphen & Fripiar, 1981).

2344 Similar to the application of stoichiometric ratios to the NAu-2 experiments, deviations from

2345 1 indicate either incongruent dissolution or non-stoichiometric dissolution, or a combination of

2346 both. Stoichiometric ratio values less than 1 indicate either the formation of secondary minerals

2347 incorporating Al, or preferential leaching of Si into solution; the inverse is true for values

2348 exceeding 1.

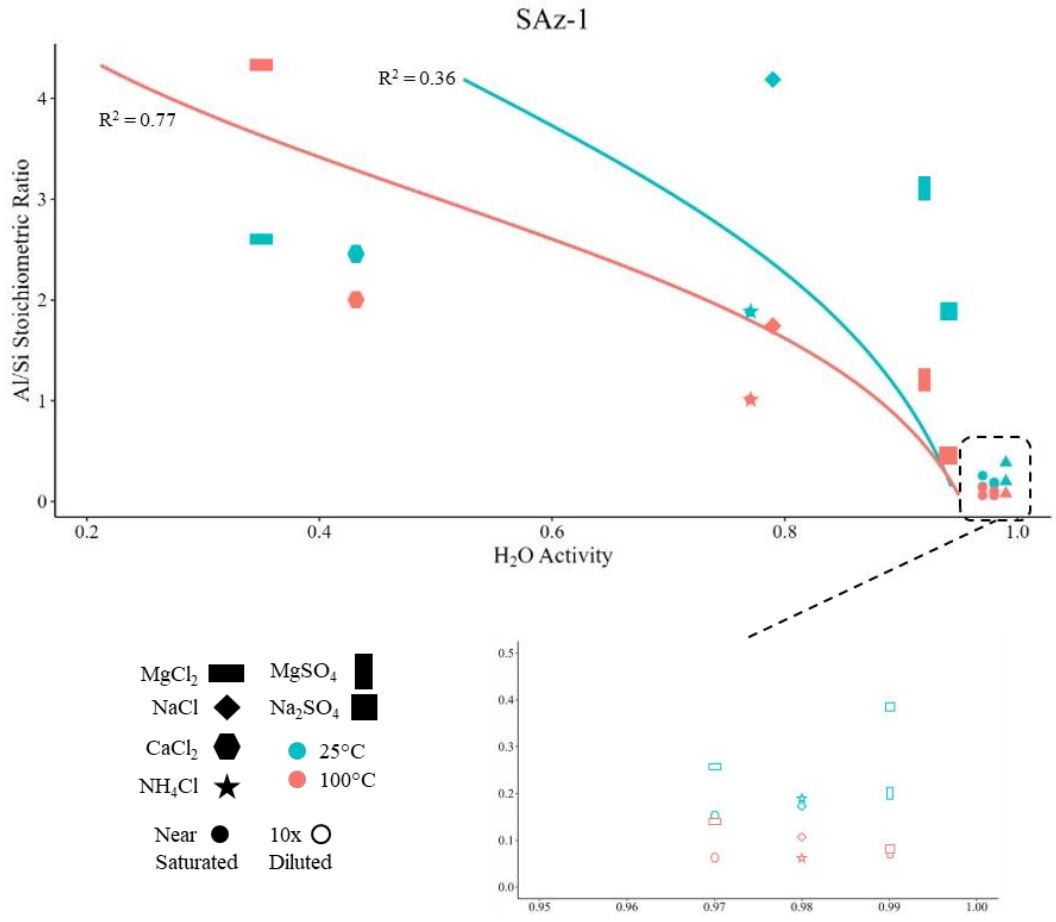

2349

2350 **Figure 11.** Al/Si stoichiometric ratio vs H_2O Activity for SAz-1 25°C and 100°C experiments.

2351 The dashed box highlights the range corresponding to the 0.9-1.0 activity of water. McFadden

pseudo R^2 = 0.36 for samples reacted at 25°C (blue dashed line). McFadden pseudo R^2 = 0.77 for samples reacted at 100°C (orange dashed line).

With the exception of near-saturated $MgCl_2$, all brines reacted with SAz-1 at 25°C had higher Al/Si stoichiometric ratios than their 100°C counterparts. In addition, the Al/Si ratios for near-saturated reacted brines were all equal to or greater than 1, while dilute reacted brines were much lower than 1, regardless of temperature. The Al/Si stoichiometric ratios had Spearman's coefficients of -0.66 and -0.83 for 25°C and 100°C, respectively. Both Spearman's coefficients were statistically significant ($\alpha = 0.05$), which indicates that a relationship between H_2O activity and the Al/Si stoichiometric ratio exists. While a Spearman's coefficient of -0.92 for 100°C is clearly a strong negative relationship, a coefficient of -0.66 for 25°C reactions implies that other factors besides H_2O activity may also influence low temperature alteration of montmorillonite (Fig. 11). Investigations involving a more detailed piecewise approach may be required to fully delineate the relationships between incongruent dissolution, non-stoichiometric dissolution, temperature, and brine composition/concentration.

4. Applications to Mars

The results of this study indicate that as near-surface waters on Mars became increasingly saltier due to evaporation or freezing, different aqueous alteration pathways may have affected clays at or near the surface. Brines influence clay alteration differently depending on their composition, concentration, and temperature of the reaction. For example, during wet periods, relatively dilute fluids would have been prevalent; by comparing the dilute brine Al/Si stoichiometric ratios for both NAu-2 and SAz-1, it is evident that NAu-2 is more sensitive to concentration and temperature differences than SAz-1. Additionally, areas on Mars such as

impact craters likely to be affected by hydrothermal activity, would have experienced different alteration pathways when compared to lower temperature lacustrine or fluvial environments.

On Mars, Al-rich clays such as kaolinite and montmorillonite have been observed to overlay Fe-bearing nontronite clays (Bishop et al., 2008). It has been well documented that transformation of smectite to mixed-layer kaolinite/smectite requires an excess of Al in solution (Środoń, 1999). However, in this study, kaolinite was not detected in either the NAu-2 or the SAz-1 experiments even with excess Al present in the reacted brines. The presence of illite detected in both groups of NAu-2 and SAz-1 subsamples, rather than kaolinite is likely the result of experimental conditions; the reactions were carried out in sealed vessels, and kaolinization of smectite requires adequate drainage to proceed (Bergaya & Lagaly, 2013; Essington, 2015). Restricted lacustrine environments on Mars therefore would likely have increased illite content relative to well drained environments where kaolinite would dominate. This dependance on drainage is similar to alteration pathways observed on Earth, however brine composition would have also influenced the alteration path and products.

In Martian environments where we observe a stratigraphic relationship between smectites and kaolinite, we would expect that the Al enriched fluids percolating downward would eventually precipitate Al-rich phases such as alunite ($KAl_3(SO_4)_2(OH)_6$ or gibbsite ($Al(OH)_3$) under acidic conditions (Fairén et al., 2017). Additionally, as Mg- and Na-rich brines exchanged Mg^{2+} or Na^{+} with the clay interlayer Ca^{2+}, the fluids would have become saturated with respect to Ca-sulfates, thus providing a mechanism for Ca-sulfate formation, which is found in abundance at locations such as Gale crater (Nachon et al., 2014; Rapin et al., 2016). Replacement of interlayer hydrated Ca^{2+} for the larger hydrated Mg^{2+} would also have caused slight localized swelling of the smectite, possibly creating fractures and veins in the surrounding rock.

The influence of both temperature and brine composition/concentration on aqueous alteration of smectites highlights the spatial and temporal variability which must be accounted for when interpreting clays on Mars. For example, in a closed lacustrine environment on Mars, initial fluid compositions would have been less salty and smectites would have released Si preferentially to solution; however, as Mars' hydrosphere shrank and fluids became more saline, smectite aqueous alteration would have released Al preferentially to Si.

5. Conclusions

While dissolution and illitization of smectites have been studied extensively over the last 100 years, the results of this study provide further context to interpret phyllosilicates on Mars and other planets. For both nontronite and montmorillonite, incongruent dissolution via illitization was observed to be dependent not only on temperature and H_2O activity, but also brine composition and concentration. Detection of illite combined with Al/Si stoichiometric ratios indicates that besides temperature and pH, brine composition and concentration strongly influence smectite alteration pathways. For example, when near-saturated NH_4Cl is reacted with nontronite or montmorillonite at 25°C or 100°C the reaction pathways are not consistent between the two smectites, reinforcing the results of previous studies. For example, Šucha et al. (1998) performed hydrothermal synthesis of illite at 300°C and reported that the formation of either NH_4- or K-illite was highly dependent on the composition of the starting material. With nontronite, much more intense illite peaks were observed in the ethylene glycol sample reacted at 100°C relative to its 25°C counterpart (Figs. 5 & 10). However, when montmorillonite was reacted with near-saturated NH_4Cl, XRD peak intensities for illite were similar between the 25°C and 100°C reactions. It has been previously discussed that different brines effect silica precipitation more or less strongly, due to ion pairing effects (Gorrepati et al., 2010). We suggest

that not all smectites are equally affected by a single brine, and that when interpreting sediments resulting from aqueous alteration by high salinity brines, disparate dissolution pathways should be considered that are a function of brine chemistry and concentration, as well as the initial clay mineralogy.

Based on the results of this study, we would expect low temperature aqueous alteration of nontronite to produce Al-enriched (relative to Si) solutions, especially in near-saturated brines. However, at elevated temperatures, dilute brines release more Si from nontronite compared to Al. This reversal in Al vs Si release ratios may reflect a kinetically controlled difference in dissolution rates between the tetrahedral or octahedral sheets, potentially leading to a solid-state like transition between individual smectite layers (Amouric & Olives, 1998).

Linear relationships between Al/Si stoichiometric ratios and activity of water were observed. This relationship may be the result of the dependence of ion pair effects on temperature (Marcus & Hefter, 2006). An alternative hypothesis is that the slower 25°C reactions allowed time for secondary minerals to precipitate, causing incongruent dissolution, thereby more strongly affecting the Al/Si stoichiometric ratio and lessening the direct activity of water effect. However, the Al/Si stoichiometric ratio of montmorillonite and nontronite reacted at 100°C, as well as nontronite reacted at 25°C, exhibited a strong relationship (Spearman's > 0.80) with H_2O activity, indicating that brine composition also affects the Al/Si stoichiometric ratio.

As demonstrated in this study, stoichiometric ratios, when combined with XRD and Raman data, provide a useful means of interpreting the influence of temperature and brine concentration on aqueous alteration of nontronite and montmorillonite. Additional studies are required to fully detail the progression of incongruent dissolution and non-stoichiometric dissolution in smectites.

Acknowledgements

This project was funded by NASA PDART grants 80NSSC18K0512 & 80NSSC23K0037. XRD data collection was performed at the Samuel Roberts Noble Microscopy Laboratory, an OU core facility supported by the Vice President for Research and Partnerships. The authors would like to thank Itunu T. Apalara for her assistance analyzing samples and Steve J. Chipera for his guidance on XRD interpretation.

References

Amouric, M., & Olives, J. (1998). Transformation mechanisms and interstratification in conversion of smectite to kaolinite: an HRTEM study. *Clays and clay minerals, 46*(5), 521-527.

Ayari, F., Srasra, E., & Trabelsi-Ayadi, M. (2007). Effect of exchangeable cations on the physicochemical properties of smectite. *Surface Engineering and Applied Electrochemistry, 43*, 369-378.

Ben Mabrouk, K., Kauffmann, T. H., Aroui, H., & Fontana, M. D. (2013). Raman study of cation effect on sulfate vibration modes in solid state and in aqueous solutions. *Journal of Raman spectroscopy, 44*(11), 1603-1608.

Bergaya, F., & Lagaly, G. (2013). *Handbook of Clay Science*: Elsevier.

Bibring, J.-P., Langevin, Y., Mustard, J. F., Poulet, F., Arvidson, R., Gendrin, A., . . . Forget, F. (2006). Global mineralogical and aqueous Mars history derived from OMEGA/Mars Express data. *Science, 312*(5772), 400-404.

Bishop, J. L. (2018). Remote detection of phyllosilicates on Mars and implications for climate and habitability. In *From habitability to life on Mars* (pp. 37-75): Elsevier.

Bishop, J. L., Dobrea, E. Z. N., McKeown, N. K., Parente, M., Ehlmann, B. L., Michalski, J. R., . . . Mustard, J. F. (2008). Phyllosilicate diversity and past aqueous activity revealed at Mawrth Vallis, Mars. *Science, 321*(5890), 830-833.

Bishop, J. L., & Murad, E. (2004). Characterization of minerals and biogeochemical markers on Mars: A Raman and IR spectroscopic study of montmorillonite. *Journal of Raman spectroscopy, 35*(6), 480-486.

Borden, D., & Giese, R. (2001). Baseline studies of the clay minerals society source clays: cation exchange capacity measurements by the ammonia-electrode method. *Clays and clay minerals, 49*(5), 444-445.

Bristow, T., Grotzinger, J. P., Rampe, E., Cuadros, J., Chipera, S., Downs, G., . . . Morris, R. (2021). Brine-driven destruction of clay minerals in Gale crater, Mars. *Science, 373*(6551), 198-204.

Bristow, T. F., Bish, D. L., Vaniman, D. T., Morris, R. V., Blake, D. F., Grotzinger, J. P., . . . Ming, D. W. (2015). The origin and implications of clay minerals from Yellowknife Bay, Gale crater, Mars. *American Mineralogist, 100*(4), 824-836.

Buckley, H., Bevan, J., Brown, K., Johnson, L., & Farmer, V. (1978). Glauconite and celadonite: two separate mineral species. *Mineralogical Magazine, 42*(323), 373-382.
Cama, J., Ganor, J., Ayora, C., & Lasaga, C. A. (2000). Smectite dissolution kinetics at 80 C and pH 8.8. *Geochimica et cosmochimica acta, 64*(15), 2701-2717.
Cappelli, C., Yokoyama, S., Cama, J., & Huertas, F. J. (2018). Montmorillonite dissolution kinetics: Experimental and reactive transport modeling interpretation. *Geochimica et cosmochimica acta, 227*, 96-122.
Chevrier, V. F., Rivera-Valentín, E. G., Soto, A., & Altheide, T. S. (2020). Global temporal and geographic stability of brines on present-day Mars. *The planetary science journal, 1*(3), 64.
Chipera, S. J., & Bish, D. L. (2001). Baseline Studies of the Clay Minerals Society Source Clays: Powder X-ray Diffraction Analyses. *Clays and clay minerals, 49*(5), 398-409. doi:10.1346/CCMN.2001.0490507
Clark, B. C., & Van Hart, D. C. (1981). The salts of Mars. *Icarus, 45*(2), 370-378.
Demaret, L., Lerman, H. N., McHugh, M., Hutchinson, I. B., Fagel, N., Eppe, G., & Malherbe, C. (2023). Raman analyses of Al and Fe/Mg-rich clays: Challenges and possibilities for planetary missions. *Journal of Raman spectroscopy, 54*(8), 823-835.
Ehlmann, B. L., Mustard, J. F., Murchie, S. L., Bibring, J.-P., Meunier, A., Fraeman, A. A., & Langevin, Y. (2011). Subsurface water and clay mineral formation during the early history of Mars. *Nature, 479*(7371), 53-60.
Ehlmann, B. L., Mustard, J. F., Swayze, G. A., Clark, R. N., Bishop, J. L., Poulet, F., . . . Wray, J. J. (2009). Identification of hydrated silicate minerals on Mars using MRO-CRISM: Geologic context near Nili Fossae and implications for aqueous alteration. *Journal of Geophysical Research: Planets, 114*(E2).
Elwood Madden, M. E., Madden, A. S., & Rimstidt, J. D. (2009). How long was Meridiani Planum wet? Applying a jarosite stopwatch to determine the duration of aqueous diagenesis. *Geology, 37*(7), 635-638.
Essington, M. E. (2015). *Soil and water chemistry: an integrative approach*: CRC press.
Fairén, A. G., Gil-Lozano, C., Uceda, E. R., Losa-Adams, E., Davila, A. F., & Gago-Duport, L. (2017). Mineral paragenesis on Mars: The roles of reactive surface area and diffusion. *Journal of Geophysical Research: Planets, 122*(9), 1855-1879.
Frost, R. L., & Kloprogge, J. T. (2000a). Raman spectroscopy of nontronites. *Applied Spectroscopy, 54*(3), 402-405.
Frost, R. L., & Kloprogge, J. T. (2000b). Vibrational spectroscopy of ferruginous smectite and nontronite. *Spectrochimica Acta Part A: Molecular and Biomolecular Spectroscopy, 56*(11), 2177-2189.
Gainey, S., Hausrath, E., Hurowitz, J., & Milliken, R. (2014). Nontronite dissolution rates and implications for Mars. *Geochimica et cosmochimica acta, 126*, 192-211.
Geyer, C., Madden, A. S. E., Rodriguez, A., Bishop, J. L., Mason, D., & Madden, M. E. (2023). The Role of Sulfate in Cation Exchange Reactions: Applications to Clay–Brine Interactions on Mars. *The planetary science journal, 4*(3), 48.
Gibbons, E., Léveillé, R., & Berlo, K. (2020). Data fusion of laser-induced breakdown and Raman spectroscopies: Enhancing clay mineral identification. *Spectrochimica Acta Part B: Atomic Spectroscopy, 170*, 105905.
Gorrepati, E. A., Wongthahan, P., Raha, S., & Fogler, H. S. (2010). Silica precipitation in acidic solutions: mechanism, pH effect, and salt effect. *Langmuir, 26*(13), 10467-10474.

Gough, R., Chevrier, V., & Tolbert, M. (2014). Formation of aqueous solutions on Mars via deliquescence of chloride–perchlorate binary mixtures. *Earth and Planetary Science Letters, 393*, 73-82.
Gough, R., Wong, J., Dickson, J., Levy, J., Head, J., Marchant, D., & Tolbert, M. (2017). Brine formation via deliquescence by salts found near Don Juan Pond, Antarctica: Laboratory experiments and field observational results. *Earth and Planetary Science Letters, 476*, 189-198.
Grim, R. E. (1968). *Clay Mineralogy* (2nd ed.): McGraw-Hill.
Grotzinger, J. P., Sumner, D. Y., Kah, L., Stack, K., Gupta, S., Edgar, L., . . . Mangold, N. (2014). A habitable fluvio-lacustrine environment at Yellowknife Bay, Gale Crater, Mars. *Science, 343*(6169), 1242777.
Guendouzi, M. E., Dinane, A., & Mounir, A. (2001). Water activities, osmotic and activity coefficients in aqueous chloride solutions at T= 298.15 K by the hygrometric method. *The Journal of Chemical Thermodynamics, 33*(9), 1059-1072.
Guendouzi, M. E., Mounir, A., & Dinane, A. (2003). Water activity, osmotic and activity coefficients of aqueous solutions of Li_2SO_4, Na_2SO_4, K_2SO_4,$(NH_4)_2SO_4$, $MgSO_4$, $MnSO_4$, $NiSO_4$, $CuSO_4$, and $ZnSO_4$ at T= 298.15 K. *The Journal of Chemical Thermodynamics, 35*(2), 209-220.
Ha, Z., & Chan, C. K. (1999). The water activities of $MgCl_2$, $Mg(NO_3)_2$, $MgSO_4$, and their mixtures. *Aerosol Science & Technology, 31*(2-3), 154-169.
Hanson, B. A. (2014). ChemoSpec: an R package for the chemometric analysis of spectroscopic data. *Package Version*, 2.0-2.
Hecht, M. H., Kounaves, S. P., Quinn, R., West, S. J., Young, S. M., Ming, D. W., . . . Hoffman, J. (2009). Detection of perchlorate and the soluble chemistry of martian soil at the Phoenix lander site. *Science, 325*(5936), 64-67.
Horgan, B. H., Anderson, R. B., Dromart, G., Amador, E. S., & Rice, M. S. (2020). The mineral diversity of Jezero crater: Evidence for possible lacustrine carbonates on Mars. Icarus, 339, 113526.
Hurowitz, J. A., Catling, D. C., & Fischer, W. W. (2023). High carbonate alkalinity lakes on Mars and their potential role in an origin of life beyond Earth. *Elements, 19*(1), 37-44.
Keeling, J. L., Raven, M. D., & Gates, W. P. (2000). Geology and characterization of two hydrothermal nontronites from weathered metamorphic rocks at the Uley graphite mine, South Australia. *Clays and clay minerals, 48*, 537-548.
Lafuente, B., Downs, R. T., Yang, H., & Stone, N. (2015). The power of databases: The RRUFF project. In (pp. 1-30). Berlin, MГjnchen, Boston: Berlin, MГjnchen, Boston: DE GRUYTER.
Li, S., He, H., Tao, Q., Zhu, J., Tan, W., Ji, S., . . . Zhang, C. (2020). Kaolinization of 2: 1 type clay minerals with different swelling properties. *American Mineralogist, 105*(5), 687-696.
Loizeau, D., Mangold, N., Poulet, F., Bibring, J. P., Gendrin, A., Ansan, V., . . . Masson, P. (2007). Phyllosilicates in the Mawrth Vallis region of Mars. *Journal of Geophysical Research: Planets, 112*(E8).
Marcus, Y., & Hefter, G. (2006). Ion pairing. *Chemical reviews, 106*(11), 4585-4621.
Marty, N. C., Cama, J., Sato, T., Chino, D., Villiéras, F., Razafitianamaharavo, A., . . . Gaucher, E. C. (2011). Dissolution kinetics of synthetic Na-smectite. An integrated experimental approach. *Geochimica et cosmochimica acta, 75*(20), 5849-5864.

McKinley, J., Worden, R., & Ruffell, A. (1999). Smectite in sandstones: a review of the controls on occurrence and behaviour during diagenesis. *Clay mineral cements in sandstones*, 109-128.
Mermut, A. R., & Cano, A. F. (2001). Baseline studies of the clay minerals society source clays: chemical analyses of major elements. *Clays and clay minerals, 49*(5), 381-386.
Mermut, A. R., & Lagaly, G. (2001). Baseline studies of the clay minerals society source clays: layer-charge determination and characteristics of those minerals containing 2: 1 layers. *Clays and clay minerals, 49*(5), 393-397.
Meunier, A., Petit, S., Cockell, C. S., El Albani, A., & Beaufort, D. (2010). The Fe-rich clay microsystems in basalt-komatiite lavas: importance of Fe-smectites for pre-biotic molecule catalysis during the Hadean eon. *Origins of Life and Evolution of Biospheres, 40*(3), 253-272.
Michalski, J. R., & Noe Dobrea, E. Z. (2007). Evidence for a sedimentary origin of clay minerals in the Mawrth Vallis region, Mars. *Geology, 35*(10), 951-954.
Miller, M. A., Madden, A. S., Madden, M. E., & Elmore, R. D. (2012). Laboratory-simulated diagenesis of nontronite. *Clays and clay minerals, 60*(6), 616-632.
Mills, M. M., Sanchez, A. C., Boisvert, L., Payne, C. B., Ho, T. A., & Wang, Y. (2023). Understanding smectite to illite transformation at elevated (> 100° C) temperature: Effects of liquid/solid ratio, interlayer cation, solution chemistry and reaction time. *Chemical Geology, 615*, 121214.
Möhlmann, D., & Thomsen, K. (2011). Properties of cryobrines on Mars. *Icarus, 212*(1), 123-130.
Moore, D. M., & Reynolds Jr, R. C. (1989). *X-ray Diffraction and the Identification and Analysis of Clay Minerals*: Oxford University Press (OUP).
Nachon, M., Clegg, S., Mangold, N., Schröder, S., Kah, L., Dromart, G., . . . Bridges, J. (2014). Calcium sulfate veins characterized by ChemCam/Curiosity at Gale crater, Mars. *Journal of Geophysical Research: Planets, 119*(9), 1991-2016.
Palmer, D. A., Bénézeth, P., & Wesolowski, D. J. (2001). Aqueous high-temperature solubility studies. I. The solubility of boehmite as functions of ionic strength (to 5 molal, NaCl), temperature (100–290 C), and pH as determined by in situ measurements. *Geochimica et cosmochimica acta, 65*(13), 2081-2095.
Parkhurst, D. L., & Appelo, C. (2013). Description of input and examples for PHREEQC version 3—a computer program for speciation, batch-reaction, one-dimensional transport, and inverse geochemical calculations. *US geological survey techniques and methods, 6*(A43), 497.
Polgári, M., Hein, J., Németh, T., Pál-Molnár, E., & Vigh, T. (2013). Celadonite and smectite formation in the Úrkút Mn-carbonate ore deposit (Hungary). *Sedimentary Geology, 294*, 157-163.
Poulet, F., Bibring, J.-P., Mustard, J., Gendrin, A., Mangold, N., Langevin, Y., . . . Gomez, C. (2005). Phyllosilicates on Mars and implications for early Martian climate. *Nature, 438*(7068), 623-627.
Rampe, E. B., Blake, D. F., Bristow, T., Ming, D. W., Vaniman, D., Morris, R., . . . Tu, V. (2020). Mineralogy and geochemistry of sedimentary rocks and eolian sediments in Gale crater, Mars: A review after six Earth years of exploration with Curiosity. *Geochemistry, 80*(2), 125605.

Rapin, W., Ehlmann, B. L., Dromart, G., Schieber, J., Thomas, N., Fischer, W. W., . . . Clark, B. C. (2019). An interval of high salinity in ancient Gale crater lake on Mars. *Nature Geoscience, 12*(11), 889-895.

Rapin, W., Meslin, P.-Y., Maurice, S., Vaniman, D., Nachon, M., Mangold, N., . . . Wiens, R. (2016). Hydration state of calcium sulfates in Gale crater, Mars: Identification of bassanite veins. *Earth and Planetary Science Letters, 452*, 197-205.

Scheller, E. L., Hollis, J. R., Cardarelli, E. L., Steele, A., Beegle, L. W., Bhartia, R., . . . Ehlmann, B. L. (2022). Aqueous alteration processes in Jezero crater, Mars− implications for organic geochemistry. *science*, eabo5204.

Schwenzer, S., Abramov, O., Allen, C., Bridges, J., Clifford, S., Filiberto, J., . . . Newsom, H. (2012). Gale Crater: Formation and post-impact hydrous environments. *Planetary and Space Science, 70*(1), 84-95.

Schwenzer, S. P., Bridges, J. C., Wiens, R. C., Conrad, P. G., Kelley, S., Leveille, R., . . . Newsom, H. (2016). Fluids during diagenesis and sulfate vein formation in sediments at Gale crater, Mars. *Meteoritics & Planetary Science, 51*(11), 2175-2202.

Squyres, S. W., & Knoll, A. H. (2005). Sedimentary rocks at Meridiani Planum: Origin, diagenesis, and implications for life on Mars. *Earth and Planetary Science Letters, 240*(1), 1-10.

Środoń, J. (1980). Precise identification of illite/smectite interstratifications by X-ray powder diffraction. *Clays and clay minerals, 28*, 401-411.

Środoń, J. (1999). Nature of mixed-layer clays and mechanisms of their formation and alteration. *Annual Review of Earth and Planetary Sciences, 27*(1), 19-53.

Steiner, M., Hausrath, E., Madden, M. E., Tschauner, O., Ehlmann, B., Olsen, A., . . . Smith, J. (2016). Dissolution of nontronite in chloride brines and implications for the aqueous history of Mars. *Geochimica et cosmochimica acta, 195*, 259-276.

Thomas, N., Ehlmann, B., Meslin, P. Y., Rapin, W., Anderson, D., Rivera-Hernández, F., . . . Mangold, N. (2019). Mars Science Laboratory observations of chloride salts in Gale crater, Mars. *Geophysical research letters, 46*(19), 10754-10763.

Uriarte, L. M., Dubessy, J., Boulet, P., Baonza, V. G., Bihannic, I., & Robert, P. (2015). Reference Raman spectra of synthesized CaCl2· nH2O solids (n= 0, 2, 4, 6). *Journal of Raman spectroscopy, 46*(10), 822-828.

Van Olphen, H., & Fripiar, J. (1981). Data handbook for clay materials and other non-metallic minerals. *Soil Science, 131*(1), 62.

Vaniman, D. T., Bish, D. L., Chipera, S. J., Fialips, C. I., William Carey, J., & Feldman, W. C. (2004). Magnesium sulphate salts and the history of water on Mars. *Nature, 431*(7009), 663-665.

Wang, A., Freeman, J. J., & Jolliff, B. L. (2015). Understanding the Raman spectral features of phyllosilicates. *Journal of Raman spectroscopy, 46*(10), 829-845. doi:10.1002/jrs.4680

Wang, A., Freeman, J. J., Jolliff, B. L., & Chou, I.-M. (2006). Sulfates on Mars: A systematic Raman spectroscopic study of hydration states of magnesium sulfates. *Geochimica et cosmochimica acta, 70*(24), 6118-6135.

Weiszburg, T. G., Tóth, E., & Beran, A. (2004). Celadonite, the 10-Å green clay mineral of the manganese carbonate ore, Úrkút, Hungary. *Acta Mineralogica-Petrographica, 45*(1), 65-80.

Wilson, M. (1999). The origin and formation of clay minerals in soils: past, present and future perspectives. *Clay Minerals, 34*(1), 7-25.

Yen, A., Ming, D., Vaniman, D., Gellert, R., Blake, D., Morris, R., . . . Edgett, K. (2017). Multiple stages of aqueous alteration along fractures in mudstone and sandstone strata in Gale Crater, Mars. *Earth and Planetary Science Letters, 471*, 186-198.

Zorzano, M. P., Mateo-Martí, E., Prieto-Ballesteros, O., Osuna, S., & Renno, N. (2009). Stability of liquid saline water on present day Mars. *Geophysical Research Letters, 36*(20).

Supplementary Material

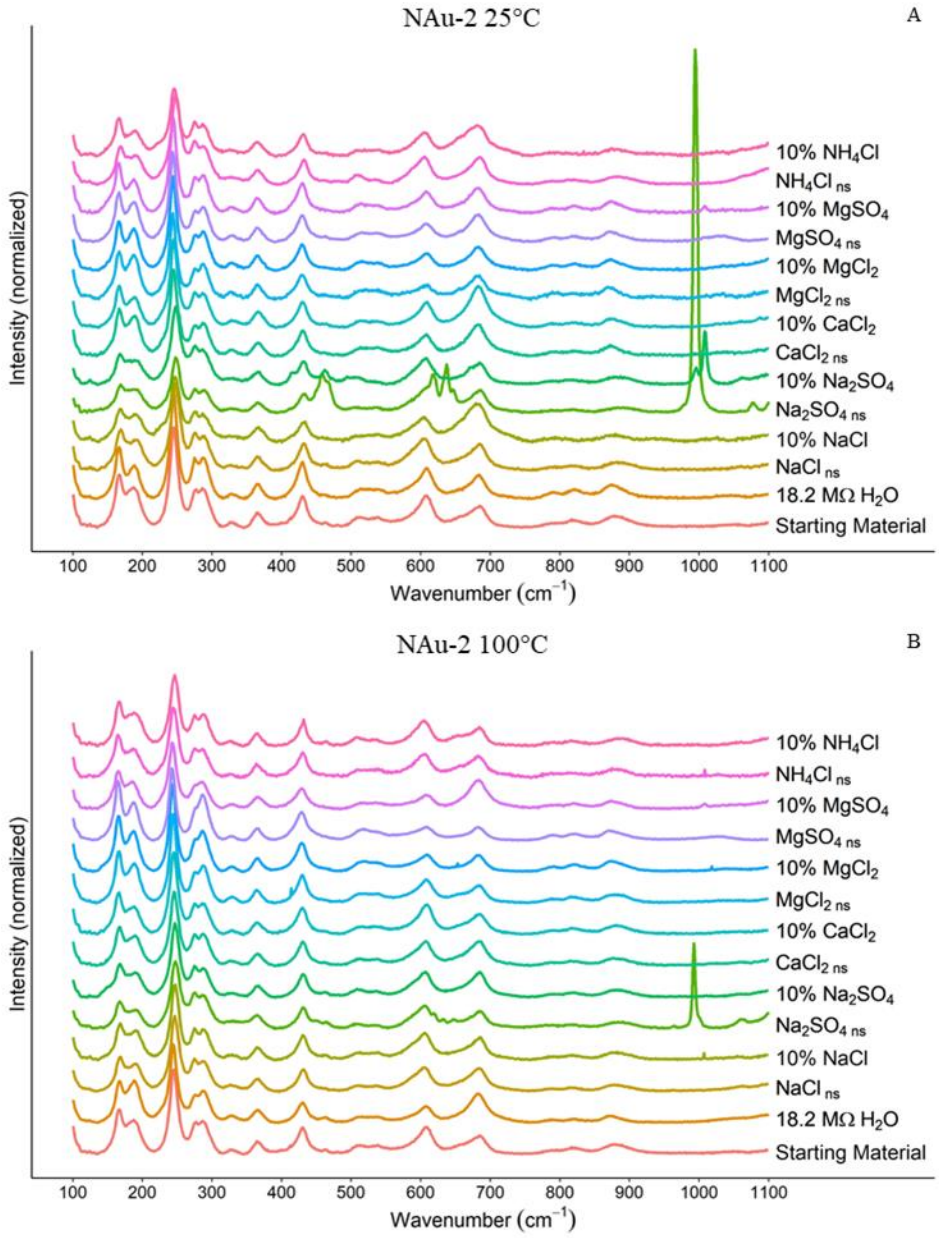

Figure A1. Raman spectra without a Savitzky-Golay smoothing filter for NAu-2 experiments.

A) NAu-2 + brines reacted at 25°C. B) Nau-2 + brines reacted at 100°C.

	NAu-2					
	25°C			100°C		
Brine	Fe	Si	Al	Fe	Si	Al
18.2 MΩ H_2O	0.22	0.61	0.04	0.01	0.32	0.00
$NaCl_{ns}$	0.02	0.92	0.30	0.02	0.50	0.91
$NaCl_{dilute}$	0.00	0.59	0.04	0.00	0.22	0.03
$Na_2SO_{4\ ns}$	0.01	0.65	0.29	0.08	0.52	0.35
$Na_2SO_{4\ dilute}$	0.02	0.34	0.03	0.01	0.67	0.03
$CaCl_{2\ ns}$	0.01	0.36	0.25	0.01	0.32	0.18
$CaCl_{2\ dilute}$	0.00	0.24	0.03	0.02	1.43	0.04
$MgCl_{2\ ns}$	0.01	0.30	0.30	0.01	0.28	0.31
$MgCl_{2\ dilute}$	0.00	0.32	0.03	0.00	1.06	0.04
$MgSO_{4\ ns}$	0.04	0.35	0.37	0.01	0.96	0.31
$MgSO_{4\ dilute}$	0.00	0.25	0.03	0.00	1.62	0.03
NH_4Cl_{ns}	0.01	0.87	0.33	0.01	1.19	0.33
NH_4Cl_{dilute}	0.01	0.41	0.03	0.00	1.44	0.03

Table A2. Elemental aqueous concentrations in m*M* for Si and Al in brines reacted with NAu-2.

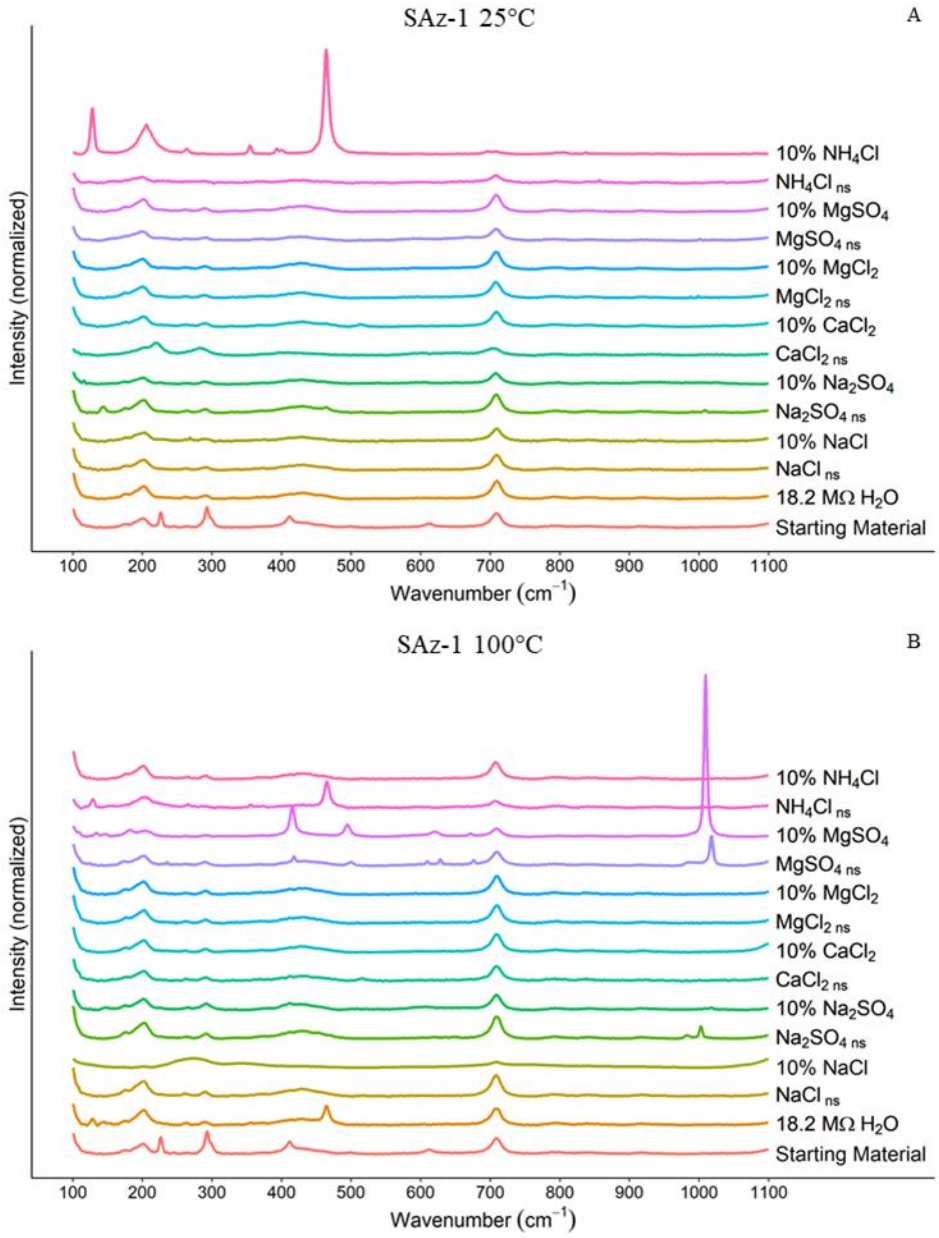

Figure A2. Raman spectra without a Savitzky-Golay smoothing filter for SAz-1 experiments. A) SAz-1 + brines reacted at 25°C. B) SAz-1 + brines reacted at 100°C.

SAz-1

	25°C		100°C	
Brine	Si	Al	Si	Al
18.2 MΩ H_2O	0.00	0.00	1.19	0.04
NaCl $_{ns}$	0.29	0.40	0.67	0.40
NaCl $_{dilute}$	0.52	0.03	0.79	0.03
Na_2SO_4 $_{ns}$	0.61	0.39	1.30	0.20
Na_2SO_4 $_{dilute}$	0.56	0.07	0.87	0.02
$CaCl_2$ $_{ns}$	0.17	0.14	0.19	0.13
$CaCl_2$ $_{dilute}$	0.47	0.02	0.85	0.02
$MgCl_2$ $_{ns}$	0.39	0.35	0.19	0.27
$MgCl_2$ $_{dilute}$	0.48	0.04	0.68	0.03
$MgSO_4$ $_{ns}$	0.31	0.33	0.56	0.23
$MgSO_4$ $_{dilute}$	0.60	0.04	1.07	0.03
NH_4Cl $_{ns}$	0.51	0.33	0.77	0.26
NH_4Cl $_{dilute}$	0.54	0.04	1.12	0.02

Table A2. Elemental aqueous concentrations in m*M* for Si and Al in brines reacted with SAz-1.

25°C	SiO_2(a)	Quartz
18.2 MΩ H_2O	-0.5	0.77
NaCl $_{ns}$	-0.32	0.95
NaCl $_{dilute}$	-0.52	0.75
Na_2SO_4 $_{ns}$	-0.47	0.8
Na_2SO_4 $_{dilute}$	-0.76	0.51
$CaCl_2$ $_{ns}$	-0.73	0.54
$CaCl_2$ $_{dilute}$	-0.91	0.36
$MgCl_2$ $_{ns}$	-0.73	0.54
$MgCl_2$ $_{dilute}$	-0.78	0.49
$MgSO_4$ $_{ns}$	-0.54	0.73
$MgSO_4$ $_{dilute}$	-0.89	0.38
NH_4Cl $_{ns}$	-0.35	0.92
NH_4Cl $_{dilute}$	-0.67	0.6

100°C	SiO_2(a)	Quartz
18.2 MΩ H_2O	-0.78	0.49
NaCl $_{ns}$	-0.59	0.68
NaCl $_{dilute}$	-0.95	0.32
Na_2SO_4 $_{ns}$	-0.57	0.7
Na_2SO_4 $_{dilute}$	-0.45	0.82
$CaCl_2$ $_{ns}$	-0.78	0.49
$CaCl_2$ $_{dilute}$	-0.13	1.14
$MgCl_2$ $_{ns}$	-0.72	0.55
$MgCl_2$ $_{dilute}$	-0.26	1.01
$MgSO_4$ $_{ns}$	-0.25	1.02
$MgSO_4$ $_{dilute}$	-0.08	1.19
NH_4Cl $_{ns}$	-0.21	1.06
NH_4Cl $_{dilute}$	-0.13	1.14

Table A3. Saturation Indices modelled using PHREEQC for NAu-2 brine reactions at 25°C (left) and 100°C (right). "SiO_2 (a)" represents amorphous silica.

25°C	SiO_2(a)	Quartz
18.2 MΩ H_2O	-3.33	-2.07
NaCl $_{ns}$	-0.82	0.45
NaCl $_{dilute}$	-0.57	0.7
Na_2SO_4 $_{ns}$	-0.5	0.77
Na_2SO_4 $_{dilute}$	-0.54	0.73
$CaCl_2$ $_{ns}$	-1.06	0.21
$CaCl_2$ $_{dilute}$	-0.62	0.65
$MgCl_2$ $_{ns}$	-0.7	0.57
$MgCl_2$ $_{dilute}$	-0.61	0.66
$MgSO_4$ $_{ns}$	-0.71	0.56
$MgSO_4$ $_{dilute}$	-0.51	0.76
NH_4Cl $_{ns}$	-0.58	0.69
NH_4Cl $_{dilute}$	-0.55	0.71

100°C	SiO_2(a)	Quartz
18.2 MΩ H_2O	-1	-0.12
NaCl $_{ns}$	-0.82	0.06
NaCl $_{dilute}$	-1.01	-0.13
Na_2SO_4 $_{ns}$	-0.97	-0.09
Na_2SO_4 $_{dilute}$	-1.25	-0.37
$CaCl_2$ $_{ns}$	-1.23	-0.35
$CaCl_2$ $_{dilute}$	-1.4	-0.52
$MgCl_2$ $_{ns}$	-1.29	-0.41
$MgCl_2$ $_{dilute}$	-1.28	-0.4
$MgSO_4$ $_{ns}$	-1.23	-0.36
$MgSO_4$ $_{dilute}$	-1.39	-0.51
NH_4Cl $_{ns}$	-0.84	0.03
NH_4Cl $_{dilute}$	-1.17	-0.29

Table A4. Saturation Indices modelled using PHREEQC for SAz-1 brine reactions at 25°C (left) and 100°C (right). "SiO_2 (a)" represents amorphous silica.

Dissertation Conclusions

The findings in this dissertation provide needed details on clay-brine reactions on Mars and other salty environments. In Chapter 1, Ca-sulfate formation resulting from cation exchange between brines and montmorillonite was discussed. Ca-sulfate formation was found to be rapid, almost instantaneous, and times required for gypsum or epsomite formation were well within even the shortest "wet" periods Mars may have experienced. Chapter 2 detailed relative humidity cycling of clay-salt mixtures and documented rapid cation exchange and migration of Ca^{2+} out of montmorillonite grains. The exchanged Ca^{2+} rapidly formed new Ca-sulfate crystals in the absence of free liquid water. Mass transport catalyzed by elevated relative humidity, albeit on a microscopic scale, is of immediate interest when investigation phenomena on Mars such as recurring slope lineae and other features which may involve water on present day Mars. Chapters 3 and 4 documented the results of reactions between near saturated/dilute brines and kaolinite, montmorillonite and nontronite at both room temperature and elevated temperature. In brine-kaolinite reactions no secondary minerals above detection limits were observed. However, non-stoichiometric dissolution of kaolinite with preferential release of Al was indicated by elemental concentrations in reacted brines. The Al/Si ratios in kaolinite reacted brines indicated a concentration-temperature interdependent dissolution pathway. Chapter 4 results were similar, with incongruent dissolution leading to the formation of illite in some samples. As with kaolinite, smectites exhibited concentration-temperature interdependence, with non-stoichiometric dissolution occurring in almost all smectite-brine reactions.

While there is always room for additional research, the preceding four studies provide a broad foundation for future investigations. Increasing our knowledge of how clay-brine reactions

progress in a Martian or salty environment will advance our understanding of the Martian hydrosphere, perhaps supporting human exploration of Mars and other planets.